BRNO UNIVERSITY OF TECHNOLOGY
VYSOKÉ UČENÍ TECHNICKÉ V BRNĚ

FACULTY OF MECHANICAL ENGINEERING
FAKULTA STROJNÍHO INŽENÝRSTVÍ

INSTITUTE OF AEROSPACE ENGINEERING
LETECKÝ ÚSTAV

DESIGN, STRESS ANALYSES AND LIMIT LOAD OF SANDWICH STRUCTURES
NAVRHOVÁNÍ, PEVNOSTNÍ KONTROLA A ÚNOSNOST SENDVIČOVÝCH KONSTRUKCÍ

DOCTORAL THESIS
DIZERTAČNÍ PRÁCE

AUTHOR   Ing. František Löffelmann
AUTOR PRÁCE

SUPERVISOR   prof. Ing. Antonín Píštěk. CSc.
ŠKOLITEL

BRNO 2021

Abstract

The thesis starts with a review of design calculations of sandwich beams, plates, and complicated structures, where FEM plays an important role. Next, optimization methods are reviewed to shed light on the wide area of mathematical programming and basic topology optimization principles up to its implementation by other authors in composite design, including representative examples of analytical and numerical optimization of sandwiches. The thesis objective is defined as an implementation of mass minimization with failure constraints aiming to make the sandwich design process easier. This is done by own implementation of gradient optimization based on topology optimization principles, known as Discrete Material Optimization (DMO), which helps to find optimal layup. Approach to material interpolation and failure constraints interpolation is developed and programmed in Python, using First Order Shear Deformation Theory (FSDT) to evaluate stresses on elements, based on element loads given by the Nastran FE solver. Gradient optimizer searches for optimal materials for each layer of the sandwich face-sheet and core from the user-defined candidates. The program is tested on examples of sequential complexity from one-element beams where the true optimum is known up to a practical task of the sandwich galley from an airliner. Results have shown that the algorithm can reach a discrete solution without (significant) violation of constraints and thus can be practically used to make conceptual sandwich design more efficient.

Key words

Sandwich, Gradient optimization, Mass minimization, Sandwich failures, Stacking sequence, Constraint aggregation, Discrete Material Optimization.

Abstrakt

Tato doktorská disertační práce je zaměřena na koncepční návrh sendvičových konstrukcí pomocí metody konečných prvků za použití diskrétní optimalizace materiálu (Discrete Material Optimization – DMO), což je gradientní metoda využívající principů multimateriálové topologické optimalizace.

V první části práce jsou popsány analytické přístupy výpočtu sendvičových nosníku a panelů, které jsou již dlouho známé a používané. Široce rozšířená je též aplikace metody konečných prvků při návrhu sendvičových konstrukcí, neboť umožňuje analyzovat i složitou geometrii a vrstvení. V rámci přehledu současného stavu poznání jsou nastíněny vybrané optimalizační metody. I když se vlastní práce zaměřuje na gradientní metody, genetické algoritmy jsou zmíněné, díky svému rozšíření v optimalizaci kompozitů a tím pádem i sendvičů. Matematické programování je dále rozvinuto v podobě nejčastěji užívané metody topologické optimalizace – SIMP (Solid Isotropic Material with Penalization), která v zahraničí posloužila jako výchozí bod pro vývoj metody DMO a jejích variant, které se z užití na optimalizaci kompozitů rozšiřují i v oblasti návrhu sendvičů. Jako příklad obecného přístupu ke konstrukční optimalizaci je shrnuta optimalizace za použití metody konečných prvku v Nastranu a tří fázová optimalizace kompozitů v OptiStructu. Přímo v oblasti sendvičů je možné v omezené míře použít analytické metody, ale těžiště praktického užití je v aplikaci numerických metod.

Cíl disertační práce byl stanoven jako programová implementace optimalizační metody, která by usnadnila proces návrhu sendvičové konstrukce za použití MKP, tedy s geometrií, kterou není snadné navrhnout pomocí analytických metod tak, aby se snížil počet návrhových cyklů, které musí inženýr ručně provádět (měnit vrstvení a kontrolovat splnění požadavků).

Optimalizační úloha je formulována jako minimalizace hmotnosti konstrukce při dodržení omezujících podmínek sendvičových poruch (maximální napětí v potahu, smyk jádra, crimping – zvlnění, wrinkling – zvrásnění), kde návrhovými proměnnými jsou materiály (včetně tloušťky a orientace vrstvy) kompozitního potahu a jádra. Metoda je založená na interpolaci hustoty dílčích materiálů pomocí RAMP (Rational Approximation of Material Properties) schématu v každé vrstvě, kdy jedna vrstva obsahuje podíly více složek materiálu. Díky vhodné penalizaci matice tuhosti vrstvy a poruch se optimalizér konverguje k diskrétnímu výsledku (ve vrstvě zůstává právě jeden materiál) na rozdíl od počáteční rovnoměrné distribuce materiálových proměnných. Logistická funkce je použita pro interpolaci hustoty jednotlivých vrstev potahu tak, aby se vrstvy odebíraly z vnější strany a návrhové veličiny se plynule měnily. Pro dosažení diskrétních výsledků, které splňují předepsaná poruchová kritéria, byly stanoveny výchozí parametry optimalizace.

Vlastní softwarová implementace je naprogramována v Pythonu, kdy uživatel nejprve definuje potenciální materiály a síť MKP modelu s okrajovými podmínkami a zatížením. Program následně provede interpolaci vlastností, tak aby mohla být použita v externím MKP řešiči, kterým je Nastran. Ten spočítá lineární statickou analýzu a vypíše vnitřní silové účinky na jednotlivých elementech, které jsou už pak vlastním programem použity k výpočtu napjatosti ve vrstvách a opakovanému vyhodnocení poruchových kritérií tak, jak je požaduje

optimalizér (IPOPT) v rámci vyčíslení omezujících podmínek, cílové funkce a jejich derivací. Po konvergenci k diskrétním výsledkům vrstvení dojde k zaokrouhlení případných nepřesností a ověření splnění poruchových kritérií na finálním modelu. Za účelem snížení výpočtové náročnosti byly implementovány agregace omezující podmínek pomocí KS funkce a „patch design", tedy sdružení elementů, které mají sdílené návrhové proměnné (vrstvení). Uživatel nakonec zkontroluje splnění ostatních podmínek, které nejsou v optimalizaci podchycení, např. deformace, ztrátu stability a konstrukční detaily.

Funkce metody byly testovány na příkladech různé složitosti, počínaje jedno-elementovým modelem sendviče zatíženého tlakem v jeho rovině, smykem a ohybem, dále série simultánně optimalizovaných nosníků sestávající z jednoho elementu. U těchto příkladů bylo řešení srovnáno se známým optimem. Příklad s vyšším počtem proměnných byly panely s trojím typem okrajových podmínek, kde je porovnána náročnost při optimalizaci každého elementu zvlášť, všech elementů se společným vrstvením, použití agregace omezujících podmínek a provázání vrstev pomocí tzv. blendingu. Složitějším příkladem je box sestávající z 25 návrhových oblastí zatížený pod tlakem na horní straně a krouticím momentem obdobně jako křídlo. Příklady z praxe jsou skříň používaná v interiéru dopravního letadla a velká kuchyňka. Na příkladech bylo demonstrováno, že optimalizace je schopna nalézt řešení, které má vysokou míru diskrétnosti a vyhovuje poruchovým kritériím nebo je jen mírně narušuje. Pro některá nastavení nebylo nalezeno skutečné minimum hmotnosti, jak lze vidět u jednoduchých příkladů. Výpočtová náročnost silně závisí na počtu proměnných a omezujících podmínek (zejména počtu elementů), takže např. vrstvení kuchyňky s hrubou sítí čítající cca 5000 elementů se optimalizovalo přibližně 14 hodin.

Přínosy disertační práce jsou v tom, že byl odzkoušen upravené postup výpočtu derivací, které umožňují snadné použití běžně používaných skořepinových MKP modelů. V rámci DMO byly zcela nově použity interpolace wrinklingu a crimpingu. Testovací příklady ukázaly, že optimalizér nekonverguje při narušení poruchových kritérií z důvodu koncentrace napětí nebo nedostatečné pevnosti využitelných materiálů, ale dobré konvergence bylo dosaženo použitím parametru, který předepisuje ignoraci malého množství poruchových kritérií. Program tedy může posloužit v inženýrské praxi pro usnadnění koncepčního návrhu sendvičových konstrukcí tím, že sníží počet ručních úprav vrstvení a přepočítávání a vyhodnocování poruch.

Klíčová slova

Sendvič, Gradientní optimalizace, Minimalizace hmotnosti, Sendvičové poruchy, Vrstvení, Agregace omezujících podmínek, Diskrétní optimalizace materiálu.

Declaration

I declare that this thesis is the result of my own work under the guidance of my supervisor and all literature and electronic sources used for the research are cited in the list of literature.

In Brno, 31st August 2021

…….....………..………………….

František Löffelmann

Acknowledgment

Content

1 Introduction

Sandwich structure combines a thick soft core in the middle of thin stiff face-sheets, which effectively transfers bending moments and satisfies high bending stiffness, which predetermines it to wide use in secondary structures required to be light and stiff under low or intermediate load levels. Sandwich structures are used and designed widely in the aerospace industry at least since Second World War. Since that, wide knowledge about them were collected and various design approaches were developed and described in engineering and scientific literature.

What is new in the recent years and decades is the use of calculations (mostly through the finite element method), not only in the validation of human-made designs, but also directly helping with design in the form of optimization used as a tool to find the best design parameters fulfilling design criteria given by an engineer. Such a growing tool is the topology optimization already established in the conceptual design of parts with isotropic materials. It uses gradient methods to solve tasks with a large number of design variables. Discrete Material Optimization (DMO) is a method based on similar principles as multimaterial topology optimization applied to design composite layups. Sandwiches, as a subgroup of fiber-reinforced composites, have a potential for ongoing research and the improvements of DMO.

The thesis implements DMO with a modified application of derivative evaluation combined with evolution within a given number of design cycles. The implementation is in the form of Python program intended as a tool which could be used by engineers and help them in finding a low mass design satisfying failure constraints on the level of global layup where an engineer defines geometry, loads and boundary conditions, and available material candidates so that the algorithm can search for the best suited combination of them.

2 State of the art

Extensive review of current trends in research and applications of sandwich structures were recently made by Birman and Kardomateas [1] which covers topics of nontraditional core concepts, nanoinclusions, smart materials, functionally graded structures, damages and various environmental effects in aerospace, civil, and marine engineering. The topic of sandwich structures is clearly very wide and so the following review focuses specifically on structural design calculations, on optimization, and application of topology optimization principles to sandwich structures.

2.1 Design calculations

From the broader view, a typical development methodology of a composite structure can be, according to the CMH-17-6 Composite Material Handbook [2], summarized to:

1. Requirements definition – usage, environment, geometry, loads. …

2. Available material assessment – preliminary selection for face-sheets, core and glue.

3. Evaluation of available manufacturing technologies.

4. Preliminary design – structural type (sandwich or laminate), number of layers and their orientation, core thickness and density, manufacturing tooling.

5. Verification tests of material properties.

6. Detailed design – design of joints, sealing. …

7. Structural details and subassembly tests, optimization of mass, cost, lifespan, …

8. Prototype test.

9. Finishing documentation.

From the broader view, sandwich is a special case of composite structure and it is often difficult to answer the question where to place a sandwich and where to use only a laminate on the product, since it depends not only on the mechanical properties and mass but also on other special requirements, reliability, and maintainability. These considerations need to be addressed in relation to the specific part and manufacturer. The review in the following paragraphs is focused to stress and deformation analysis, since it is a wider background of the theses.

2.1.1 Sandwich beams

Difference between analytical calculation of the sandwich beams and homogeneous beams is that sandwiches have, due to soft core and thin face-sheets, small shear stiffness so that shear deformation cannot be neglected. Instead of Bernoulli equation for bending, it is necessary to use more general Timoshenko formulation which includes shear effects

$$D\frac{d^4 w}{dx^4} = \left(1 - \frac{D}{S}\frac{d^2}{dx^2}\right)q \quad , \tag{1}$$

which can be rewritten in more demonstrative form of partial differential equations for bending and shear displacements $w = w_b + w_s$,

$$D\frac{d^4 w_b}{dx^4} = q \quad , \quad S\frac{d^2 w_s}{dx^2} = -q \quad , \tag{2}$$

where q is distributed load; bending and shear stiffness are defined as

$$D = \frac{E_1 t_1 E_2 t_2 d^2}{E_1 t_1 + E_2 t_2} \quad , \quad S = \frac{G_c d^2}{t_c} \quad , \tag{3}$$

where E_1. E_2 are elastic modules of the top and bottom face-sheet, G_c is shear module of the core, t_1, t_2, t_c denotes face-sheet and core thickness, $d = t_c + \frac{t_1 + t_2}{2}$ is a distance of face-sheet centers.

The governing equation (1), which deduction is explained, e.g., by Zenkert [3], is valid with typical sandwich assumptions that face-sheets transfer in-plane loads and bending moments, but do not transfer shear force, whereas the core does not transfer in-plane loads and bending moments, but transfer whole shear force. Error is small if the core has low modulus in the in-plane direction and face-sheets are thin in compare to the core. Conditions for the error less than 1 percent are if

$$\frac{d}{t_f} > 5{,}77 \quad , \quad \frac{6 E_f t_f d^2}{E_c t_c^3} > 100 \quad . \tag{4}$$

Simplification is drawn in Figure 1. In practical applications, it is possible for simplicity to use beam equations to calculate real panels with neglected side boundary conditions.
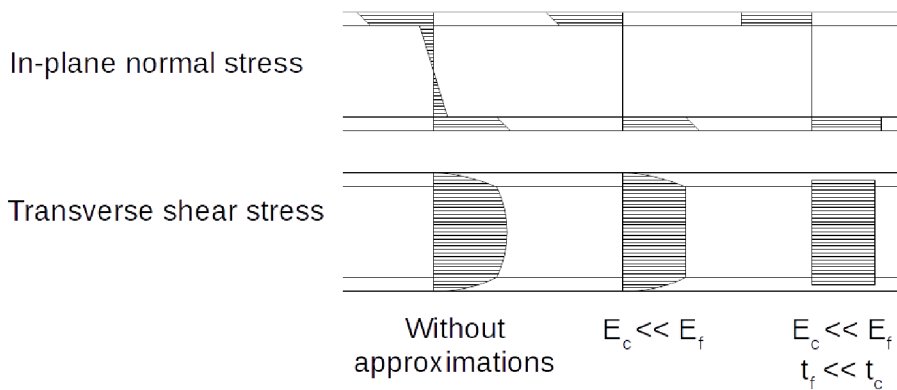

Figure 1: Simplification of the stresses across a sandwich[32].

Theories of higher orders can be used to work with more precise deformation across the sandwich, e.g., polynomial distribution instead of linear or involving nonzero out-of-plane stress. These theories have application, e.g., in detailed calculations in the area where the

sandwich changes its thickness since tapered face-sheets carry also the shear force [5, 7, 9]. Accurateness of the results might be comparable with FEM, but setting the equations requires considerable insight and they finally need to be solved numerically.

2.1.2 Classical panels

Wide attention was paid to the simple panels with constant layup and analytical methods for their design were developed. Their applicability fits rather to the panels on large aircraft where the structure can be divided into idealized panels (flat or with one curvature or cylindrical) with analytical boundary conditions on the edges (simply supported, clamped, or free) and clear loads (tension/compression, shear, bending moments acting on the whole edge, and pressure acting on the surface). These loads can be calculated analytically or from the global FE model. Several sources are described in the subsequent paragraphs.

As for the beam, panel behavior can be described by a set of differential governing equations containing chosen independent variables, e.g., displacement w and shear forces T_x, T_y. According to over the thickness stress variation, first-order shear deformation theory (FSDT), which application is described in detail in appendix Layer stress calculation 9.1, or higher-order shear deformation theories (HSDT) can be used. Solution of the governing equations for specific boundary conditions gives deformation distribution which can be finally used to calculate stresses. Buckling and natural frequencies can be calculated as well. Equations can be solved by numerical methods or approximately with help of energetic methods, e.g., Ritz method which supposes the solution in the form

$$
\begin{aligned}
w &= \sum_{m=1}^{M_1} \sum_{n=1}^{N_1} A_{mn} w_{mn}(x,y) \\
T_x &= \sum_{m=1}^{M_2} \sum_{n=1}^{N_2} B_{mn} T_{xmn}(x,y) \quad , \\
T_y &= \sum_{m=1}^{M_2} \sum_{n=1}^{N_2} C_{mn} T_{ymn}(x,y)
\end{aligned}
\tag{5}
$$

where A_{mn}, B_{mn}, C_{mn} are unknown coefficients – amplitudes of the chosen functions w_{mn}, T_{xmn}, T_{ymn} which are usually in the form of function multiplication $X_m Y_n$.

Solutions for various boundary conditions were collected into diagrams which can be used for practical calculations and design. Many of them can be found in the handbook CMH-17-6 [2], which is a revision of canceled MIL-HDBK-23 from 1974. Regarding the time of original publishing, both handbooks are oriented rather to the metal materials and mostly analytical approaches since composite materials were not so common and computers did not allow wide use of FEA. By sequential use of proper diagrams, it is possible to determine needed core thickness, face-sheet thickness, core shear module for flat panels with isotropic or orthotropic face-sheets and core. For combined loads, it is recommended to use additive equation, e.g., for compression and shear loads

$$
R_c + R_s^2 = 1 \quad ,
\tag{6}
$$

where $R = \dfrac{N}{N_{cr}}$ is ratio of real load to the critical load. Similar methodology is described for sandwich cylinders. Sandwich failures are checked afterwards.

Another significant source is Bruhn [11], who dedicated a detailed chapter to sandwich strength calculations (again flat and curved panels, and cylinders for various load combinations) and also focused on metal structures with hexagonal and square cell cores, and corrugated cores, where core properties are approximated by empirical relations based on the core density. Face-sheet plasticity is considered. Design of the flat panel with given load and allowable stress follows the points:

1. Determination of the face-sheet thickness according to compression load.

2. Determining the core thickness and its shear modulus to prevent global buckling.

3. Define core parameters for sufficient strength in the out-of-plane direction loads and selecting elastic module and shear module to prevent wrinkling.

4. Define the core size to prevent dimpling.

5. In the case of sandwich cylinders, the extra point is to check the bending stiffness of the cylinder preventing buckling.

Kollar [13] describes the deduction of formulas for long plates (based on the analogy with sandwich beams), plates with orthotropic layup loaded with pressure, buckling of long plates simply supported and clamped, and orthotropic simply supported plates. Kollar mentions also analytical formulas for natural frequencies of sandwich plates.

ASM Handobook [15] contains the methodology for sandwich panel design loaded with uniform pressure by the help of superposition of two perpendicular beams which gives conservative results of stress in the face-sheet and core. The handbook also recommends how to reinforce the tapered endings of the sandwich with composite face-sheets.

Much simpler approach is summarized in the document [17] from the composite material producer Hexcel. General approach to design a sandwich panel is:

1. Panel definition (geometry and boundary conditions) and load definition.

2. Constraints definition – displacements, thickness, mass, and safety factor.

3. Preliminary calculation – choosing panel thickness and core thickness and material, stiffness calculation without shear deformation, next calculating displacement and core shear stress.

4. Design optimization – core and face-sheet thickness modification, core material modification.

5. Detailed calculation – with shear deformation included, calculating stress in the core and face-sheets.

6. Checks – global buckling, displacement, crimping, wrinkling, intracell buckling, and core crush.

This approach is usable for manual calculation. Big simplification is the neglection of the shear deformation during the optimization phase. Several typical loads of sandwich beams and an example of the simply supported panel loaded with uniform pressure are described in the cited source.

2.1.3 Finite element analysis

Finite element method (FEM) enables several different approaches to sandwich calculations. When whole structures are calculated, the sandwiches are modeled by shell elements with composite layup where the special layer acts as a core. It is necessary to use a proper element type which does not neglect the shear deformation. Specialized programs might contain even element types programmed directly with formulations valid for sandwiches, but general software packages usually do not contain these element types. During postprocessing, sandwich failures are evaluated from the stresses in the core and face-sheet on each element according to analytical failure criteria. Buckling need to be checked separately by linear buckling analysis or by nonlinear static analysis. Regarding sandwich assumptions, Hexcel document [17] recommends for the honeycomb core to use the following material data: shear modulus in L (ribbon) direction $G_{xz} = G_L$ and W (transverse) direction $G_{yz} = G_W$, and compression modulus $E_z = E_c$. Other characteristics can be defined as close to zero $E_x \approx E_y \approx G_{xy} \approx 0$, $\nu_{xy} \approx \nu_{xz} \approx \nu_{yz} \approx 0$.
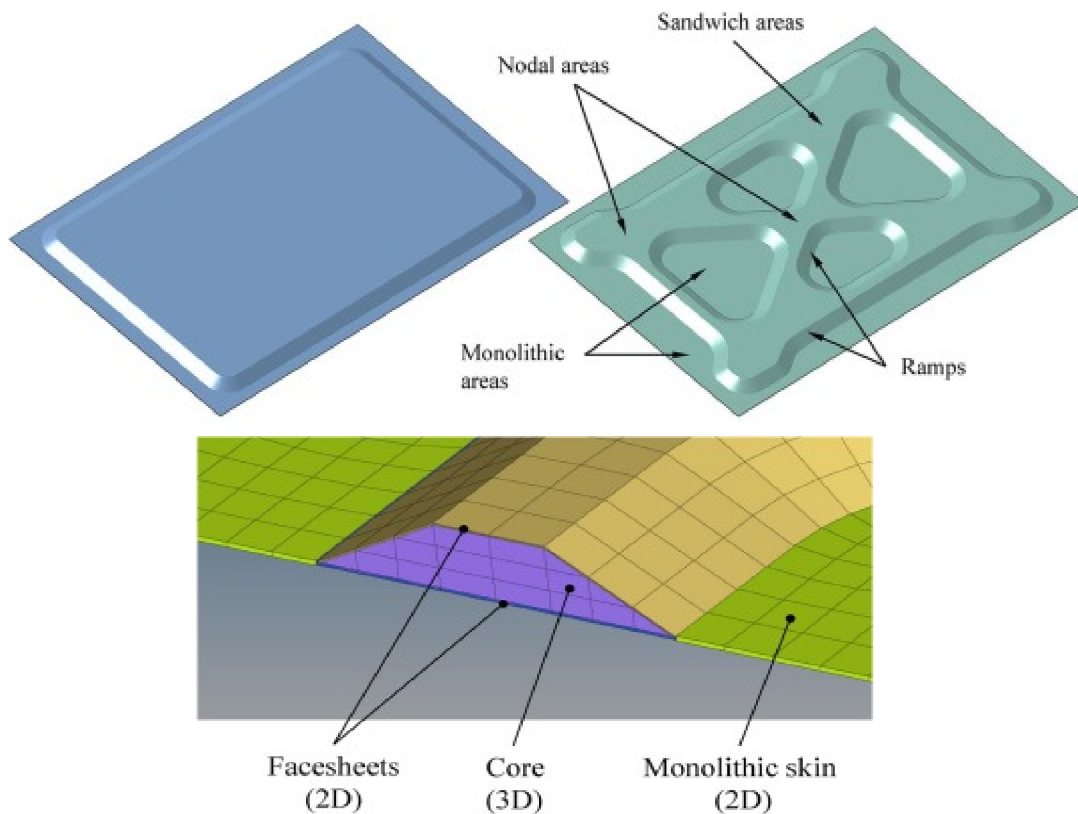

Figure 2: Example of the model combining 2D and 3D elements on helicopter panel [27]

Sandwich needs to be modeled more in detail if stress distribution is required inside detailed structural parts such as joints, core inserts, geometrical changes, and so on. It is usually enough to model the core as a continuum by 3D elements and modeling face-sheets by shell elements with offset from the core or without the offset on the slightly thicker core. Depending on the task, in case of plane strain, the core can be modeled by 2D elements and face-sheets only as 1D beam elements. Continuous 3D elements can be used even for honeycomb core with homogenized material properties found experimentally or from the FE model of the representative sandwich section, where shell elements represent face-sheet and core walls if they are not represented by very fine 3D elements to catch precisely local stress [19, 21], but using 2D elements for honeycomb and corrugated walls is more common for quite detailed models of the specimens [23, 25]. Example combining 2D for faces and 3D elements for the core is in Figure 2, which is after the optimization for buckling on helicopter fuselage panels [27].

2.1.3.1 Complicated structures

When solving a practical task, it is often not possible to split the structure to simple geometrical parts (flat panels or panels with one curvature or cylindrical geometry) having constant layup and loaded uniformly along its edges and by uniform pressure. In these cases, analytical methods are hard to use so that FEM is necessary during design if it is not to be tested only experimentally. Thanks to easiness and precision, FEM is also often used during panel design where analytical methods could be used well. For example, designing the layup of the light aircraft wing, analytical methods can be used with enough precision in the global scale, but when designing a fuselage of a light aircraft [4, 6], using FEM is much more precise than approximate analytical methods because these fuselages used to be geometrically more complicated.

Design and strength checks of sandwich (laminated) structures, which are done in [4, 6] at the Institute of Aerospace Engineering, have rather global modeling character since structural details (such as hinge reinforcement, web-skin connection, sandwich-laminate transition) are rather made according to the technological possibilities and experience of the manufacturer. The workflow is shown in Figure 3. Geometry is used to create a relatively rough mesh with loads and boundary conditions. Here are two options of modeling critical load cases: one way is to model real cases, second way is to model experimental tests which should proof them. Modeling of the experimental test is more idealized, but the test should be proposed to verify critical sections of the structure and moreover, it is possible to validate FE model directly with the experiment, which would be less representative in case of modeling the real case (e.g., due to loading through test tools instead of aerodynamic loads acting on the whole skin). The first layup is placed intuitively in Patran (Laminate modeler) with respect to manufacturing. Than FEA is made. Postprocessing is done in the in-house program COMPOST [31], which calculates sandwich and laminate failures for all elements. According to the results (over-stressed and low used areas in the model), layup is manually modified, again regarding manufacturing, and the analysis is repeated. Since the postprocessing is laborious (e.g., for 7 load cases), this optimization is repeated usually 10-15 times. In Figure 4 depicts a tail area during postprocessing.
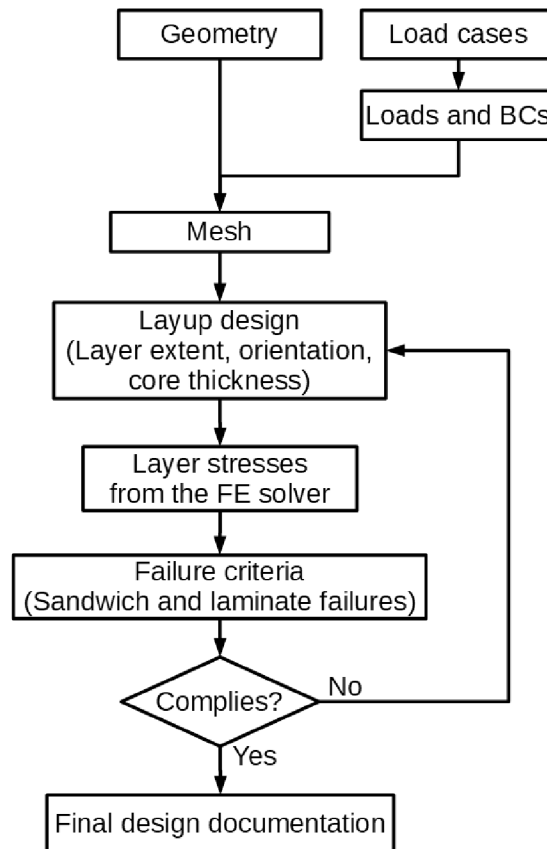
Figure 3: Schema of the workflow for designing a light aircraft layup.

When a light composite airplane fuselage is designed, thin wall structure principles can be assumed, e.g., that the bending moment on the wing is transferred by the axial forces in the beam flanges and the skin transfers only its small portion. If a sandwich is used in this case, the core function is primarily to increase the buckling resistance of large areas of the skin rather than increasing the bending moment transfer by sandwich face-sheets. In this regard and due to technological reasons, several load carrying layers are placed on one side (usually the smooth side of the skin). They are usually supplemented by the foam core and covered with only one closing layer, although in the areas of local bending both face-sheets need to be reinforced by additional layers.
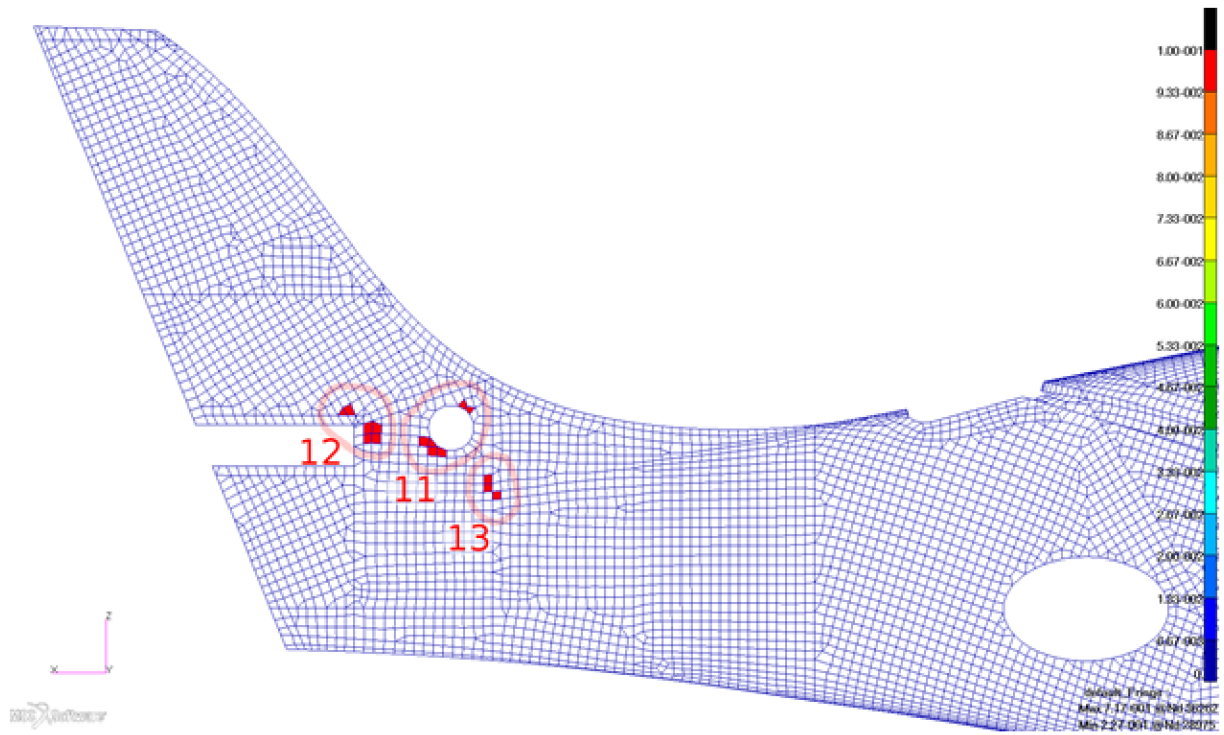
Figure 4: Example of the critical sandwich elements during side load of the tail of 4 seat aircraft. In the area 11 and 12 core shear is critical, resp. core crush in the area 13 [6].

2.2 Optimization

2.2.1 Optimization methods

A lot of methods were developed for the optimization of various tasks. In this chapter, methods related to composite optimization or directly to the thesis are briefly introduced.

2.2.1.1 Genetic algorithms

Genetic algorithms (GA) are widely used in composite optimization as can be found in extensive review papers [8, 10, 12, 14]. GA work on probability bases and fall into the heuristic category. A series of individuals carries genes where design variables are coded. Goal function is evaluated in each iteration for each individual and individuals get fitting parameters, which defines the probability with which the individual will continue to the next iteration. Another tool is crossover, which means that two individuals swap part of the genes. Mutation means that some variables in the gene are changed with a given probability. GA do not require to derive gradients and can be easily parallelized. Thanks to the probability base, they are less prone to end in the local optimum. By their nature, GA work with discrete variables, which makes them convenient for composite layup optimization. Disadvantage is in a high number of goal function evaluations (e.g., in case of wing composite panels layup [33] it was needed 300 iterations with initial population of 400 individuals), so that models for optimization by GA need to be easy to evaluate in each iteration and they should contain rather small number of design variables.

2.2.1.2 Mathematical programming

To minimize goal function f($\mathbf{x}$) with constraint functions g($\mathbf{x}$). Lagrange function is typically minimized

$$L(\mathbf{x},\boldsymbol{\lambda}) = f(\mathbf{x}) + \sum \lambda_i g_i(\mathbf{x}) \tag{7}$$

where Lagrange multiplicators $\boldsymbol{\lambda}$ are minimized together with variables $\mathbf{x}$. Typical approach to find minimum is to solve equation system where partial derivatives of the Lagrange function are set to zero vector. The minimum can be proved by calculating Hessian matrix (matrix of the second derivatives) which should be positive definite. Since this approach could be quite difficult in general, for specific types of goal and constraint functions, efficient methods were developed. Example of structural optimization with mathematical programming of the stiffened panel can be found in the paper by Píštěk and Pešák [34] and a wider description was given by Píštěk [35] including a heuristic approach based on the criteria of fully loaded structure.

Important task in gradient optimization methods is derivative calculation which often takes significant portion of the optimization time. If we assume that functions are continuously differentiable, there are basically three options how to evaluate derivatives:

1. Symbolic differentiation – formula for the function derivative is made by hand or with the help of mathematical software, which might give quite complicated result, but it

can be used for substitution without user interaction. If the function is clearly defined for analytical differentiation, it is usually more efficient than next approaches.

2. Numerical differentiation – the derivative is computed by the forward, backward, or central difference which require to evaluate one (two for more precise central difference) extra functional value(s) in the chosen step from the point where the derivative is required. It is easy to implement, but it could be prohibitive for a high number of variables or if the function takes long to evaluate, e.g., in the case of calculating a large FE model.

3. Automatic differentiation (AD) – AD works on the principle of chain rule applied to the function implemented in the given programming language. First, the original function code is decomposed into intrinsic functions which are effectively symbolically differentiated. Second, intrinsic functions and their derivatives are multiplied together according to the chain rule and combined towards more complicated parts up to the original function. This procedure can be done as a transformation of the original function code or by modification during the code compilation. Brief explanation can be found in the presentation by Berland [36]. AD is reported to be computationally efficient even in calculation higher order derivatives, when a user defines still only nonderived original function.

Since Python programming language was selected to work with in this thesis, the initial focus was on the methods which are available through Python libraries. Large library for scientific computing SciPy [37] contains two algorithms for constrained nonlinear problems: Trust-constrained algorithms and SLSQP (Sequential Least SQuares Programming) [38]. For constrained problems, "Trust constrained algorithms" use the interior point algorithm with changing barrier parameters (preventing constraints violation) for the solution of sequential subproblems.

Another available optimizer is IPOPT (Interior Point Optimizer) [39] which can be also called from Python, but originally works in C++. IPOPT is open-source package which is also available in MSC.Nastran for large scale optimization (topology optimization).

2.2.1.3   Topology optimization with SIMP method

In 1989, Bendsøe [16] introduced Solid Isotropic Materials with Penalization (SIMP) method to seek the distribution of material in the design space. SIMP method is established as the most common method of topology optimization. Design variables are element pseudo densities $x_e \in (0, 1\rangle$, which are continuous so that gradient optimization can be efficiently used for large scale problems. To converge results back to the discrete solution (solid or void material), the penalization coefficient p is defined with recommended values from 2 to 5 (or increasing during iterations) as shown in Figure 5. Element stiffness matrix is interpolated as

$$K_e = x_e^p K_0 \quad , \tag{8}$$

where $\mathbf{K}_0$ is the element stiffness matrix with original solid material. Optimization is typically formulated to minimize compliance given by force vector $\mathbf{F}$ and displacement vector $\mathbf{u}$

$$min \quad \boldsymbol{F}^T \boldsymbol{u} \quad , \tag{9}$$

with equality constraint of static equilibrium typical for finite element method

$$\left(\sum_{e=1}^{N} x_e^p \boldsymbol{K_0} \right) \boldsymbol{u} = \boldsymbol{F} \quad , \tag{10}$$

where the term in the parentheses is global stiffness matrix assembled from penalized element matrices.
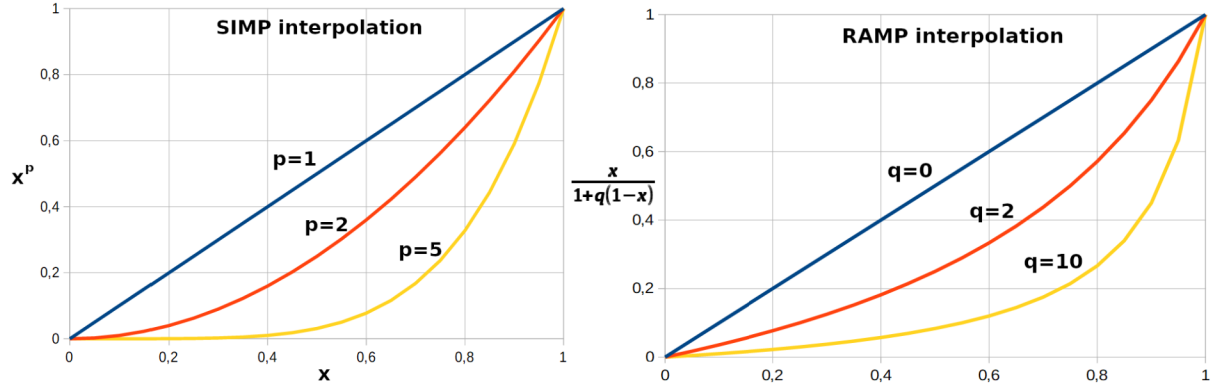
Figure 5: SIMP and RAMP interpolation.

Since minimal compliance (i.e. maximal stiffness) would be achieved when all elements are solid, another constraint is prescribed to limit volume summed over elements v_e

$$\sum_{e=1}^{N} v_e x_e^p \leq V \quad . \tag{11}$$

Derivative of the goal function (sensitivity) can be found analytically for the element e as

$$\frac{\partial f}{\partial x_e} = - p \, x_e^{p-1} \boldsymbol{u}^T \boldsymbol{K_0} \boldsymbol{u} \tag{12}$$

Sensitivity is usually filtered to suppress so called checkerboard effect where neighboring elements are alternately solid and void in the pattern. Than some of the optimization method is used, e.g., optimal criterion method, SLP (Sequential Linear Programming), or often MMA (Method of Moving Asymptotes) [40]. Schema of the implementation is in Figure 6.
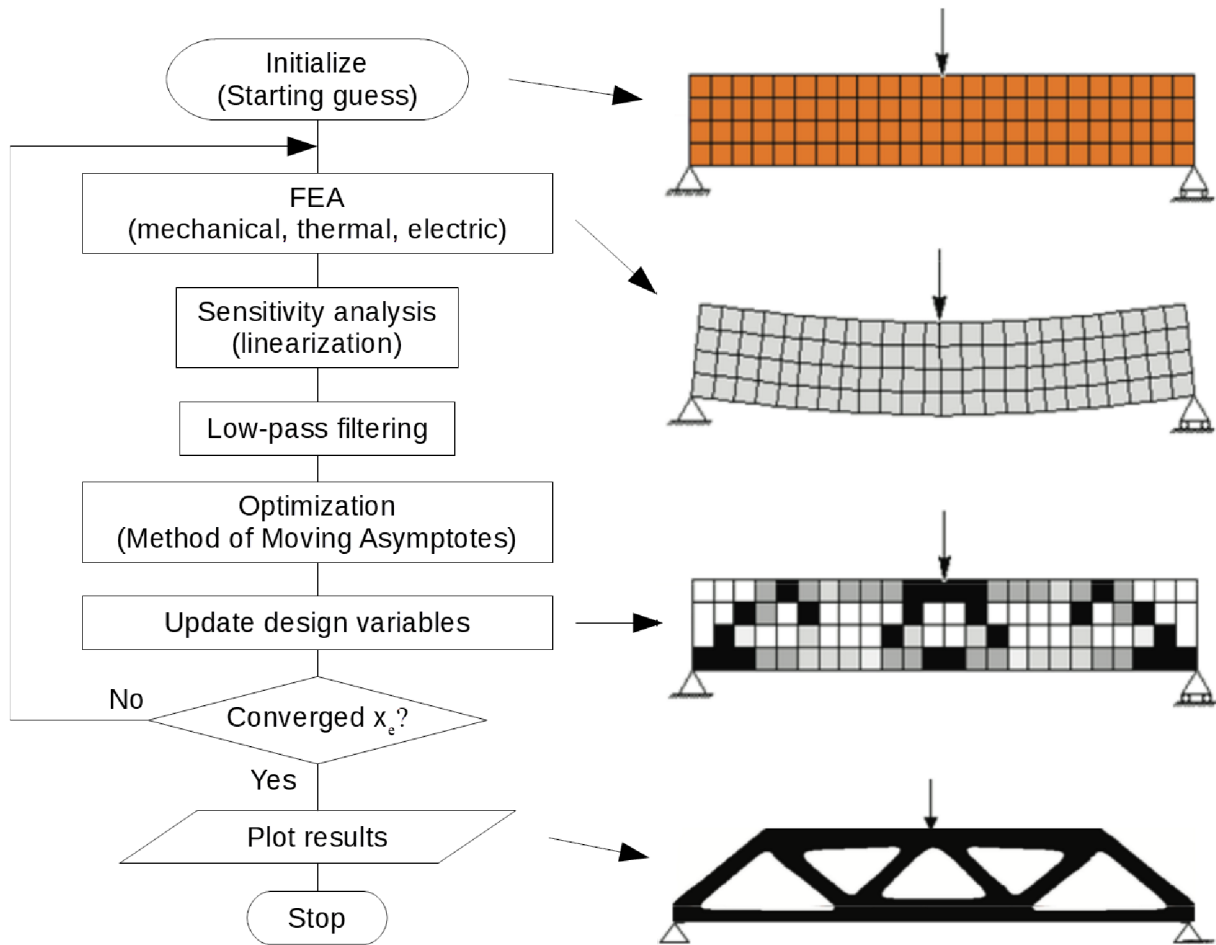
Figure 6: Schema of the SIMP method [71].

Multi-material interpolation

When multi-material topology optimization is carried out, interpolation contains weighted sum of stiffness matrices

$$\boldsymbol{K} = \sum_{i=1}^{n_M} w_i \boldsymbol{K_i} \quad , \tag{13}$$

where the weight coefficient can be defined in more ways, e.g.,

$$w_i = x_i^p \prod_{j=1}^{n_M} \left(1 - x_{j \neq i}^p\right) \tag{14}$$

and the term in parentheses binds i-th material variable x_i with other material variables x_j.

RAMP interpolation

Rational Approximation of Material Properties (RAMP) interpolation is another scheme which was suggested by Stolpe and Svanberg [41] to replace SIMP interpolation from equation (8) in the form

$$K_e = \frac{x_e}{1+q(1-x_e)} K_0 \quad , \tag{15}$$

where q is penalization parameter causing similar effect as p in SIMP scheme (Figure 5). Numerical advantage of RAMP scheme is nonzero value and nonzero gradient at point $x_e=0$, which prevents instability in frequency analysis.

Stress constraints and constraint aggregation

Two difficulties were reported when applying stress constraints in topology optimization. First, when the element variable vanishes, the stress constraint is singular since the compliant element has large strain. Cheng and Guo [42] applied so-called ε-relaxation in the solution of truss structures, which prevents the stress singularity in void elements. Similar approach was later used by Duysinx and Sigmund [43] on continuous structures. Alternative to the ε-relaxation was investigated by Bruggi [44] who achieved a similar effect by use of different SIMP penalization of the stress and stiffness.

Second, difficulty with stress constraints is due to the large number of elements in topology optimization. Prescribing stress constraints on each element would be prohibitive, so most of the studies use aggregation by one of the following functions, where only one or several constraints are passed to the optimizer. P-norm used by Duysinx and Sigmund [43] is

$$\sigma_{PN} = \left(\frac{1}{n} \sum_i^n \left(\frac{\sigma_i}{\sigma_{limit}} \right)^p \right)^{1/p} \quad , \tag{16}$$

where n is number of constraints (elements), the higher power p is, the closer σ_{PN} is to the maximum stress value, but too high p can decrease numerical stability.

Other option is KS function [45]

$$KS = \max_i g_i + \frac{1}{\rho_{KS}} \ln \left(\sum_j^n \exp \left[\rho_{KS} \left(g_j - \max_i g_i \right) \right] \right) \quad , \tag{17}$$

where g is constraint function, the higher coefficient ρ_{KS} the closer KS function is to the maximum constraint, but too high ρ_{KS} can decrease numerical stability. Maximum terms in the formula should prevent data type overflow due to exponential function.

An overview of various approaches to mass minimization with stress constraints was given by Le et al. [46]. Other aggregation functions are possible as were suggested by Kennedy and Hicken [47]. When many local constraints are aggregated to one constraint, it leads inevitably to decrease in the precision of original ones. Logically, there were attempts [48, 49] to aggregate not to one but to a set of constraints by clustering constraints according to stress level, element proximity, or physical meaning to find a good compromise between calculation demands and precision.

There was also a study by Kennedy [50] which avoided the need of constraint aggregation by using full-space barrier method which was able to solve the task efficiently with a large number of stress constraints.

2.2.1.4   *Composite optimization with DMO method*

Stegmann and Lund [18] applied topology optimization approach to the layer composite to minimize compliance and in the second paper [20] to maximize the lowest eigenfrequency. Material interpolation from equation (14) was used in the form for the constitutive matrix of the layer so that layer stiffness matrix would be

$$Q = \sum_{i=1}^{n_M} \left[x_i^p \prod_{j=1}^{n_M} \left(1 - x_{j \neq i}^p \right) \right] Q_i \quad , \tag{18}$$

where n_M is number of potential materials on the layer and x_i is the i-th material pseudo density (design variable), Q_i is the i-th material constitutive matrix. This interpolation scheme converges to one material with $x_i = 1$ and others close to 0, but during iteration sum of x_i on the layer is not 1, which means that this scheme needs to be modified in case of frequency minimization where the element mass matrix is to be interpolated as well. Scheme used by Lund and Stegmann [20] for this purpose is extended by the normalizing term

$$Q = \sum_{i=1}^{n_M} \left[\frac{1}{\sum_{k=1}^{n_M} w_k} x_i^p \prod_{j=1}^{n_M} \left(1 - x_{j \neq i}^p \right) \right] Q_i \quad , \tag{19}$$

but it was reported to converge slower. This approach is called DMO (Discrete Material Optimization) and can be used also for the variable material orientation if we consider each orientation as a new material variable. In the original form, DMO was used to minimize the compliance with variable materials and orientations, so that sensitivity analysis can be done in the same way as in the topology optimization, i.e. by the use of eq. (12). Later, Lund [22] modified the method also for buckling optimization.

Sohouli et al. [51] developed a Matlab composite optimization framework involving Abaqus solver. The main idea was to split DMO to two levels, where the first optimization was with material variables and constant orientations, the second level was with orientation variables and constant materials. Variables were then updated in the common model and the optimization ran again until convergence. Each of the optimizations has a lower number of variables and can run in parallel. The approach was called Decoupled Discrete Material Optimization (DDMO) and was described and tested on plate and beam examples minimizing compliance with mass (cost) and manufacturing constraints, preventing large orientation changes between adjacent patches. DDMO was reported to converge to better results than the original DMO.

Thickness variation

Original DMO has a fixed number of layers. Søren et al. [24] described DMO including thickness optimization by defining new density variable $\rho_{el} \in [0, 1]$ on each element e and its layer l. Using RAMP scheme on the layer, the interpolation equation (18) takes the form

$$Q = Q_0 + \frac{\rho_{el}}{1 + r(1 - \rho_{el})} \sum_{i=1}^{n_M} \frac{x_i}{1 + q(1 - x_i)} \Delta Q_i \quad , \tag{20}$$

where $\mathbf{Q_0}$ holds properties for void layer and $\mathbf{\Delta Q} = \mathbf{Q} - \mathbf{Q_0}$, r and q are penalization coefficients. Optimization was done to minimize compliance with constraints on total mass and density being lower in outer layers $\rho_{el} < \rho_e(l+1)$, and constraints limiting number of dropped layers in the same location and layer continuity. Authors tested several optimization schemes with Sequential Linear Programming. The approach was used for composite optimization without sandwich core. Subsequent paper Søren et al. [52] called the method Discrete Material and Thickness Optimization (DMTO). The method is modified for practical tasks to minimize mass constrained with buckling load factors, eigenfrequencies, displacements, and basic manufacturing constraints. Patches were applied to group elements and design domains for thickness variables and for material candidates were made independently. In the example (main spar of the wind turbine blade), the foam material candidate was included but its thickness was the same as of GFRP candidate and none sandwich constraints were applied. Dealing with face-sheet thickness was improved by Sørensen and Lund [53] where the thickness was controlled by one independent variable which drives the layer variables through the filtering function. Recent study by Sjølund et al. [26] improved DMTO for sandwiches with variable thickness core and face-sheets. They used the method to minimize the mass with displacement and buckling constraints.

2.2.2 Finite element analysis and optimization

Possibilities of optimization within large FEA programs are described on the example of MSC.Nastran according to its manual [54].

In Nastran, the concept of design variables, the goal function, and constraint functions are handled with an added layer of design properties (e.g., material property, element thickness, node coordinate) which can be directly (or through an equation) linked to design variables passed to the gradient optimizer. IPOPT [39] and MSCADS optimizers are implemented in MSC.Nastran. MSCADS is MSC derivative of the code developed originally for NASA by Vanderplaats [55] as ADS (Automated Design Synthesis). If not selected by the user, a specific gradient method is automatically chosen according to character of the task (number of variables, linear or nonlinear constraints, etc.). Another specific term is the design response which can be output from FE analysis (e.g., nodal displacement, stress, buckling factor as load case dependent or model mass as global response) or design responses calculated by user-defined equations from primary ones. Goal function is given by the value of one design response. Design constraints are imposed on the design responses. Nastran contains a large number of in-build formulas to calculate analytical sensitivities for various design responses, otherwise sensitivities are calculated by the finite difference method. Scheme of optimization is in Figure 7.

To decrease the number of full FE analysis, the optimizer iterates over the approximate model before updating the design properties in the original model used in the full FE analysis. To decrease size of the optimization task, design variables can be linked (which is in fact the

same as a patch design where several elements in the patch are driven by the same design variable), and constraints which are far from being violated are temporarily deleted. In this way, the optimizer works with an approximate model which is easier to evaluate, but precise enough in the given iteration.
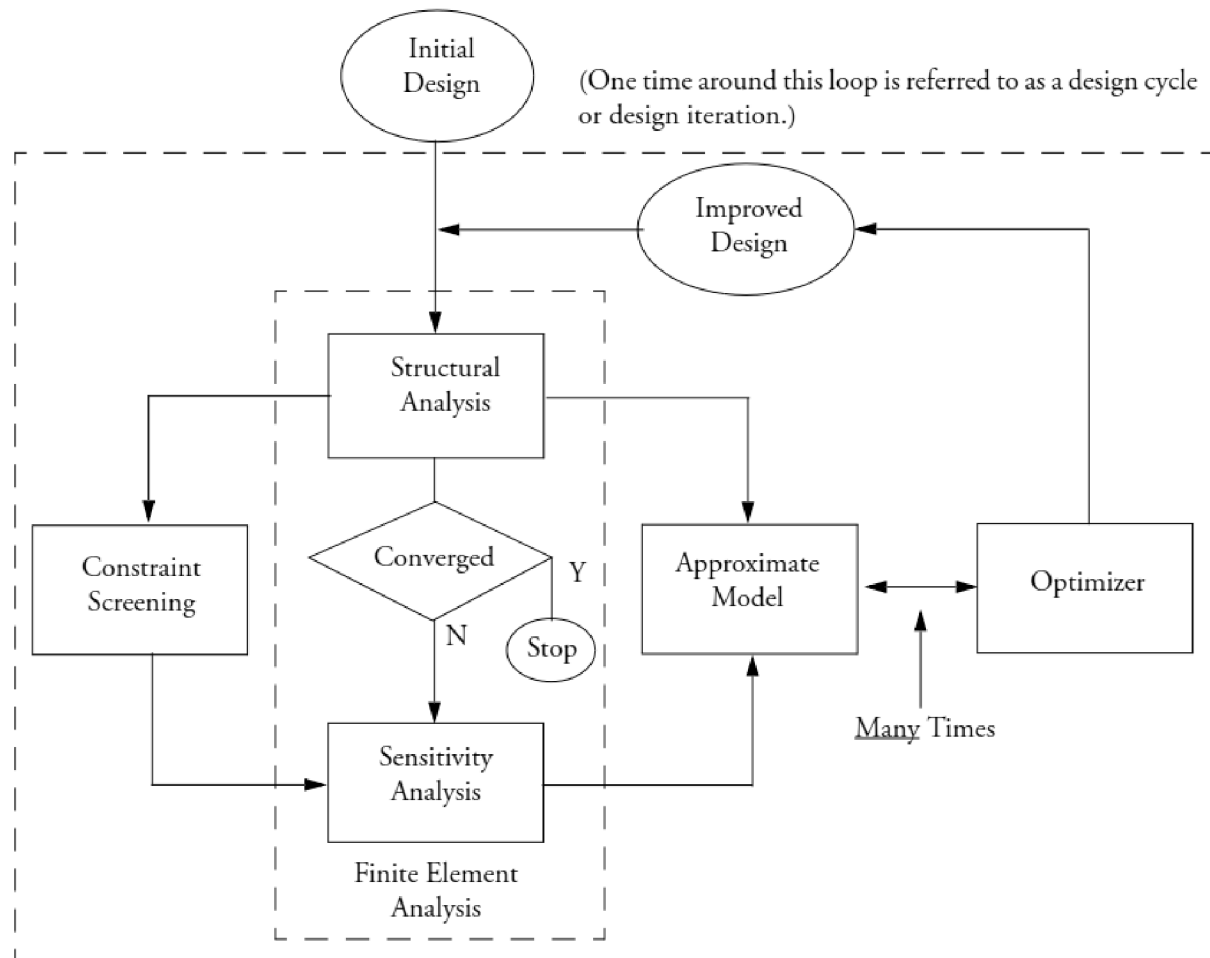
Figure 7: Scheme of the optimization in Nastran [54].

Zhou et al. [56] described three-phase process of composite optimization in OptiStruct, which is used in designing wing layup of airliners with high number of layers. Phases are shown in Figure 8:

1) Free-size optimization is used to find the concept design of material orientation and placement. Design variables are on thickness of so-called superplies (plies with a given orientation). Global responses are used in the goal function – compliance or key displacements. Manufacturing constraints at this stage involve the minimal and maximal percentage of the orientation and total laminate thickness.

2) Ply-bundle sizing optimization is used to split superplies to plies of a given orientation, real thickness, and a covering specific area. Additional constraints are applied on failures, buckling, and laminate behavior.

26

3) Detailed optimization of the plies contains other constraints on consecutive number of plies of the same orientation, pairing +/- angles, predefined covering layups, etc.
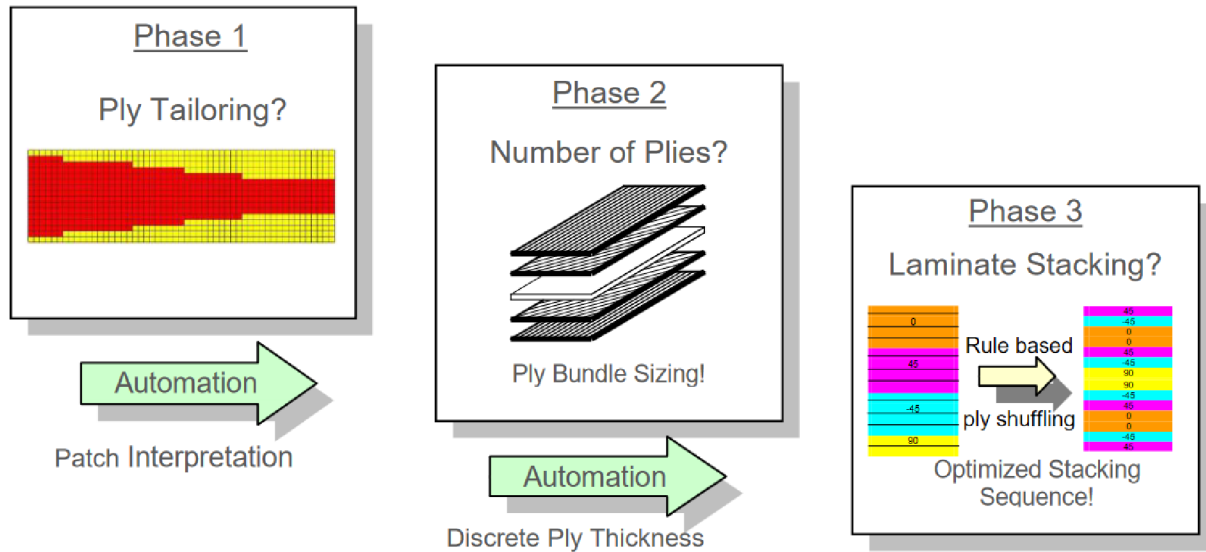
Figure 8: Phases of composite optimization in OptiStruct [56].

2.2.3 Analytical approaches to sandwich optimization

Due to the high number of variables and constraints, only relatively simple methods for sandwich beam optimization are described here.

Prescribed bending stiffness or beam strength

Kuenzi [57] and Theulen [58] describe the deduction of the formula for minimal mass with one prescribed parameter. When mass of glue is neglected, optimum for the fixed bending stiffness is for the core mass W_c being double times mass of both face-sheets together W_f

$$W_c = 2 W_f \ . \tag{21}$$

If maximum bending stress in the face-sheets is taken as a fixed parameter, than minimal sandwich mass is at

$$W_c = W_f \ . \tag{22}$$

Provided that core elastic properties are proportional to the face-sheet properties in ratio of their densities, minimum mass limited by wrinkling will be in the same case as with fixed bending strength, i.e. $W_c = W_f$. In case of dimpling instead of wrinkling limit, similar method leads to $W_f = 3 W_c$.

Prescribed beam deformation or strength

For practical purposes, total stiffness (bending and shear, not only the shear stiffness as in the previous paragraph) is more interesting and load capacity is not limited only by bending stress. Zenkert [3] summarized a method to find optimal sandwich beam with given boundary conditions and prescribed materials.

Let's have a prescribed beam deflection and variable thickness of the core and of face-sheet (same for top and bottom). Face-sheet thickness can be expressed from the equation of the beam deflection and inserted to the goal function (sandwich mass)

$$W \approx \rho_c d + 2 \rho_f t_f \quad , \tag{23}$$

where ρ_c, ρ_f are core and face-sheet densities, t_f is face-sheet thickness, d is distance between face-sheet centers which is roughly thickness of the core. Optimal thicknesses can be found by a graphical solution of the equation $\dfrac{\partial W}{\partial d} = 0$ and back substitution. If the variable is core density and if it is possible to describe core shear module G_c with a relation of the constant C_G and exponent n

$$G_c = C_G \rho_c^n \quad , \tag{24}$$

then thicknesses d, t_f, and core density ρ_c can be found by partial derivation of the mass equation with deflection equation.

When n = 1, optimum directs to increasing core thickness, decreasing core density, and thinning face-sheets, so that real choice would be limited by maximal allowable sandwich thickness and corresponding t_f and ρ_c. For n = 2 (foams) solution gives specific values of the design variables.

Repeating same approach with substitution of some failure condition instead of deflection equation into the goal function, it is possible to calculate optimum for each failure separately and pick the lowest possible design variable values. Optimality criterion is often assumed to be at a design point where all failure combinations occur together. With this condition, it is possible to express each design variable from different failure criteria and substitute them to the goal function, for example, the combination of the core shear failure with face-sheet yielding or wrinkling is possible to use.

2.2.4 Numerical sandwich optimization

Since analytical methods are limited to examples which can be explicitly expressed and differentiated, numerical optimization is often easier for more complex geometries or parametrization. Various design parameters can be optimized, e.g., core material (density), orientation and thickness, wall thickness and cell size of hexagonal core or angle of corrugated core; number of layers and stacking sequence when laminated face-sheets are used. The following examples are related to optimization on the global level (selecting materials, thicknesses, and stacking sequence).

Wind turbine blades

Sjølund and Lund [59] used DMO in wind turbine blade design. Regarding the task scale (~28000 solid-shell elements) and a set of constrains on buckling, displacement, failure indices, and manufacturing, the authors decided to optimize only the thicknesses (laminate or laminated face-sheets and core thickness) of predefined ply groups with constant properties. Initial state was defined as conventional layup. High number of stress constraints (~1000000)

was reduced (to 353) by P-norm functions used on patches. Authors used the internal design optimization tool MUST (MUltidisciplinary Synthesis Tool) with Sequential linear programming and semianalytical gradients. Recently, Sjølund et al. [26] applied DMTO to sandwich optimization with variable core thickness and face-sheets with displacement and buckling constraints.

Blending design

Soremekun [60] used composite optimization denoted as blending design, where neighboring panels are pressed to share bottom composite layers so that layers do not need to be disrupted on the common boundaries during manufacturing. As an example, GA were used to optimize 3×3 sandwich panels with evaluation of panel buckling, face-sheet strength, wrinkling, and dimpling failures. In the first step, layup of each panel was designed separately. In the second step, layer linking between panels were optimized with change of the layer number and orientation (0°, 45°, 90°). The goal function f(x) was modified by additional term penalizing unsuitable solutions by β coefficient or advantaging solutions which fulfilled technological constraints by coefficient ε

$$f(\boldsymbol{x}) = \sum_{i=1}^{n_p} \begin{cases} f_i + \beta\, g_{min}^i & if\ g_{min}^i < 0 \\ f_i + \varepsilon\, g_{min}^i & otherwise \end{cases} \quad , \tag{25}$$

where g_{min}^i is a constraint of the i-th panel of total panel number n_p. The final variant was only by 2.5% heavier than optimum without technological constraints.

Composite car body

By the use of current software packages, it is possible to use optimization problems complexly. Velea et al. [28] described multicriteria optimization of the small car body. Multi-criteria optimization enables to reach convenient parameters not only from the mass point of view but also safety and driving properties which were quantified by torsional stiffness in the longitudinal direction, stiffness during front impact, and a few other cases.

First, the free size optimization was solved as one criterion optimization (mass minimization) with defined minimal and maximal layer thicknesses (glass fabric, PUR core, glass fabric) to find load paths as can be seen in Figure 9 where the foam core thickness is displayed. Thicknesses of other layers were found in the same way.
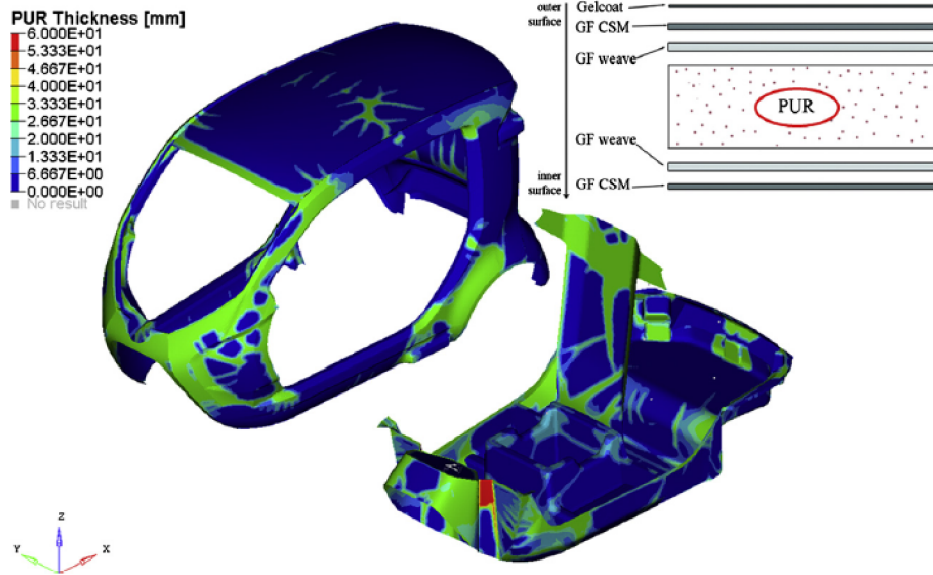
Figure 9: Foam core thickness distribution after the free size optimization [28].

Second, size optimization was carried out. Based on the technological possibilities, surfaces to contain different cores were defined manually (well-shaped PUR, stronger PVC, honeycomb to prevent buckling). In this step, 7 criteria were evaluated by weighting coefficients, 42 sections were defined manually (each with constant layer thicknesses), and thicknesses were sought on them. In total, more than 5000 design points were evaluated. Final variant was selected according to minimum of the cost function made of weighted contributions of prescribed criteria.

2.3 Summary of review

The review focused on sandwich design and optimization. State of the art in this broad field can be summarized to:

1) Traditional approach to sandwich design covered in (hand)books describes the analytic design of sandwich beams and plates, so it is limited to basic geometry and boundary conditions.

2) Practical tasks are typically solved with FE models of various detail. Structures are often optimized by repeated manual modifications of layup and evaluation of design requirements.

3) Non-gradient methods (especially genetic algorithms) are used in sandwich optimization as a subtopic of optimization of fiber-reinforced composites. Such methods can reach a robust solution (close to the global optimum), but their computational demands quickly arise with the number of variables when FE model needs to be involved.

4) Optimization of some simple tasks is possible through basic optimization methods, but tasks of real complexity are designed in several phases, which can combine several types of optimization tools and manual modifications to cover all requirements from conceptual design to manufacturing.

5) In 2014, Discrete Material Optimization (DMO) was introduced. DMO is gradient method and it has been used for fixed and later variable thickness composite optimization. Goal function and constraints consist of responses on compliance, mass, natural frequency, composite failures, manufacturing rules, but not specific sandwich failures such as wrinkling and crimping.

3   Thesis objective

The goal of the thesis is to implement an automated optimization algorithm to improve the design process of sandwich structures regarding stress and load capacity. Attention should be paid to the structures with relatively low number of plies with the ability to solve tasks with geometry and loads more complicated than classical panels, which can be designed by the existing analytical approaches. Examples of the structures of interest are light aircraft fuselages or airliner interior components. The implementation should contribute to the quality of the designed structure and shorten the time needed for designing a new product. Used methods should be programmed and the workflow should be validated by comparison of theoretical and practical examples. Focus of the work is illustrated in Table 3.1.

Table 3.1: Thesis objective reasoning.

Sandwich design characteristics	Potential improvements
Simple sandwich panels with uniform loads and structures, which can be split to them, can be sequentially designed by the existing approaches working with separated panels.	Sandwich design of the whole structure considering nonuniform load, potentially with complicated geometry where FEM is needed.
Details (like inserts, sandwich endings), especially in the case of sandwiches with few layers, are designed according to the technological possibilities and standard processes of the manufacturer.	Put attention rather to global characteristics (number and orientation of the layers, core material, and thickness) than details.
Trend in design methodologies is to use automated optimization from the beginning according to loads, boundary conditions, and design constraints (including manufacturing) rather than cyclical intuitive design with sequential stress analysis. In the case of topology optimization with isotropic material, terms like "Design by load" or "Design for manufacturing" are used in the simulation software marketing.	Focus on the initial design phase of the layup where optimization has the biggest impact.
	Minimize design cycles where repetitive human work is needed.
Optimal results might be hard to implement in the industry.	Consider manufacturing constraints.
Need for validation.	Comparison with "optimal" results of simple examples or studies from the literature. If possible, cooperate with the industry to design a product which will be experimentally tested.

Although gradient methods contain an inherent risk of trapping in the local minimum or infeasible design, this can be partially diminished by convenient penalization. Gradient

optimization also requires continuous variables to determine derivatives. Contrary, the sandwich design contains rather discrete variables (number of laminated face-sheet layers, available core materials, etc.), which requires to be transformed to continuous ones and forced to converge to discrete values or to be rounded, as performed in a classical topology optimization on solid-void material. Provided that gradients can be efficiently evaluated, this approach can efficiently reach the local optimum even with a large number of design variables.

The thesis focuses on the core functionality of the sandwich optimization regarding sandwich failure constrains. The scope of the scientific work is specified in these aims:

1) Implement gradient optimization of the sandwich structures based on DMO connected to FE model with general geometry.

    a) Minimize mass of the structure

    b) Include constrains on sandwich failures

    c) Consider manufacturing constraints

2) Demonstrate convergence to the optimum by simple examples

3) Demonstrate the application to the practical design task.

4 Methods

The basic idea is to apply the principles of topology optimization to sandwich structures. Topology optimization uses typically gradient methods, which can be efficiently used when discrete variables are represented by penalized continuous variables. This means that the key question is to transform the original discrete problem (composite layup) to the continuous problem, which converges to the discrete solution due to convenient penalization. Such approach is described in chapter 4.1 Optimization approach. Section 4.1.6 Failure constraints develops composite and specific sandwich failure constraints in the form which fits to the model with interpolated materials. Chapter 4.2 Software implementation describes application of the mathematical model in the Python program, connection with FEA solver, connection of the robust mathematical optimizer, and several heuristic features, which diminishes the difficulties which appeared during algorithm testing and which increases the scope of the tasks on which the program can be used. Finally, chapter 4.3 User workflow introduces how the program can be used.

4.1 Optimization approach

4.1.1 Problem formulation

The first step is to define the goal function, constraints and design variables. General goal is the overall costs of the component, including manufacturing, operation, service, and disposal. This is, however, a vague term, because overall costs can be only estimated in relation to a specific product, based on the situation on the market and experience with similar products, which means that cost estimation is an important but also a difficult step in product development and that it needs to be done by an informed engineer or a development team. In the aircraft industry, a crucial cost factor is the mass which needs to be carried on by an aircraft, so that mass minimization is typical goal of the optimization and it can be used in a wide range of applications. From the implementation point of view, the advantage is that it can be clearly defined and analytically differentiated.

The structure will be represented by the FE model, where each element can obtain an independent design layup. Unknown orientations and materials of the face-sheet and the core are parameterized by one variable for each material, which includes specific orientation and thickness by the concept of DMO. Such an approach is reasonable when there is a short list of predefined materials, orientations and core thicknesses, which is the common case for manufacturers who keep a limited number of stock items. Use of multiple material variables per each element requires a constraint on their sum to satisfy the physical meaning of having one mixed material in the layer. The number of composite layers in the face-sheet is controlled by the face-sheet thickness variable, so that the layers from outside have diminished stiffness as void elements in classical topology optimization independently on their material variable.

Failure constraints follow common sandwich failures. Features improving manufacturability are discussed in the program implementation. Optimization problem can be mathematically formulated as

$$
\begin{aligned}
& \min M(\boldsymbol{x}) \\
& \quad 0 \leq x_{ijk} \leq 1 \quad \text{material variables} \\
& \quad \frac{0.99}{n_L} \leq x_{Tk} \leq 1 \quad \text{face-sheet thickness variables} \\
& \quad \sum_{i}^{n_{MC}, n_{MF}} x_{ijk} = 1 \quad \text{at each element layer} \qquad , \\
& \quad FI_\sigma < 1 \quad \text{face-sheet stress} \\
& \quad FI_\tau < 1 \quad \text{core shear} \\
& \quad FI_{cr} < 1 \quad \text{crimping} \\
& \quad FI_{wr} < 1 \quad \text{wrinkling}
\end{aligned}
\tag{26}
$$

where the material variables x_{ijk} can be between 0 (not used) and 1 (used) as in topology optimization. Indices denote i-th material candidate, j-th layer, k-th element (or patch). In the meaning of this work, term "material" includes also orientation and thickness so that orientation and layer thickness are dependent parameters, not directly design variables. Face sheet thickness variables x_T have lower bound on relative thickness of one layer $1/n_L$ (considering n_L as number of layers and for numerical reasons used as $0.99/n_L$), which denotes that face-sheet contains at least one layer. Sum of n_{MC} core material candidates (n_{MF} face material candidates) on the layer must be 1 to fulfill physical meaning. Failure constraints are nonlinear and are prescribed on face-sheet stresses, core shear, element crimping, and wrinkling of each face-sheet. Vector notation means that they are calculated on each layer as will be explained later.

4.1.2 Goal function

The goal function is a mass of the structure penalized in material density

$$
M(\boldsymbol{x}) = \sum_{k}^{n_E} A_k \sum_{j}^{n_L} t_{Mjk}(\boldsymbol{x}) \rho_{Mjk}(\boldsymbol{x}) \quad ,
\tag{27}
$$

where n_E is the total number of finite elements, A_k is element area, t_{Mjk} is j-th layer thickness interpolated linearly

$$
t_{Mjk} = \sum_{i}^{n_{MC}, n_{MF}} x_{ijk} t_i \quad .
\tag{28}
$$

RAMP interpolation

ρ_{Mjk} is a density interpolated with penalization as

$$\rho_{Mjk} = \begin{cases} \rho_{Ljk}(x_{Tk}) \displaystyle\sum_i^{n_{MF}} \dfrac{x_{ijk}}{1+q(1-x_{ijk})} \rho_i & \text{for face-sheet} \\[2em] \displaystyle\sum_i^{n_{MC}} \dfrac{x_{ijk}}{1+q(1-x_{ijk})} \rho_i & \text{for core} \end{cases} , \tag{29}$$

where ρ_{Ljk} is the layer density and will be explained later, ρ_i is the density of i-th material (in physical meaning, so that it determines a cost of the material per volume). A fraction in the sum is RAMP interpolation. In topology optimization, interpolation is used with $q > 0$ to decrease intermediate element stiffness as shown in Figure 5. In this thesis, mass is penalized with coefficient selected as $-1 < q < 0$, so the intermediate material has higher mass. Figure 10 shows the case for two candidate materials with variables x_1 and x_2. Blue and red curves denote the mass contribution of each material component related to x axis, which is drawn as a portion of the first material (red) $x_1 = x$, and for the second material (blue) $x_2 = 1 - x$. After the summation, the intermediate values are larger value so that gradient directs the minimization towards the clear first material or clear second material. The graph also demonstrates why the starting point for design variables (x_1, x_2) is chosen to be in the middle, i.e., uniform distribution of the candidate materials $(x_1 = x_2 = 0.5)$, otherwise the optimization would be biased and it might be difficult to overcome the gradient which is steep when the actual design point is close to discrete values. Interpolation in the figure is drawn for $q = -0.7$, which proved to be a robust value in the test examples.

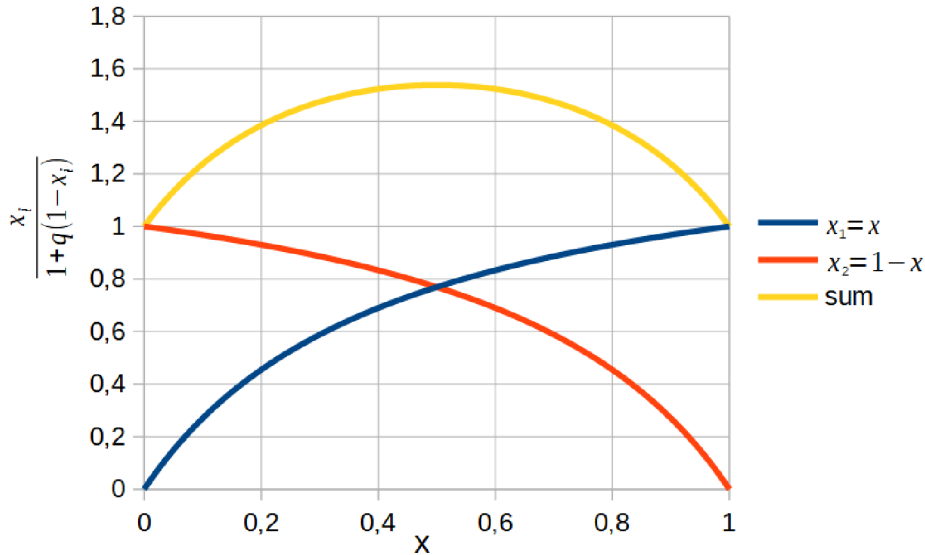*Figure 10: Penalization term for two material candidates with same densities and for q = -0.7 [68].*

If we consider the same (physical) densities of both materials, Figure 36 represents the shape of the layer density defined in eq. (29). In practical cases, materials can differ in density: Glass/epoxy composite density is 1.19 times higher than the carbon/epoxy composite

(considering V_f = 0.35); the candidate core materials can differ much more in density and so this case is demonstrated in Figure 11, where the second material has density 2 times larger than the first. The starting point will be still in the middle (x_1 = x_2 = 0.5), so that the goal function gradient will direct towards the lighter material, unless it is pressed by failure constraints over the top of the curve to finally fall on the side of the heavier material.
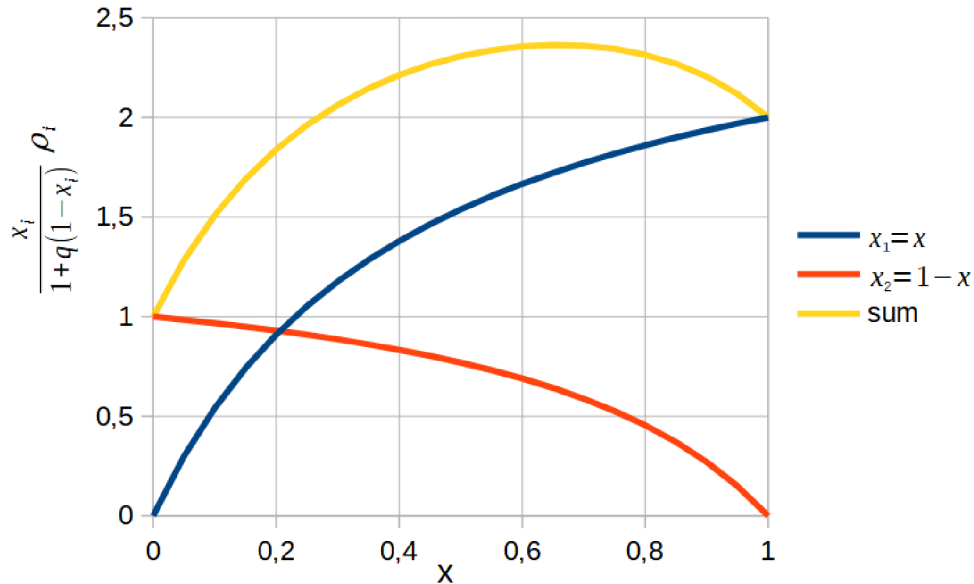

Figure 11: Density penalization for two material candidates where one has density $\rho_1 = 1$, second material $\rho_2 = 2$; for q = -0.7.

The situation with more material candidates is analogous and more difficult to display, but three materials can be still drawn on a paper, as shown in Figure 12. The base of the drawing is a triangle. Material variables are distributed in the way that each corner is occupied by one material variable. There is a proportional combination of the materials inside of the triangle with equations for x_1, x_2, and x_3 dependent in x and y position on the paper. Colored triangle shows RAMP interpolation of these three materials. We can see high values in the middle of the triangle where the materials mix. Middles of the triangle edges mix only two materials (the third is zero) and so corresponds to the previously explained case of two materials. Corners have the lowest interpolation value so that the goal function optimization will direct towards the corners with just one material. Starting point of the optimization will be set to the triangle center (x_1 = x_2 = x_2 = 0.333). The drawing is for the case where all materials have the same density. One can note that in this specific case the goal function gradient is 0 and so the optimization might stay with mixed variables. It can theoretically happen but is unlikely, since in a practical case, the number of face-sheet layers will decrease due to the thickness variable gradient and so some constraint (which is also penalized) will become violated and causes the variables to move towards one of the materials.

If the materials will have different densities. Figure 12 will slightly change so that the highest point of the interpolation value (including material density) will move towards the heaviest material, so that the starting point in the middle of the triangle will slightly help moving towards the lighter material(s).

Variables

$$x_1 = 1 - x - \frac{y}{\sqrt{3}} \qquad x_2 = x - \frac{y}{\sqrt{3}} \qquad x_3 = \frac{2y}{\sqrt{3}}$$
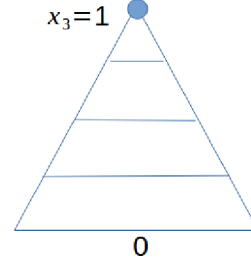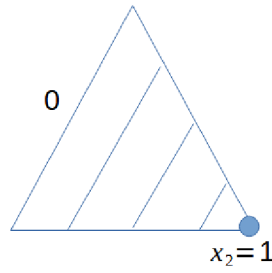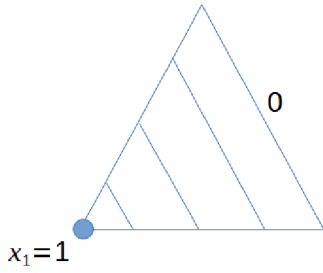
Interpolation

$$\sum \frac{x_i}{1+q(1-x_i)} = \frac{x_1}{1+q(1-x_1)} + \frac{x_2}{1+q(1-x_2)} + \frac{x_3}{1+q(1-x_3)}$$
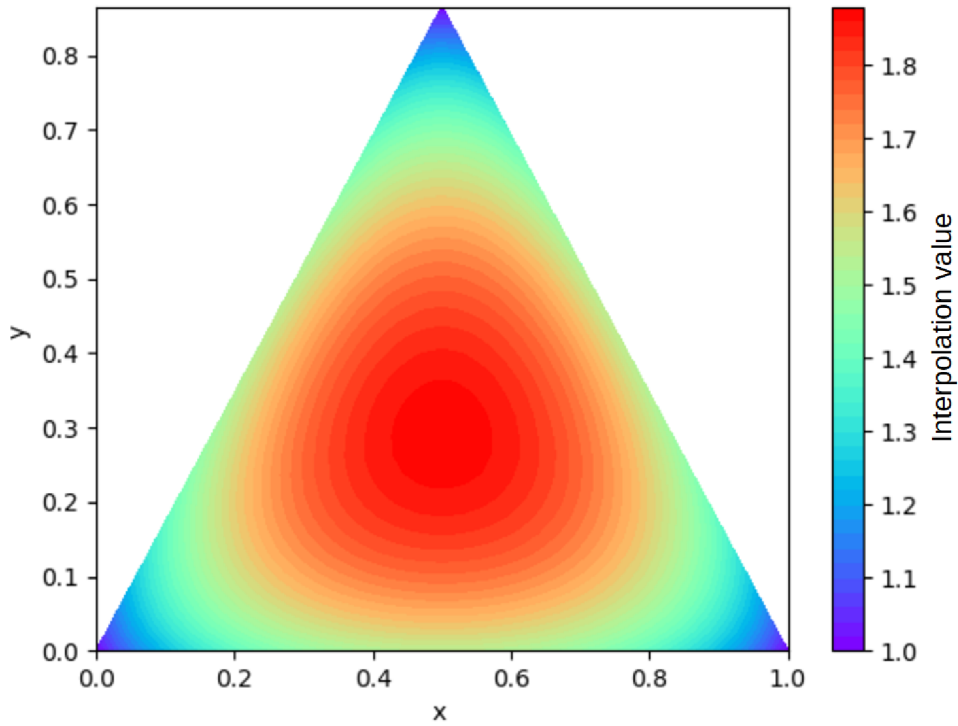
Figure 12: Interpolation value for 3 candidate materials with same density.

Layer density ρ_{Ljk}

Layer density $\rho_{Ljk} \in \langle 0,1 \rangle$ in eq. (29) serves as a coefficient determining how much the j-th layer on k-th element is active. ρ_{Ljk} is defined by the S shape function (also called logistic function) dependent on the thickness variable x_{Tk}. Its shape is drawn in Figure 13, where c = 0.5 marks center of the curve on x axis, k controls the steepness. This function will determine the density of the given layer.

$$\frac{1}{1+\exp[k(c-x)]}$$
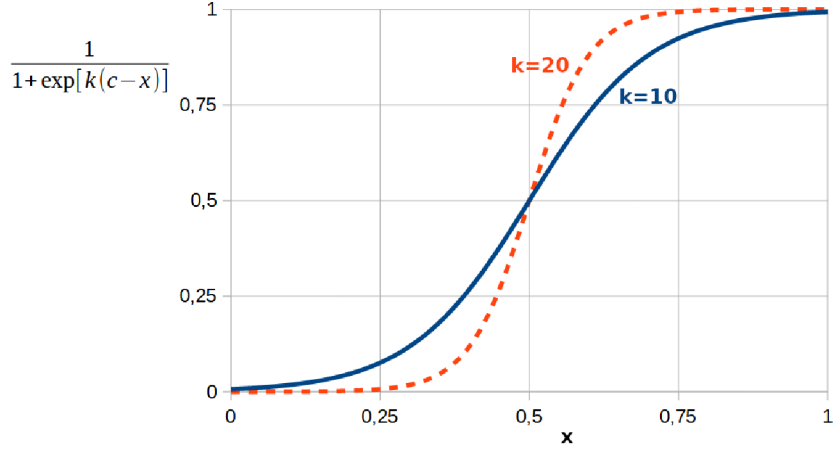
Figure 13: Example of S shape function with center at c = 0.5.

The S shape function for each j-th layer is in the form

$$\rho_{Ljk} = \frac{1}{1+\exp\left[k\left(x_{Ljk}-x_{Tk}\right)\right]} \quad , x_{Ljk} = \frac{j-1}{n_L} \quad , j=1,2,\ldots,n_L \quad , \tag{30}$$

where x_{Ljk} is the position of the beginning of the j-th layer measured from the core to the outer face-sheet surface; it is constant during the optimization and does not depend on the thickness of the material but only on the relative position from the core. Face-sheet thickness variable x_{Tk} is measured in the same way. Value of the steepness coefficient

$$k = 2n_L \ln(19) \tag{31}$$

was derived from equation (30) substituting ρ_{Ljk} = 0.05, and $\left(x_{Ljk}-x_{Tk}\right) = \dfrac{1}{2n_L}$, which means

that layer density changes from 0.05 to 0.95 within the length of relative layer thickness. Densities are shown in Figure 14 for face-sheet with three layers. Curves for x_{Lj} = 0. 0.333, 0.666 are for densities of first, second, and third layer, their sum corresponds to the shape of the goal function as it dependents on x_T.

If k is high, graph resembles stairs, so that x_T being within the span of the layer counts almost all its density, which is useful when the optimization is close to finish (reaching discrete results). Waves are supposed to favor positions with lower gradient, i.e. in the middle of the physical layer instead of in the region with large gradient where physical layers touches, so that rounding x_T to obtain discrete number of layers in the face-sheet will be clearer. However, sliding over more layers would cause large changes of the gradient (specifically $\dfrac{\partial M}{\partial x_T}$)

which is proportional to waviness of the red sum curve in Figure 14. Contrary, if k is lower, the curves (and the gradient) are smoother, which help the optimizer to change x_T easily, but it causes overlaps of the layer densities, which is not convenient for the final rounding since it would change the results significantly. The practical approach is to start with lower k and increase it during the optimization. If it is not written otherwise, k is set to linearly change from $n_L\ln(19)$ to $2.2n_L\ln(19)$ in the thesis since it proved as a robust setting for various examples.
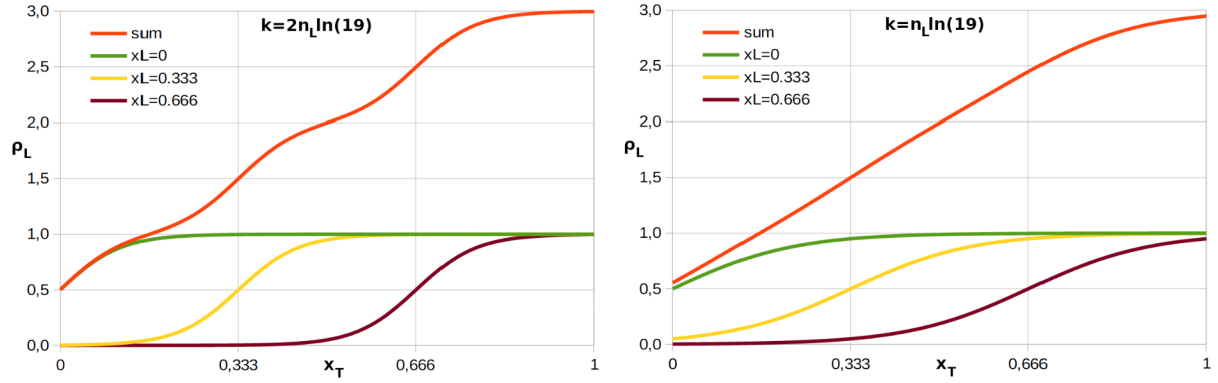
Figure 14: Layer densities of the face-sheet with three layers used in the goal function. Right graph is for k two times lower[68].

4.1.3 Goal function derivatives

The goal function in equation (27) and its members were defined to be smooth. Their partial derivatives can be analytically derived and efficiently evaluated during the optimization.

The derivative by the face-sheet thickness variable is:

$$\frac{\partial M}{\partial x_{Tk}} = A_k \sum_j^{n_L} t_{Mjk} \frac{\partial \rho_{Mjk}}{\partial x_{Tk}} \quad , \tag{32}$$

where on the j-th layer

$$\frac{\partial \rho_{Mjk}}{\partial x_{Tk}} = \frac{\partial \rho_{Ljk}}{\partial x_{Tk}} \sum_i^{n_{MF}} \frac{x_{ijk}}{1 + q(1 - x_{ijk})} \rho_i \tag{33}$$

and

$$\frac{\partial \rho_{Ljk}}{\partial x_{Tk}} = \frac{k \ \exp[k(x_{Ljk} - x_{Tk})]}{\{1 + \exp[k(x_{Ljk} - x_{Tk})]\}^2} \quad . \tag{34}$$

The derivative by the material variable is:

$$\frac{\partial M}{\partial x_{ijk}} = A_k \left(\frac{\partial t_{Mjk}}{\partial x_{ijk}} \rho_{Mjk} + t_{Mjk} \frac{\partial \rho_{Mjk}}{\partial x_{ijk}} \right) \quad , \tag{35}$$

where

$$\frac{\partial t_{Mjk}}{\partial x_{ijk}} = t_i \tag{36}$$

thanks to linear interpolation and for the face-sheet

$$\frac{\partial \rho_{Mjk}}{\partial x_{ijk}} = \rho_{Ljk} \frac{q+1}{(q x_{ijk} - q - 1)^2} \rho_i \quad , \tag{37}$$

40

or without ρ_{Ljk} for the core

$$\frac{\partial \rho_{Mjk}}{\partial x_{ijk}} = \frac{q+1}{\left(q\,x_{ijk}-q-1\right)^2} \quad. \tag{38}$$

After rearrangement, derivatives can be written as the following formulas: derivative by the face-sheet thickness variable is

$$\frac{\partial M}{\partial x_{Tk}} = A_k \sum_j^{n_L} t_{Mjk} \frac{k\ \exp\left[k\left(x_{Ljk}-x_{Tk}\right)\right]}{\left\{1+\exp\left[k\left(x_{Ljk}-x_{Tk}\right)\right]\right\}^2} \sum_i^{n_{MF}} \frac{x_{ijk}}{1+q\left(1-x_{ijk}\right)}\rho_i \quad,$$
$$x_{Ljk}=\frac{j-1}{n_L} \quad, j=1,2,...,n_L \tag{39}$$

derivative by the face sheet material variable is

$$\frac{\partial M}{\partial x_{ijk}} = A_k \left(t_i \rho_{Mjk}+t_{Mjk}\rho_{Ljk}\frac{q+1}{\left(q\,x_{ijk}-q-1\right)^2}\rho_i \right) \quad, \tag{40}$$

derivative by the core material is the same formula with dropped ρ_{Ljk}.

In the practical design, symmetry of the face-sheets is often used (top and bottom face-sheets have same layup), so that optimization can work only with variables on the bottom face-sheet and top face-sheet is mirrored. In this case, equation (40) should be multiplied by 2 for the face-sheet.

Second practical feature is patch design, when more elements share the layups and driven by same design variables. In this case, A_k in equations (39) and (40) is area of the patch instead of separate element area.

4.1.4 Stiffness and thickness interpolation

Layers stiffness matrix

The layer stiffness matrix is linearly interpolated as:

$$\bar{\boldsymbol{Q}}_{jk} = \sum_i^{n_{MC},n_{MF}} x_{ijk}\bar{\boldsymbol{Q}}_i \quad, \tag{41}$$

where $\bar{\boldsymbol{Q}}_i$ is the stiffness matrix of i-th material candidate in the finite element coordinate system according to FSDT described in appendix 9.1, so the interpolation is done in common coordinate system. Note that $\bar{\boldsymbol{Q}}_{jk}$ does not depend on the layer thickness nor face-sheet thickness variable x_{Tk}.

Layer thickness

The layer thickness is linearly interpolated as in the goal function, but it includes the layer density $\bar{\rho}_{Ljk}$ which is modified from the one in densities inside the goal function. The layer thickness is defined as:

$$t_{jk}=\begin{cases}\bar{\rho}_{Ljk}\sum_{i}^{n_{MF}}x_{ijk}t_i & \text{for face-sheet}\\[2em]\sum_{i}^{n_{MC}}x_{ijk}t_i & \text{for core}\end{cases}\qquad .$$ (42)

The layer density $\bar{\rho}_{Ljk}(x_T)$ includes dependency on the face-sheet thickness, i.e., if the layer is active or not, which needs to be controlled by the thickness rather than stiffness matrix $\bar{\boldsymbol{Q}}_{jk}$. Figure 15 shows the initial thickness of the face-sheet when $x_T = 1$. When x_T decreases during the optimization, the outer layers are "squeezed" in thickness, so that the outermost layers are very thin, but not having thickness 0, so that their derivatives can still be evaluated during the optimization. At the end of the optimization, the thickness x_T is rounded upwards and rounded thicknesses correspond to discrete values of the candidate materials. The "squeezing" of thicknesses and keeping original stiffness matrix $\bar{\boldsymbol{Q}}_{jk}$ is important in a wrinkling evaluation, where a quadratic moment of the face-sheet to its own neutral plane is needed. Note that the use of fixed layer thickness and penalized stiffness matrix is an intuitive application of the topology optimization principle, which would be equivalent for the in-plane stiffness, but would not work properly for bending stiffness due to the quadratic dependency on the cross-sectional thickness.
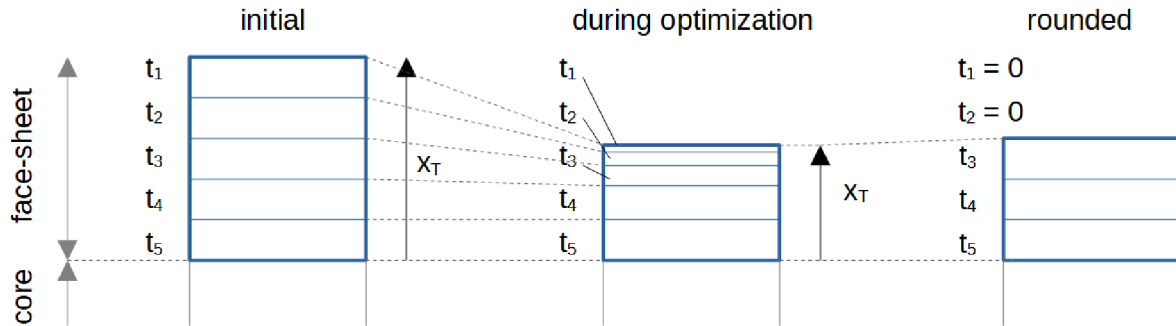

Figure 15: Thickness of the face-sheet layers controlled by the thickness variable x_T.
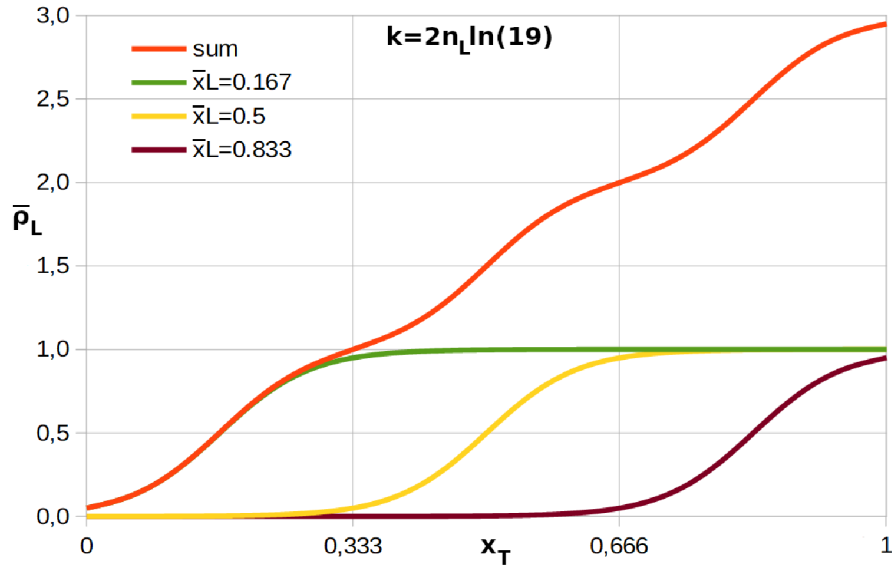
Figure 16: Shifted layer density used for properties out of the goal function [68].

The layer densities are defined by S shape function as:

$$\bar{\rho}_{Ljk} = \frac{1}{1+\exp[k(\bar{x}_{Ljk}-x_{Tk})]} \quad , \bar{x}_{Ljk} = \frac{j-0.5}{n_L} \quad , j=1,2,\dots,n_L \quad , \tag{43}$$

which are shifted from the densities defined for the goal function in equation (30). The shift is given by $\bar{x}_{Ljk}$ which is smaller by half of the relative layer thickness $0.5/n_L$ and corresponds to the layer middle (compare Figure 16 and 14, where x_{Ljk} corresponds with the layer beginning). The logic of using one layer density for the goal function and one shifted for physical thickness is that the goal function aims towards a step of the mass on boundary between layers, so that the goal function gradient close to the boundary is larger than in the middle of the layer, and so the optimizer would tend to finish just below the boundary (not to strongly increase cost), which will use fully properties of the layer after rounding layer up to the discrete. Contrary, physical thickness (using $\bar{\rho}_L$ instead of ρ_L) changes within the scope of the layer respecting their physical position, e.g., for $k = 2n_L\ln(19)$ layer density $\bar{\rho}_L$ changes from 5% to 95% within the range of the layer thickness. It can be seen also in Figure 16 that, e.g., at point $x_T = 2/3$, purple (outermost) layer will have the thickness 5% of the material thickness ($\bar{\rho}_{L1k}=0.05$), yellow (middle) layer will have the thickness 95% of the material thickness ($\bar{\rho}_{L2k}=0.95$), and green (inner) layer will have almost 100%, i.e. $\bar{\rho}_{L3k}=0.99985$. The strategy of increasing k during the optimization as was explained for the goal function is the same here – k is lower at the beginning and so the overlaps are more significant in smoothing the gradients; at the end, the overlaps are small (below 5%) which prevents abrupt changes due to final rounding.

4.1.5 Real mass of the structure

The optimization might finish with some elements not fully discrete, or if unsuccessful, it can finish with most elements not fully discrete, which was often the case during searching for convenient optimization parameters in the beginning of the work. In such cases, the real physical mass of the structure differs from the goal function (penalized mass) not only during the optimization but also at the end of the optimization. So that for practical insight to the optimization process, real mass of the structure can be monitored during the optimization and so it is calculated formally as

$$m(\boldsymbol{x}) = \sum_{k}^{n_E} A_k \sum_{j}^{n_L} t_{jk}(\boldsymbol{x}) \rho_{mjk}(\boldsymbol{x}) \quad , \tag{44}$$

where the thickness t_{jk} from equation (42) contains layer density $\bar{\rho}_{Ljk}$ from equation (43), which is more precise for actual mass, instead of equation (30) which was more convenient for the gradient of the goal function.

Since layer density is now involved in the thickness, it is dropped from physical density (compared to the goal function) and is now linearly interpolated without RAMP scheme

$$\rho_{mjk}(\boldsymbol{x}) = \sum_{i}^{n_{MC}, n_{MF}} x_{ijk} \rho_i \quad . \tag{45}$$

4.1.6 Failure constraints

Failure constraints are of the basic form

$$FI \leq 1 \quad , \tag{46}$$

where FI is a failure index which will be defined separately for each failure type. This form is common in composite design and is also convenient for the optimizer from the numerical point of view because all FI values are expected to be between 0 and 1. Less or equality is written in the formula since the optimizer keeps values on the limit and it would be hard to enforce values which are just "a little" below. Element index k and layer index j are removed in this section.

Penalization of the failure constraints will be defined precisely for each failure type, but the overall principle is the same for all. The effect of FI and goal function penalization is shown together in Figure 17 since it affects the convergence to discrete results. Cases consist of the two material interpolation where the left material is heavier and better resists the loading (has lower FI) compared to the right material, e.g., lighter and stronger core. Figure 17 shows four cases:

a) A situation when FI is linearly interpolated without penalization. Optimization starts in the middle marked with dash-dot line where FI < 1 (below green line), so that the failure constraint is not active and optimization is driven by the goal function (M) gradient (blue arrow). When it reaches point 2, failure constraint becomes active at

point 3, but with the opposite constraint gradient, so the optimization sticks to point 3 without reaching the discrete solution.

b) Materials and loads are the same as in a), but with penalized FI. Optimization starts with an active failure constraint due to penalization (point 1), so that FI gradient directs the solution towards the stronger left material. When it reaches point 2, the constraint is not active any more and the solution is directed by the goal function gradient (blue arrow) towards the discrete solution (point 4). This is an ideal case when optimization finds the best solution, however, the cases c) and d) describe unfavorable situations.

c) In this case, the penalization causes a rather small constraint violation, so that FI gradient directs the optimization towards the left stronger material (red arrow), however, this direction is not optimal, since both materials are feasible, the green line denoting FI = 1 is above the discrete ends of the red curve, so the lighter right material is optimal, but when the optimization reaches point 2, failure constraint is fulfilled and control is overtaken by the goal function gradient (point 3) which already directs towards stronger material (point 4).

d) The difference from case c) is that left material is much stronger then right material. When optimization reaches point 2, the goal function gradient directs towards the right lighter material, but it activates the failure constraint again, so the solution is locked at this point (3, resp. 2).
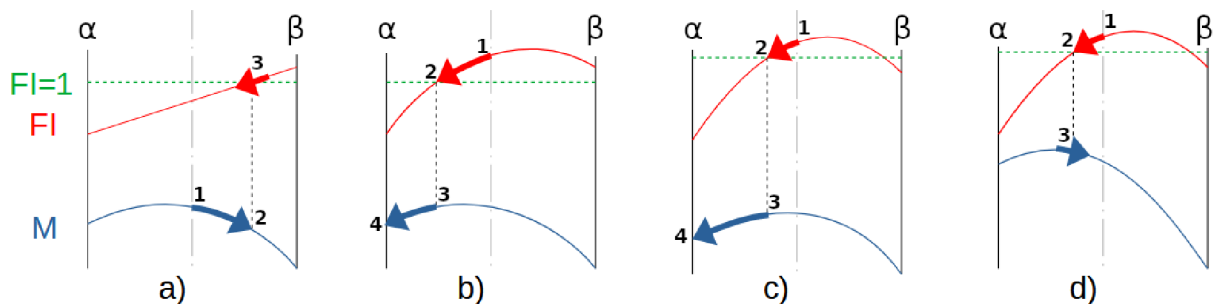
Figure 17: Schema of the mass and failure index interpolation in different situations.

Figure 18 b) shows same situations with the highlighted range Δ, which is the range between the maximums of the constraint value FI and the goal function M. When FI = 1 within this range, the optimization sticks due to opposing gradients. as was the case in Figure 17 d). For the cases in Figure 18:

a) Range Δ is large when FI is not penalized. The case without any penalization of FI and M is not shown, but one can imagine that Δ would span the whole range between α and β.

b) Δ is the distance between peaks.

c) Higher penalization in FI shifts slightly the FI peak towards the center which leads to slightly smaller Δ. The same would be true for M.

d) Large difference between M(α) and M(β) shifts peak of the goal function out of the center, which increases Δ. The same would be true for FI.
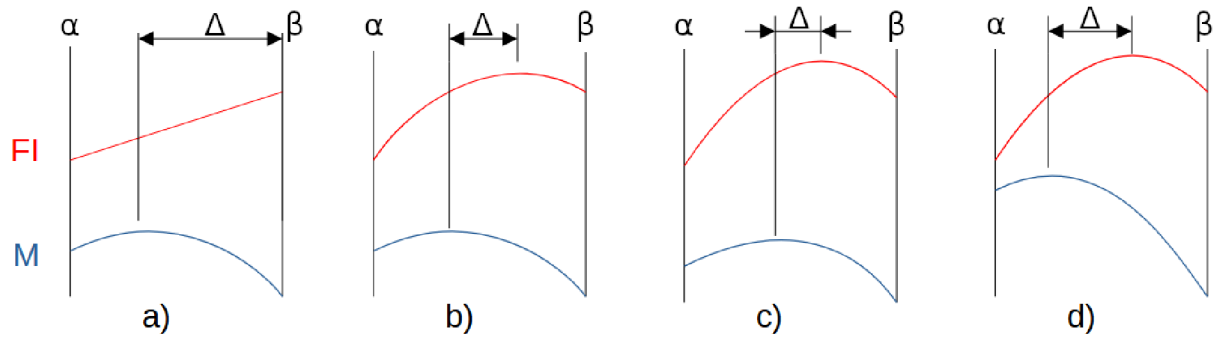
Figure 18: Range of the opposite gradients of failure constraint and goal function.

Different M(α) and M(β) is typical for cores of different thickness and/or different physical density. Face-sheet materials can differ only in orientation, so their strength would be different in the evaluated direction, but M(α) could equal to M(β), so the goal function curve will have the peak in the center which would decrease Δ.

The explanation of the range Δ may lead to impression that the optimization is prone to sticking to nondiscrete results. Test examples were used to check various optimization parameters which resulted in robust settings for materials of common use and led to low amount of nondiscrete elements.

Calculation of the stresses and stiffnesses is done by First Order Shear Deformation Theory (FSDT). This chapter contains only details related closely to the applied constraints. Complete relations are explained in the appendix 9.1.

Max stress criterion

First, max stress criteria of the face-sheet layers are evaluated for each material in its local coordinate system for allowable stresses of the face-sheet materials S_{xxt}, S_{xxc}, S_{yyt}, S_{yyc}, S_{xy}, where t and c denotes tension and compression, so that failure indices of i-th material are

$$FI^i_{xxt} = \frac{\sigma_{xx}}{S^i_{xxt}} \quad , \quad FI^i_{xxc} = \frac{\sigma_{xx}}{S^i_{xxc}} \quad , \quad FI^i_{yyt} = \frac{\sigma_{yy}}{S^i_{yyt}} \quad , \quad FI^i_{yyc} = \frac{\sigma_{yy}}{S^i_{yyc}} \quad , \quad FI^i_{xy} = \frac{|\tau_{xy}|}{S^i_{xy}} \quad , \tag{47}$$

where failures are evaluated on the top and again on the bottom side of the layer to respect stress changes over the thickness. Final failure criteria on the layer is a maximum of candidate material failure indices defined above and penalized by the RAMP scheme as

$$FI_\sigma = \sum_i^{n_{MF}} \frac{x_i}{1+q(1-x_i)} max(FI^i) \quad . \tag{48}$$

Same penalization as for density is used, again with q = -0.7, so that intermediate material will have larger FI as was shown, e.g., in Figure 10 and which corresponds with explanation in Figure 17. Bruggi [44] and Lund [61] used similar approach to failure penalization.

Note that other laminate failure criteria can be easily implemented by replacing FI^i in equation (48) with value from other failure criteria (e.g., max strain, Tsai-Hill, or Tsai-Wu) on i-th material.

Core shear

Core shear failure is evaluated for the core shear stresses τ_{xz} and τ_{yz} in the same manner as max stress criterion of the face-sheet layers. For allowable core shear stress S_{xz} and S_{yz}, failure of each material is

$$FI^i_{xz} = \frac{|\tau_{xz}|}{S^i_{xz}} \quad , \quad FI^i_{yz} = \frac{|\tau_{yz}|}{S^i_{yz}} \tag{49}$$

and final failure criteria is

$$FI_\tau = \sum_i^{n_{MC}} \frac{x_i}{1+q(1-x_i)} max\left(FI^i_{xz}, FI^i_{yz} \right) \quad . \tag{50}$$

Crimping

Crimping is a core failure similar to anti-symmetric wrinkling where length of the half wave approaches zero. It is caused by insufficient core shear strength. Crimping failure indices are calculated in principal directions 1 and 2 as

$$FI_1 = \frac{-N_1}{G_{c1}t_c} \quad , \quad FI_2 = \frac{-N_2}{G_{c2}t_c} \quad , \tag{51}$$

where t_c is core thickness, principal load is calculated from element internal membrane forces N_{xx}, N_{yy}, N_{xy} as

$$N_{1,2} = \frac{N_{xx}+N_{yy}}{2} \pm \sqrt{\left(\frac{N_{xx}-N_{yy}}{2} \right)^2 + N^2_{xy}} \tag{52}$$

and corresponding rotation angle is

$$\theta_p = \begin{cases} 0 & \text{if } N_{xx}=N_{yy} \wedge N_{xy}=0 \\ \dfrac{\pi}{4} & \text{if } N_{xx}=N_{yy} \wedge N_{xy}>0 \\ -\dfrac{\pi}{4} & \text{if } N_{xx}=N_{yy} \wedge N_{xy}<0 \\ \dfrac{\pi}{2} & \text{if } N_{xx}<N_{yy} \wedge N_{xy}=0 \\ \dfrac{1}{2} arctg\left(\dfrac{2N_{xy}}{|N_{xx}-N_{yy}|} \right) + \dfrac{\pi}{2} & \text{if } N_{xx}<N_{yy} \wedge N_{xy}>0 \\ \dfrac{1}{2} arctg\left(\dfrac{2N_{xy}}{|N_{xx}-N_{yy}|} \right) - \dfrac{\pi}{2} & \text{if } N_{xx}<N_{yy} \wedge N_{xy}<0 \\ \dfrac{1}{2} arctg\left(\dfrac{2N_{xy}}{|N_{xx}-N_{yy}|} \right) & \text{if } N_{xx}>N_{yy} \end{cases} \quad . \tag{53}$$

Angle θ_p is used to rotate core shear stiffness (due to interpolation already transformed to the element coordinate system). Transformation from element to principal coordinate system for anisotropic material gives core shear module

$$
\begin{aligned}
G_{c1} &= \bar{Q}_{44}\cos^2\theta_p + \bar{Q}_{55}\sin^2\theta_p + 2\bar{Q}_{45}\sin\theta_p\cos\theta_p \\
G_{c2} &= \bar{Q}_{55}\cos^2\theta_p + \bar{Q}_{44}\sin^2\theta_p - 2\bar{Q}_{45}\sin\theta_p\cos\theta_p
\end{aligned}
\quad,
\tag{54}
$$

where $\bar{Q}_{44}$, $\bar{Q}_{55}$, and $\bar{Q}_{45}$ are stiffness matrix members in element coordinate system defined in eq. (88).

The FI penalization cannot be directly included in eq. (51) as in max stress criterion, since there is no direct design variable interpolation in eq. (51). Material properties (G_{c1}, G_{c2}, t_c) depends on the interpolation and thus they need to include penalization to follow explanation in Figure 17, however, stiffness matrix and layer thickness were defined with linear interpolation, i.e. without penalization in eq. (41) and (42) to keep stiffness of the FE model directly within design materials. Stiffness penalization of the FE model would change load distribution among finite elements, which was considered undesirable after some experimenting. This discrepancy was solved by definition of special stiffness matrix $\widetilde{\boldsymbol{Q}}_{jk}$ which replaces $\bar{\boldsymbol{Q}}_{jk}$ (eq. (41)) just only for the crimping and wrinkling evaluation, so the stiffness matrix in element coordinate system is

$$
\widetilde{\boldsymbol{Q}}_{jk} = \sum_i^{n_{MF},\,n_{MC}} \frac{x_{ijk}}{1 + \widetilde{q}\left(1 - x_{ijk}\right)} \bar{\boldsymbol{Q}}_i \quad,
\tag{55}
$$

where $\widetilde{q} > 0$ to penalize intermediate values in the opposite way from Figure 10 where intermediate values were increased. Based on the test examples, $\widetilde{q} = 5$ is applied which is plotted in Figure 19. Now, intermediate values of the stiffness matrix are decreased, including core shear modulus which is used in eq. (51). Since G_{c1} is in denominator, it will have similar effect on the crimping FI as the opposite penalization on the max stress FI.

Note again, that $\widetilde{\boldsymbol{Q}}_{jk}$ is used only for determining stiffness in crimping and wrinkling evaluation. Layer stress calculation and finite element properties uses linearly interpolated $\bar{\boldsymbol{Q}}_{jk}$.
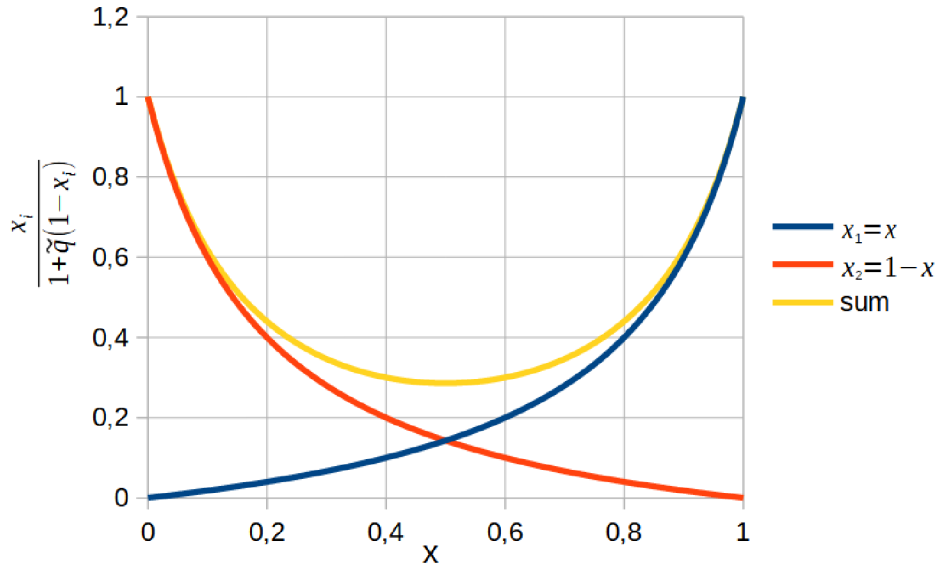
Figure 19: Penalization term for two material candidates with same densities and for $\tilde{q}=5$ [68].

Wrinkling

Wrinkling is a local stability failure of the face-sheet loaded in compression. In the literature, several formulas were theoretically derived in dependence on core thickness and type [62, 63], but significant influence is also due to face-sheet waviness depending on manufacturing quality [2]. For uni-axial loading, Hoff and Mautner [29] suggested to use

$$\sigma_{wr}=k_{wr}\left(E_f E_c G_c\right)^{1/3} \tag{56}$$

with conservative value $k_{wr}=0.5$ for the design if more precise value is not available from experiments. Effective face-sheet module is

$$E_f=\frac{12\left(1-v^2\right)D_f}{t_f^3} \quad , \tag{57}$$

where D_f is bending stiffness of the face-sheet.

In case of combined loading, failure index will be calculated according to Sullins [30]. Principal loads and directions are calculated for the face-sheet by eq. (52) and (53). If only one principal load is in compression, wrinkling is evaluated as uni-axial. If both are in compression, failure index is defined by addition equation

$$FI_{wr}=\begin{cases} R_1^3+R_2 & if\ R_1\leq 1 \\ R_1^{1/3}+R_2 & else \end{cases} \quad , \tag{58}$$

where $R_1=\dfrac{-N_{f1}}{N_{wr1}}$ and $R_2=\dfrac{-N_{f2}}{N_{wr2}}$, which in fact denote separated wrinkling failure indices in the first and second principal directions of the face-sheet loads. Sullins [30] defined first row, i.e. $R_1^3+R_2=1$ to fit experimental results from bidirectionally loaded panels, so this relation just corresponds with the state of wrinkling failure. In the optimization, it is

necessary to evaluate FI not only before the failure (the structure withstands the loads) but also above when FI > 1, which is a nonphysical situation, but the optimizer still needs reasonable values to continue and converge to a feasible state. Figure 20 shows the functions R_1^3 and R_2 which define FI_{wr} contributions from loads in the first and second principal directions. Intuitively, the second direction (i.e. more intensive compression) should have a larger contribution whether R > 1 or R < 1, but R_1^3 could overcome R_2 if $R_1 > 1$. Because of this situation, equation (58) defines second case $R_1^{1/3} + R_2$ which fulfills the intuitive requirement so that the weaker compressive load contributes less to the wrinkling failure index FI_{wr}.
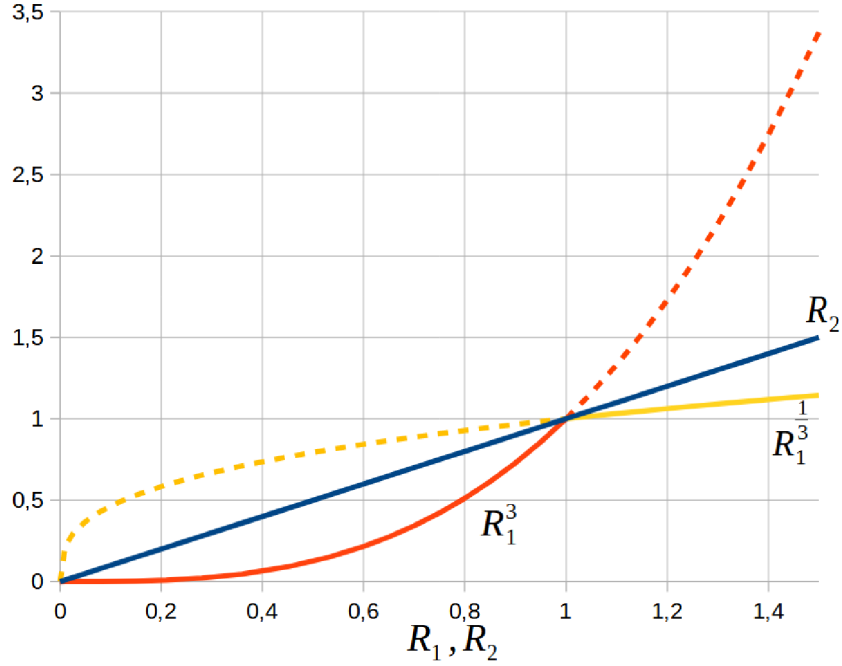
Figure 20: Members of the addition equation for wrinkling [68].

In-plane loads of the face-sheet are calculated from the stresses obtained by eq. (98) in the global coordinate system

$$N_{fxx} = \sum_j^{n_L} t_j \sigma_{xxj} \quad , \quad N_{fyy} = \sum_j^{n_L} t_j \sigma_{yyj} \quad , \quad N_{fxy} = \sum_j^{n_L} t_j \sigma_{xyj} \quad , \tag{59}$$

where n_L is number of the given face-sheet layers. Principal loads of the face-sheet N_{f1} and N_{f2} are evaluated again by eq. (52) and (53). In each principal direction, wrinkling force is according to eq. (56)

$$N_{wri} = k_{wr} \left(E_{fiN} E_c G_{ci} \right)^{1/3}, \quad i=1,2 \quad , \tag{60}$$

but thickness is dropped from effective modulus

$$E_{fiN} = 12 \left(1 - \nu_{12} \nu_{21} \right) D_{fi}, \quad i=1,2 \quad , \tag{61}$$

core shear modulus is transformed to principal directions G_{c1}, G_{c2} by eq. (54). With simplifying assumption of symmetrical laminate, i.e. $\mathbf{B} = \mathbf{0}$, $D_{16} = D_{26} = 0$, faces-sheet bending stiffness is evaluated as

$$D_{fi} = \frac{D_{ii}(\theta_p)}{1 - \nu_{12}\nu_{21}}, \quad i = 1,2 \quad , \tag{62}$$

where Poisson numbers are

$$\nu_{21} = \frac{A_{12}(\theta_p)}{A_{11}(\theta_p)} \quad , \quad \nu_{12} = \frac{A_{12}(\theta_p)}{A_{22}(\theta_p)} \quad . \tag{63}$$

Bending stiffnesses $D_{11}(\theta_p)$, $D_{22}(\theta_p)$, and membrane stiffness matrix members $A_{11}(\theta_p)$, $A_{12}(\theta_p)$, $A_{22}(\theta_p)$ of the face-sheet laminate are transformed from element coordinate system to the principal directions 1 and 2 by θ_p in the same manner as $\bar{\mathbf{Q}}$ in eq. (88).

The same approach is used to calculate wrinkling of the opposite face-sheet.

4.1.7 Blending constraints

Blending design enforces the continuity of the layers between elements (patches). A direct approach would lead to linear constraints on design variables similar to material constraints (enforcing the sum of the material variables on the element layer). IPOPT optimizer tries to fulfill constraints for "any" cost in the goal function which means that the direct approach would enforce all bottom layers to have the same material. That can be useful on a small model, but it may be too restrictive on a complex one. To control how strongly blending should be enforced, a penalization term is added to the goal function instead of a direct constraint on the optimizer side.

Penalization term

Goal function from eq. (27) contains additional term for blending penalization M_b:

$$M(\mathbf{x}) = \left[\sum_k^{n_E} A_k \sum_j^{n_L} t_{Mjk}(\mathbf{x}) \rho_{Mjk}(\mathbf{x}) \right] + M_b(\mathbf{x}) \quad , \tag{64}$$

where penalization term is defined as

$$M_b = \sum_{k1,k2}^{n_P} \sum_j^{n_L} (M_{jk1} + M_{jk2}) b_0 \sum_{i1,i2}^{n_M} |x_{i1jk1} - x_{i2jk2}| \quad , \tag{65}$$

where first sum is for set n_P of element pairs k1, k2. The penalization is done for every j-th layer; M_{jk1} and M_{jk2} denotes penalized layer mass of element k1 and k2

$$M_{jk} = A_k t_{Mjk}(\mathbf{x}) \rho_{Mjk}(\mathbf{x}) \quad . \tag{66}$$

Coefficient b_0 controls how strongly blending is enforced. Third sum consists of absolute value of differences between material variables between element pairs.

Derivatives

Layer masses M_{jk} are in fact dependent on material variables x_{ijk} and thickness variable x_{Tk}, but the term serves more like a scale of the penalization term and it is derived as a constant, so that $\dfrac{\partial M_b}{\partial x_{Tk}} \approx 0$. Absolute value has not a derivative at 0. To improve convergence, absolute value term is replaced

$$\left| x_{i1jk1} - x_{i2jk2} \right| = \left| \Delta_{12} \right| \approx \sqrt{\Delta_{12}^2 + b_\varepsilon} \quad , \tag{67}$$

where b_ε is small tolerance which controls how smooth the function is as shown in Figure 21. The term with a root is used only for derivative. Goal function contains absolute value, which gives 0 at $\Delta_{12}=0$.

$$\Delta_{12} = x_{i1jk1} - x_{i2jk2}$$
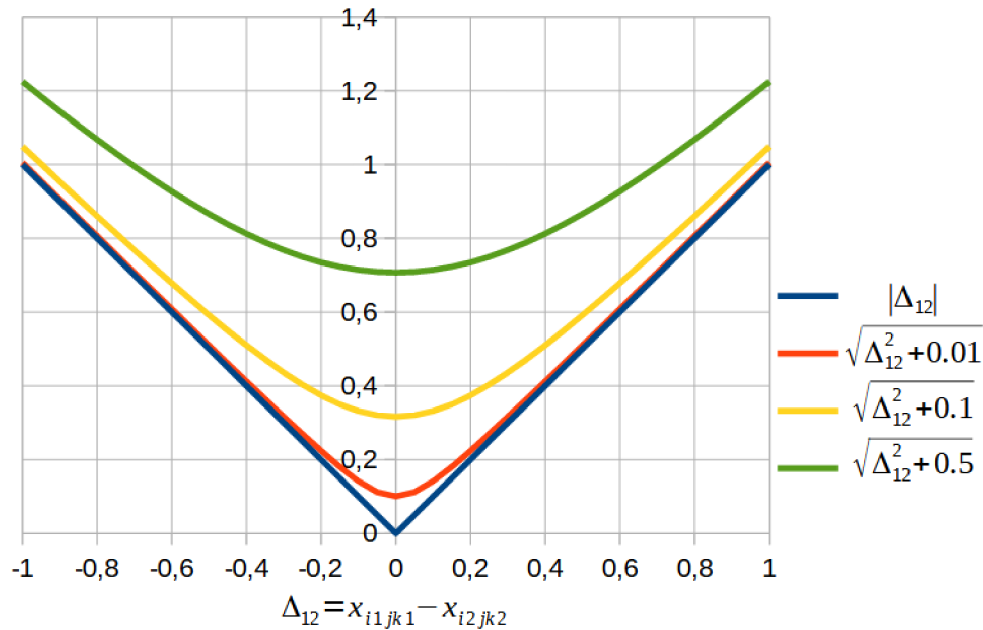
Figure 21: Relaxation of the absolute value function.

Goal function derivative by material variable from eq. (40) is increased (decreased) by the term from blending penalization

$$
\begin{aligned}
\frac{\partial M}{\partial x_{i1jk1}} &= \left(\frac{\partial M}{\partial x_{i1jk1}} \right)_{noblending} + \left(M_{jk1} + M_{jk2} \right) b_0 \frac{\Delta_{12}}{\sqrt{\Delta_{12}^2 + b_\varepsilon}} \\
\frac{\partial M}{\partial x_{i2jk2}} &= \left(\frac{\partial M}{\partial x_{i2jk2}} \right)_{noblending} - \left(M_{jk1} + M_{jk2} \right) b_0 \frac{\Delta_{12}}{\sqrt{\Delta_{12}^2 + b_\varepsilon}}
\end{aligned}
\tag{68}
$$

4.2   Software implementation

Python programming language was chosen since it is a relatively easy to learn and widely used scripting language. Engineering programs such as Abaqus or MSC.Apex support it for writing macros. Python is available freely, including professional editing programs where the most popular are PyCharm and Spider. Python code is compiled directly during the run, and so manual compilation after the code changes is not needed. This advantage is paid by lower speed compared to lower level languages such as C++ or Fortran. However, thanks to a wide range of libraries, extensive operations can be done by external libraries which are written in more efficient languages, but are wrapped in Python interface.
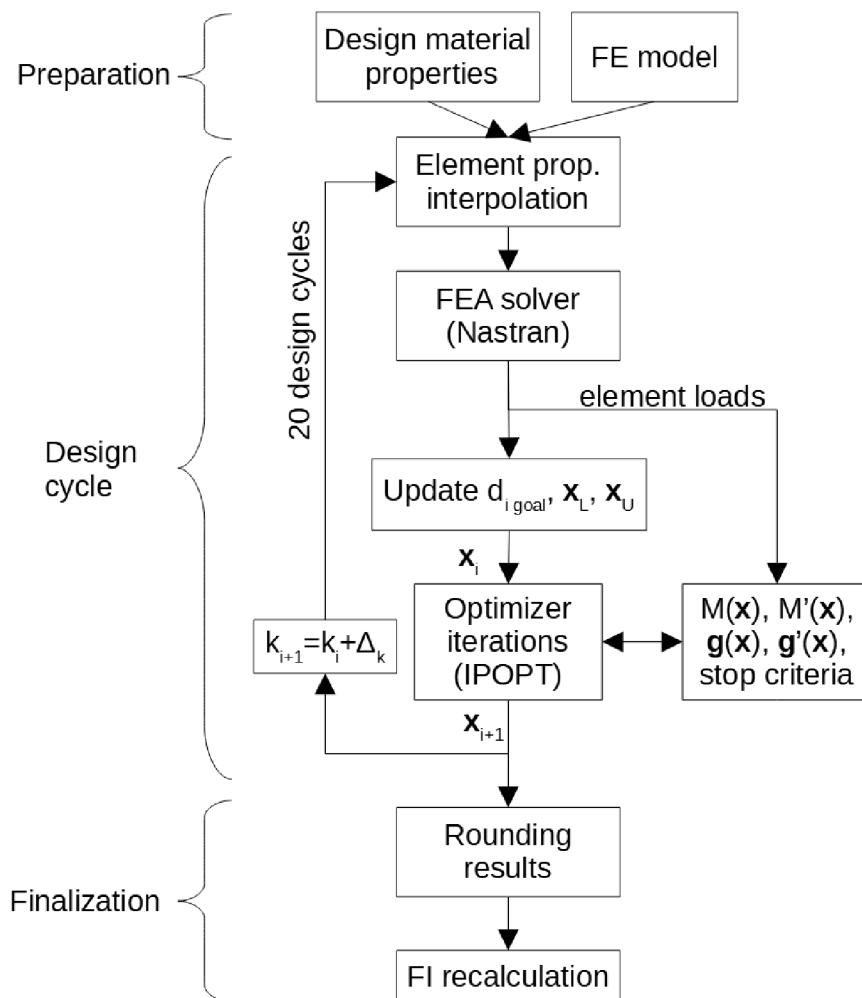
Figure 22: Algorithm flowchart [68].

Basic flowchart of the algorithm is in Figure 22. Inputs consist of candidate materials, their properties, and FE model with mesh, boundary conditions and loads. Design cycle starts with material interpolation where potential materials are combined with artificial element properties to replace properties in the input FE model. FEA solver solves the linear static analysis to calculate element loads. Goal discreteness $d_{i\,goal}$, box constraints $\mathbf{x}_L$, $\mathbf{x}_U$ are updated for values in the given design cycle to prevent extensive changes. Next, the optimizer tries to

improve design variables and (within its own iterations) calls subfunctions to evaluate the goal function, constraint function and their gradients. Twenty design cycles repeat with the evolving coefficient k in S shape function for face-sheet thickness. Finally, design variables are rounded to discrete values and the model with rounded properties is recalculated to check its validity.

Following description goes through the algorithm in detail, including important options and parameters. It is application of the method given in the chapter 4.1 and FSDT described in appendix 9.1.

4.2.1 Preparation

The program starts with an optimization parameters definition, a candidate materials definition that includes evaluation of the material stiffness matrix in the element coordinate system (eq. (88)) including transverse shear, which will be repeatedly used to evaluate stresses.

Layup

Design layup defines the maximum number of bottom layers, top layers (if not symmetric), candidate materials defined above for face-sheets and for the core. Multiple layups can be defined with different number of layers and/properties. It is also possible to define a layup without a sandwich core, but the optimization is not intended to start with a sandwich and decide whether using a core is optimal or not. Elements included in layups are recognized by their Nastran property id associated with each design layup, so that the FE model can contain other elements which are not subjected to optimization. Design layup determines design variables (for face-sheet thickness and materials) which will be defined on each element that has given design layup.

Patches

To decrease number of design variables and to obtain results which can be easily manufactured, user can define patches by element numbers. If element is in the patch, design variables are created only for the first element and sheared with others through the patch.

Number of design variables can be enumerated as

$$\left(n_E + n_P\right)\left(n_{MC} + n_L n_{MF}\right) \quad , \tag{69}$$

where each independent element and patch ($n_E + n_P$) contain design variables for n_{MC} number of potential core materials and each layer contains n_{MF} potential face-sheet materials. Potential "materials" include all layer properties: physical material, thickness, and orientation. E.g., model with 50 elements, softer and stiffer isotropic core, both of two thicknesses, and 5 layers with 1 fabric oriented in 0° or 45° will have $\left(50+0\right)\left(4+5{\cdot}2\right)=700$ design variables. When all 50 elements are in one patch, it would be only $\left(0+1\right)\left(4+5{\cdot}2\right)=14$ which is easier to handle by the optimizer.

Nastran input file

Mesh is read from *.bdf file created in Patran and which defines elements with property id. Specific properties of such elements do not matter because they will be overwritten in each design cycle. When the id is associated to some design layup, design variables are initialized on the element or associated to the guiding element if they are in a patch. Element areas (and patch areas) are calculated from the corresponding nodes. Candidate materials are uniformly distributed without preference, but loading initial design variable values from the file is possible, so the optimization can be restarted from older results. Nastran input must contain a request for element forces to be written in the HDF5 output file.

Linear and quadratic shell elements are recognized (CQUAD4, CQUAD8, CTRIA3, CTRIA6). Element areas (and patch areas) calculated at this phase are later used in the mass evaluation. The advantage is that unrecognized keys in *.bdf file are left untouched and replicated during design cycles, so that the model can contain other element types or connectors.

Multiple load cases can be defined in the *.bdf file or multiple *.bdf files can be defined which contain other load cases. The later approach is slower but might be useful when additional load cases require a modified model.

Constraint preparation

Set of constraints depend on the number of elements, design layup, and material candidates. They are fixed during design cycles, so that material constrain matrix can be defined in the preparation phase. Linear material constrains $\sum_{i}^{n_{MC},n_{MF}} x_{ijk}=1$ at each element layer are defined in the form of the matrix $\mathbf{J}_{mat}$ which binds candidate materials within the layers, in a matrix notation:

$$\boldsymbol{J}_{mat}\boldsymbol{x}=\boldsymbol{1} \quad , \tag{70}$$

where $\mathbf{J}_{mat}$ is shown in Figure 23 for layup with symmetry of the face-sheets, 3 face-sheet layers with 3 material candidates and 3 material candidates for the core. The green rectangle bounds one element, columns correspond to each design variable (face-sheet thickness, 3+3+3 face-sheet materials, and 3 core materials). Each row binds variables of the element in a specific layer.
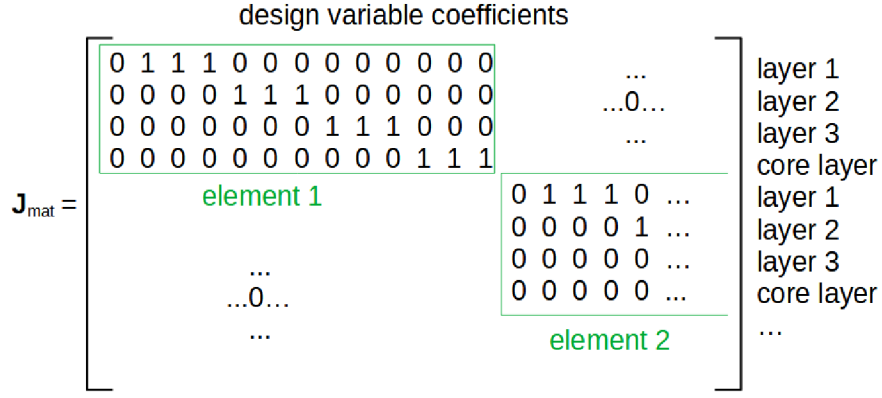
design variable coefficients

$$
\mathbf{J}_{mat} =
\begin{bmatrix}
\begin{array}{cccccccccccc}
0 & 1 & 1 & 1 & 0 & 0 & 0 & 0 & 0 & 0 & 0 & 0 & 0 \\
0 & 0 & 0 & 0 & 1 & 1 & 1 & 0 & 0 & 0 & 0 & 0 & 0 \\
0 & 0 & 0 & 0 & 0 & 0 & 0 & 1 & 1 & 1 & 0 & 0 & 0 \\
0 & 0 & 0 & 0 & 0 & 0 & 0 & 0 & 0 & 1 & 1 & 1 \\
\end{array}
\end{bmatrix}
$$

Figure 23: Example of the material constraint matrix.

Discreteness

Discreteness is used for the optimization process monitoring. It is evaluated before the first design cycle and than during each optimizer iteration.

Core discreteness for k-th element is defined as

$$
d_{kC} = \max_{i \in (0, n_{MC})} x_{i\bar{j}k} \quad , \tag{71}
$$

which is simply maximum of material variables on the core layer ($\bar{j}$ -th layer)

Face-sheet discreteness

$$
d_{kF} = \frac{\sum_{j}^{n_{LF}} \bar{\rho}_{Ljk} \max_{i \in (0, n_{MF})} x_{ijk}}{\sum_{j}^{n_{LF}} \bar{\rho}_{Ljk}} \tag{72}
$$

is given by the maximum material variables on face sheet layers n_{LF} weighted by layer density from eq. (43), so that "empty" layers ($\bar{\rho}_{Ljk} \to 0$) does not contribute significantly to discreteness. Checking separately discreteness of the core and face-sheet gives detail insight to convergence. Average element discreteness is calculated by eq. (72) as if the core is next layer with unit density, formally

$$
d_k = \frac{\left(\max_{i \in (0, n_{MC})} x_{i\bar{j}k} \right) + \sum_{j}^{n_{LF}} \bar{\rho}_{Ljk} \max_{i \in (0, n_{MF})} x_{ijk}}{1 + \sum_{j}^{n_{LF}} \bar{\rho}_{Ljk}} \quad . \tag{73}
$$

Finally, average of all elements gives one value which can be plotted during optimization. For example, in case of three candidate materials for the face-sheet and for the core, initial discreteness will be 0.333. Ideally, discreteness should reach 1 at the end of the optimization.

Blending preparation

Blending pairs are defined for all neighboring elements which shear at least 2 nodes except the pairs inside a patch. Pairs are created for layers counted from the core on neighboring elements so that blending can work also between elements with different design layups (different number of candidate layers).

4.2.2 Design cycle

The algorithm (Figure 22) combines gradient optimization (IPOPT optimizer which makes several iterations) and evolution of the model within the design cycle, which is similar to the approach used within Nastran optimization (Figure 7). The difference is that gradients are simplified, neglecting the derivative by the element loads and that element loads are fixed during the optimizer run, so their evaluation does not require full FEA – running Nastran for each **x** perturbation within a finite difference evaluation would be unbearable. Failure constraint derivatives are evaluated independently on each element (the effect of the stiffness change of neighboring elements is neglected). These simplifications are payed off by the slower evolution of the model within design cycles (outer loop) which is controlled by heuristic parameters:

1) The number of design cycles is fixedly defined to be i_{dc} = 20, which behaved robustly on the test examples.

2) The steepness coefficient starts at k = 0.5 k' and incrementally grows to k = 1.1 k' where $k'=2n_L \ln(19)$ corresponds to layer density change from 5% to 95% within layer thickness as discussed in the chapter 4.1.2. Here, coefficients 0.5 and 1.1 are based on experience with test examples.

3) Similar evolution strategy was implemented with penalization coefficients $\tilde{q}$, q (separate parameters for density, stiffness, and for failures in eq. (29) (48) (50) (55)), but results were rather worse so that these parameters were fixed on best values $\tilde{q}=5$ and q = -0.7.

4) Sequential evolution of the model is controlled by the goal discreteness $d_{i\,goal}$, which defines ideal speed of the average discreteness changes (not too fast which would decrease quality of the solution). It is linear interpolation between initial average discreteness d_0 and 0.999 as a goal in the last design cycle. Formally, goal discreteness in i-th design cycle is:

$$d_{i\,goal}=d_0+\frac{0.999-d_0}{i_{dc}}i \quad .$$

(74)

Element property interpolation

Layer properties (layer stiffness matrix, thickness, density) are interpolated according to eq. (41, 42, 45) and used to assemble the element stiffness matrix ABD and shear stiffness matrix

according to FSDT as described in appendix 9.1. Usually, PCOMP or PCOMPG card is used in Nastran input to define layers of the composite, however, these cards cannot be used since they allow only 2D isotropic or orthotropic materials with transverse shear properties. In our case, interpolation of orthotropic materials with different orientations leads to anisotropic material in the layer and transverse shear properties must be used for sandwiches. As a result, a more general PSHELL card is used by the optimization program. It defines shell properties by total thickness, density (average of the sandwich layers is used), and stiffness matrices, specifically in the form of matrices defined in MAT2 cards as:

$$G_1 = \frac{A}{t_{tot}} \quad , \quad G_2 = \frac{12\,B}{t_{tot}^3} \quad , \quad G_3 = \frac{A_{shear}}{t_{tot}} \quad , \quad G_4 = \frac{-B}{t_{tot}^2} \quad , \tag{75}$$

where A is the membrane, B membrane-bending coupling, D bending. and transverse shear A_{shear} matrices, and t_{tot} is the total element thickness. Default shear correction factor K=0.833333, i.e. 5/6, is used for pure laminates only, 1 is used for sandwich (when a core is present). New material properties are written to the input file which is a copy of the original Nastran input file.

According to Nastran manual, PSHELL card does not include transverse shear in linear buckling analysis, but buckling is not used in this thesis.

FEA solver

MSC.Nastran makes linear static analysis (SOL101) on the FE model. Optional Nastran parameters can be used to set number of CPU threads or allocated memory. The later is important to decrease when multiple optimizations are run in parallel (a user runs the whole optimization with different parameters simultaneously), because MSC.Nastran allocates 50% of the memory by default which would rise the error when running the second Nastran analysis on the same computer.

Nastran writes results to the HDF5 file. The script reads element loads (membrane forces, bending moments, and shear forces per unit width). Number of load cases are recognized from the repetition of the results on the first element in HDF5 file (results are accumulated in one data field). Stresses and failures are evaluated later for evolving design variables within iterations in the optimizer without (time consuming) Nastran interaction, so the loads are updated only out of the optimizer.

Optimizer

Trials were done with three optimizers from which only the last one is finally implemented. SciPy library [37] contains two methods for constrained large-scale nonlinear tasks. First, Trust-constrained method [64] was used, but it did not converge well on small test examples. Second, SLSQP [38] was used in the similar way, which performed well on small test examples, but calculation time quickly increased with the number of variables and constraints, which would be major bottleneck for practical tasks. This was the motivation to implement third optimizer, IPOPT [39], which is used through cyipopt wrapper (i.e. library that enables

to call programs written in one programming language, C in case of IPOPT, by commands of second language, Python in this case). The installation required compilation of the IPOPT on Windows, which might bring difficulties in getting whole optimization working on other computers. The implementation required more coding compared to previous optimizers, but IPOPT enabled to apply user-defined convergence criteria and converged much faster on large tasks, so that only IPOPT was kept.

The optimizer solves optimization problem:

$$\min M(\boldsymbol{x})$$
$$max\left(0,x_{ijk}^{D-1}-\Delta_{max}\right)\leq x_{ijk}^{D}\leq min\left(1,x_{ijk}^{D-1}-\Delta_{max}\right)$$
$$max\left(\frac{0.99}{n_L},x_{Tk}^{D-1}-\Delta_{max}\right)\leq x_{Tk}^{D}\leq min\left(1,x_{Tk}^{D-1}-\Delta_{max}\right)$$
$$\sum_{i}^{n_{MC},n_{MF}} x_{ijk}^{D}=1$$
$$\boldsymbol{FI}<\boldsymbol{1}$$

(76)

where D is design cycle number. The difference from the original problem is given in eq. (26) is that the box constraints on material and thickness variables (x_{ijk}, x_{Tk}) are tightened, i.e. the maximal change during the design cycle is limited to Δ_{max} = 0.2, which prevents abrupt changes in the stiffness of the structure and consequently the element load distribution.

IPOPT optimization is defined through a Python class, which contains functions to evaluate the goal function, its gradient, constraints (linear and nonlinear), their derivatives (Jacobian matrix), and an intermediate function which is called each iteration to the check convergence criteria.

Goal function

Thicknesses and densities of all layers from eq. (28-30) are interpolated by actual variables and substituted to the eq. (27) to evaluate the goal function. If blending is used ($b_0 \neq 0$), the goal function contains the blending penalization term according to eq. (65).

Goal function gradient

Since IPOPT calls the gradient function independently from the goal function (**x** may differ), thicknesses and densities need to be interpolated again (values are not shared with those evaluated during the goal function). Derivatives by thickness and material variables are then evaluated according to eq. (39) and (40) and filled into the gradient vector respecting the order of variables. When blending is used, gradient of the goal function increases by derivative of the blending penalization term in eq. (68).

Constraints

Vector of linear constraints is evaluated by multiplication of the material constraint matrix (Figure 23) and design variable vector **x**, so they satisfy material constraints $\sum x_{ijk} = 1$ in eq. (26, 76) per each layer.

Vector of nonlinear (failure) constrains is evaluated on each element for the element loads previously calculated by Nastran. Layer stresses are calculated according to FSDT described in appendix 9.1 (ABD matrix is assembled and numerically inverted), failures are calculated on each element for max stress criteria of the face-sheet layers, core shear, crimping, and wrinkling by eq. (48, 50, 51, 58). If the model has multiple load cases, failure constrains are evaluated for all loads found in HDF5 results, e.g., 3 load cases will cause number of nonlinear constraints (and evaluated failure indices) to be 3times compared to a model with one load case.

IPOPT input does not distinguish linear and nonlinear constraints (contrary to SLSQP), so that their values are concatenated to one constraint vector. Lower bound is 1 for material constraints and $-\infty$ for failure constraints. Upper bound is 1 for all constraints. (The optimizer accepts equality constraints $\sum x_{ijk} = 1$ defined as inequalities with same upper and lower bounds.)

Constraint aggregation

The review chapter showed that the number of constraints can be decreased by p-norm or KS function aggregation. KS function was implemented. Since it results in one value which should approach to the maximum and IPOPT scales constraints internally. KS function is not evaluated on this level. Maximum from failure constrains is given to IPOPT

$$\boldsymbol{FI} \rightarrow max(\boldsymbol{FI}) \ . \tag{77}$$

KS function is used later when evaluating derivatives.

Constraint ignoring

Difficulties with convergence were encountered when some elements in the model were failing even with the strongest materials. That can be explained by the priority on fulfilling all constraints, so that the optimizer can violate material constraints (e.g., that materials overlap on the layer $\sum x_{ijk} > 1$ so that the summary material exceeds 100%). Even if constraints are violated on few elements, the optimizer does not improve the goal function too much, which leads to poor results on the rest of the model. Such situation may happen with a model containing stress concentration, concentrated loads, or with poor elements. For ordinary analysis, an engineer interpreting the results may consider such failing elements to be irrelevant.

Heuristic approach to overcome such situations has been developed. Parameter A_{ign} defines the fraction of the design domain area on which the failure constraints will be ignored. The implementation is:

1) At the beginning, none elements are "ignored".

2) The optimizer calls the function to evaluate constraints in each iteration. Elements with the highest FI are marked as "candidates" for ignoring, other elements are unmarked. The number of candidates respects A_{ign}, e.g., if A_{ign}=0.1, then elements with the highest FI, filling 10% of the design domain area, are marked.

3) At the end of the constrains evaluation, failure constraints on the ignored elements are set to 0.

4) At the end of the design cycle, the ignored elements are reset and candidates are activated for ignoring.

5) Final recalculation of the optimization results is done without ignoring.

Whole optimization can run for several A_{ign} so that the engineer can compare the elements which are failing at the end of the optimization and consider local reinforcement. Including reinforcing materials in the optimization would lead to high calculation demands and if the reinforcing material differs strongly from the other materials, it might decrease the convergence or quality of the solution.

Constraint ignoring is implemented for the case without constraint aggregation.

Jacobian

Constraint derivatives are filled to the Jacobian matrix which structure is shown in Figure 24. It consists of two parts. First, derivatives of material constraints which were linear, so that this part is directly the material constraint matrix $\mathbf{J}_{mat}$ as can be seen from eq. (70). $\mathbf{J}_{mat}$ in Figure 24 is for clarity shown for the same case as it is in Figure 23. Second, derivatives of the failure constraints $\mathbf{J}_{FI}$ which are nonlinear. General shape of $\mathbf{J}_{FI}$ is:

$$
\mathbf{J}_{FI} = \begin{bmatrix} \dfrac{\partial FI_1}{\partial x_1} & \dfrac{\partial FI_1}{\partial x_2} & \cdots & \dfrac{\partial FI_1}{\partial x_n} \\ \dfrac{\partial FI_2}{\partial x_1} & \dfrac{\partial FI_2}{\partial x_2} & & \\ \cdots & & \cdots & \\ \dfrac{\partial FI_m}{\partial x_1} & & & \dfrac{\partial FI_m}{\partial x_n} \end{bmatrix} ,
\tag{78}
$$

so that members a^e_{ij} in Figure 24 correspond to $\dfrac{\partial FI_i}{\partial x_j}$ on element e. They are evaluated as:

$$
a^e_{ij} = \frac{\partial FI_i}{\partial x_j} \approx \frac{FI_i(\mathbf{x}+\Delta_j) - FI_i(\mathbf{x})}{\Delta_j} ,
\tag{79}
$$

where finite difference in j-th variable $\Delta_j = 10^{-9}$ is used. Eq. (79) requires high number of FI evaluation on each element for each optimizer iteration and so it is the most time consuming operation of the whole optimization even when only the red diagonal in Figure 24 is filled.
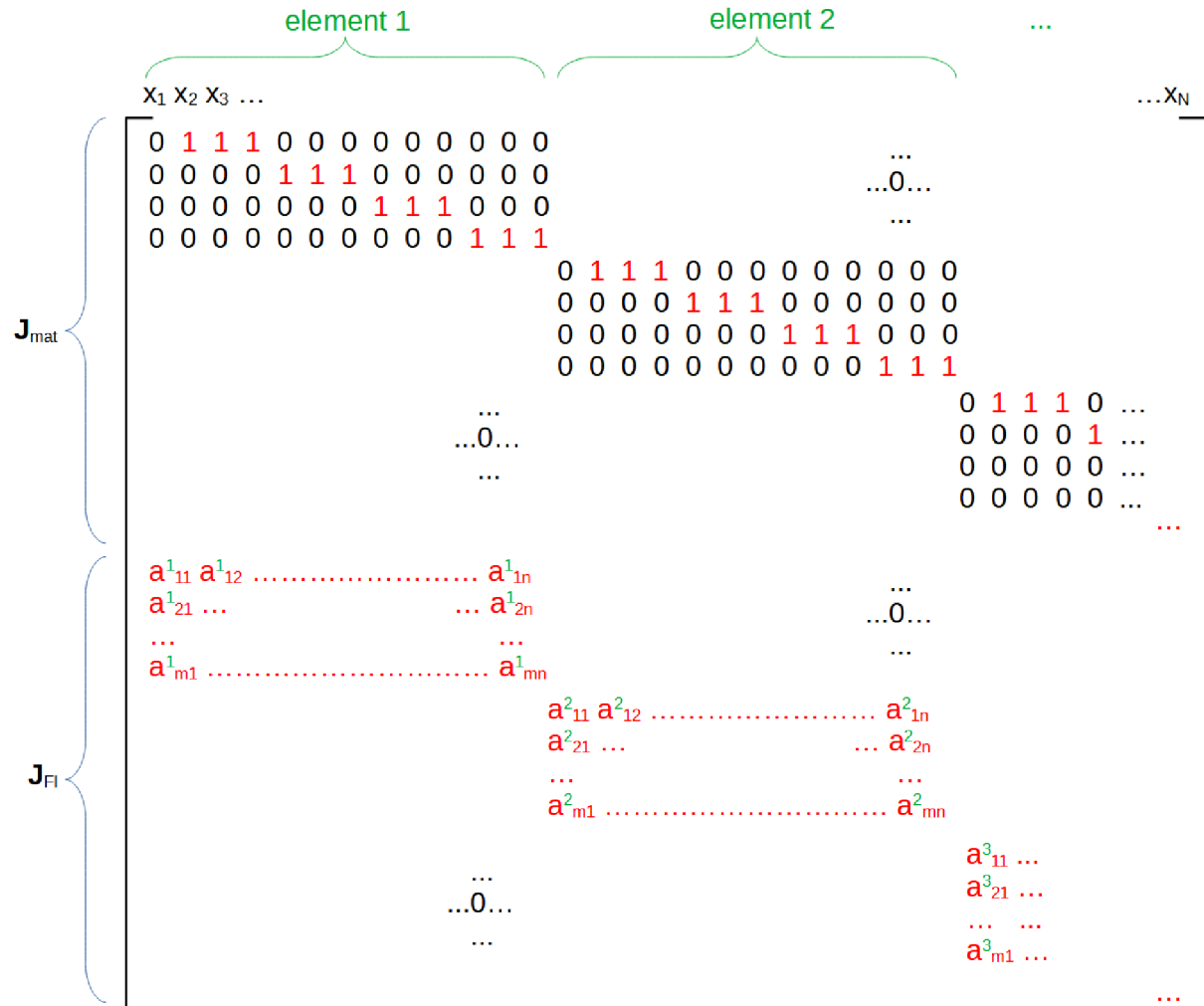
Figure 24: Structure of the Jacobian matrix

Since the evaluation of failures is time consuming, an additional parameter was defined: cut_low_FI_threshold. It is a threshold FI below which Jacobian members a^e_{ij} are not evaluated and is set to 0, e.g., cut_low_FI_threshold = 0.5 denotes that eq. (79) will be skipped ($a^e_{ij} = 0$ for all i and j) if all failure indices of the element e are below 0.5. Default value is -∞ so that eq. (79) is used for all elements. Using a higher threshold is useful especially when patch design is used, since patches consist of a higher number of elements, but only a few of them are critical and so drives the optimization and the given threshold decreases the calculation time without significant change in the optimization results.

The possibility to define Jacobina as a sparse matrix is a significant advantage of IPOPT optimizer as regards large-scale problems. Since SLSQP accepts Jacobian as a dense matrix, it required far more memory and calculation time on large test examples. IPOPT requires

structure of the Jacobian to be explicitly defined as pairs locating each nonzero member. Pairs for nonzero members are created according to Figure 24.

Jacobian with aggregated constraints

If failure constraints are aggregated to one FI, eq. (78) will simplify to one row:

$$J_{FI\,aggr.}=\left[\frac{\partial FI}{\partial x_1}\quad\frac{\partial FI}{\partial x_2}\quad\cdots\quad\frac{\partial FI}{\partial x_n}\right]\quad. \tag{80}$$

Maximum of failure constraints max(**FI**) is used in the constraint function, but it is not convenient for derivation, since most of the variables has none influence on the max. value. Thus, aggregation with KS function is used, so that:

$$\frac{\partial FI}{\partial x_j}\approx\frac{\partial KS}{\partial x_j}\approx\frac{KS(x+\Delta_j)-KS(x)}{\Delta_j}\quad. \tag{81}$$

where KS function [45] is in the form

$$KS=max(\boldsymbol{FI})+\frac{1}{\rho_{KS}}\ln\left(\sum_i^m \exp\left[\rho_{KS}(FI_i-max(\boldsymbol{FI}))\right]\right)\quad. \tag{82}$$

where m is number of constraints, coefficient ρ_{KS} controls how close the KS function is to the maximum, values from 2 to 100 were tried.

Trials were done also with aggregation per elements, where groups for aggregation consisted of element constraints, so that final number of failure constraints were decreased to number of elements, but it gave worse results than aggregation to one constraints from all elements, so only this was kept in the code.

Convergence criteria of the optimizer

Due to the evolution of the loads, the optimizer is not supposed to have full convergence, thus the number of IPOPT iterations is limited by the conditions which are tested by the function called at the end of each IPOPT iteration as shown in Figure 25. Conditions are:

1) Average element discreteness d (average of eq. (73)) is above the goal discreteness of the i-th design cycle $d_{i\,goal}$. It means that the desired evolution change of discreteness is achieved and so the optimizer may finish.

2) First, maximum of failure index is below the threshold 1.001, which means that the constraints are feasible or only slightly violated and so the optimizer can finish. Or second, the average change of design variables x is above half of their maximum change, so the optimizer should finish, otherwise the optimizer will press the variables to their bounds even if they help decreasing constrains only a little – next design cycles are assumed to change bounds and so the variables (which are effective in decreasing constrains) could be changed, one half was selected heuristically as a part of max. changes.

3) Optimizer is finished when achieving the maximal number of iterations j = i_{dc}, where 10 is used, based on the test examples.
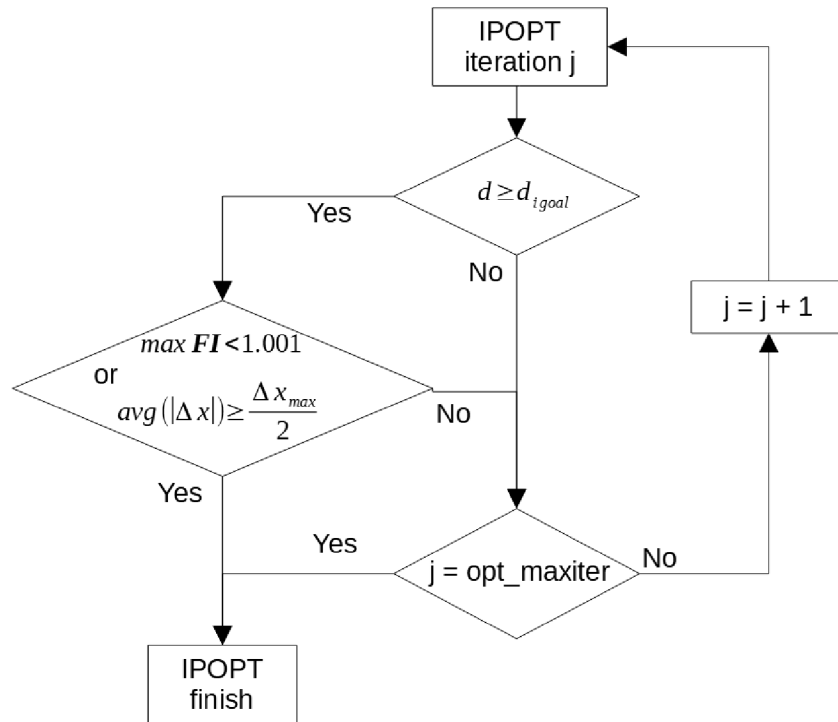

Figure 25: Convergence criteria for IPOPT iterations

4.2.3 Finalization

After the end of the design cycle, design variables are rounded to obtain one discrete material on each layer according to the highest portion of the candidate material, which is necessary for the elements which finish without clearly discrete result. Final values are defined close to 0 or close to 1 to prevent numerical errors when evaluating failures by the same functions as were used during optimization, because the interpolation is still involved. Presence of the face-sheet layer is determined from layer density, $\rho_{Ljk} < 0.5$ means empty layer, $\rho_{Ljk} \geq 0.5$ means active layer.

Rounded variables are used to create input for Nastran and to recalculate the model to check failures. Constraints are evaluated and saved for the check by a user.

Since rounding the core according to the portion with the highest design variable can violate constraints due to lose of the thicker or higher density core, alternative rounding is used for the core. If there is a heavier core with a portion of the design variable larger than 1%, the core is rounded to the heavier (even if it was present only by a few percent), supposing that the heavier core will satisfy constraints. These layups are also recalculated by Nastran again and constraints are evaluated, so the user can choose which rounding is better in the specific case. This option of rounding to the heavier core was implemented due to difficulties with convergence which occurred with older settings. Actual default settings have not required this step on test examples.

64

Outputs

Output data are saved to several files in the working directory for later browsing, plotting graphs or restarting the optimization. Table 4.1 explains details.

Table 4.1: Output files

File type	Data	Comment
*.bdf *.h5 …	Nastran input and analysis results	Nastran analysis bdf input is written in each design cycle. Element forces are loaded from HDF5. These files are usually not needed by the user.
*rounded.bdf …	Nastran input and analysis results	Nastran files from the final solution with rounded materials.
*round_core_heavier.bdf …	Nastran input and analysis results	Same as the previous, but the core is rounded to the heavier if heavier material content is above 1%.
*variables.npy	Design variables	Binary file with design variables, which can be used for the restart of the optimization from the selected design cycle.
*.vtk	Mesh data. Element discreteness. Face-sheet disc. Core disc. Layer materials	Results are from each design cycle for viewing in Paraview. Discreteness is averaged on element, for the core and averaged for face-sheets. Prevailing (rounded) materials in each layer are mapped on the mesh according to the material number in user input.
*constraints.vtk	Mesh data. Max. FI Face-sheet Max stress FI Core shear FI Crimping FI 1 and 2 Wrinkling FI top and bottom	Failure indices in final rounded results for viewing in Paraview. Each layer can be displayed for each load case.
*constraints_maxLC.vtk	…	Same as the previous, but only max. values from all load cases are printed for each failure type.
*constraints_core_heavier.vtk	…	Same as *constraints.vtk, but after rounding to heavier core material.
*constraints_core_heavier_maxLC.vtk	…	Same as previous, but only max. values from all load cases are printed for each failure type.

printed_log.log	Mass Max. FI Face-sheet max. FI Max. core shear FI Max. crimping FI Max. wrinkling FI Average element disc. Average face-sheet disc. Average core disc.	ASCII file with debugging information and with an overview of values at the end of each design cycle, which can be used to plot the evolution of FI (by type) and discreteness. List of ignored elements due to the parameter A_{ign} is given.
*_log.log	...	Similar as previous, including input parameters.

4.3   User workflow

Figure 26 summarizes the workflow during sandwich structure design when the optimization program is used (With optimization). First, the usual FE model is created. Second order shell elements with relatively large element size can be used for the optimization model to keep a low number of design variables and constraints. Boundary conditions and loads are prescribed as usual, preferably trying to avoid stress concentrations, because the optimization aims to design a global layup, so that small details (local reinforcements) are out of the scope of the optimization so the local concentrations would make difficulties in convergence. Multiple load cases can be used. Nastran input file should the contain output request for internal forces acting on shell elements of the design domain.
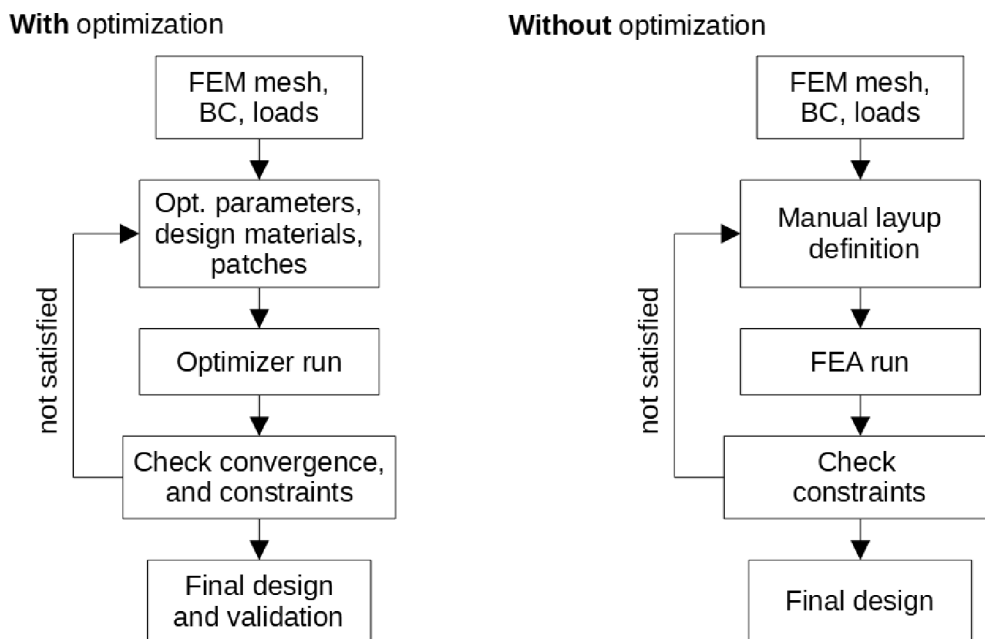

Figure 26: User workflow.

In the FE model, simple properties are prescribed on the optimized elements, since they will be overwritten by the optimizer, but the orientation of the material must be defined if all

elements do not have the same orientation. Properties of the design materials (elastic constants, layer thickness and orientation) are prescribed in the program input together with the optimization properties discussed in the previous chapter and listed in Table 4.2. When the model contains patches, the ignoring area A_{ign} can be defined, so that areas which will require local reinforcement will be found and the optimization can be run several times for varying A_{ign}. When patch design is used, the speed can be increased by using the parameter cut_low_FI_threshold.

The optimization is started from a Python console, so that only Nastran solver and Python with appropriate libraries (bisect, operator, time, datetime, os, subprocess, sys, numpy, sympy, h5py, ipopt) are needed.

Outputs are checked, especially convergence to discrete values (if convergence is low, rounding errors might be high) and failure indices (maximum and specific failures) which can be easily displayed in Paraview. If the results are not satisfactory, the optimization can be launched again with altered parameters.

The optimization model can be used for further processing if it was not created only with optimization intention at the beginning (e.g., due to the rough mesh in a large model needed to satisfy a reasonable optimization time). According to the task, total displacement or buckling can be validated since it is not included in the optimization. Structural details out of the optimization scope need to be designed by common engineering practices.

Figure 26 right shows the workflow without the optimization program, where the initial layup needs to be guessed manually according to engineering experience, including manufacturing preferences which might be missing in the optimization. Instead of the loop where optimization is run one or several times with various parameters, if the optimization is not used, the engineer needs to manually evaluate the results from FEA and modify the layup to improve the model behavior, mostly by reinforcing the failing area or changing layer orientations. If the mass is to be minimal, the engineer tries several modifications, all time manually evaluating results. Final design may involve additional features which do not need to be evaluated by FEA. It can be seen that the workflow with optimization replaces laborious modifications with a simple change of optimization parameters. On the other side, the optimization may lack some of the constraints or manufacturing rules, so that they need to be added manually at the end and validated, but the final validation is expected to be done only ones.

Table 4.2: Overview of the main optimization parameters

Parameter	Default value	Comment
q	-0.7	Penalization coefficient for density in the goal function, for max stress and core shear criteria in eq. (29), (48), and (50)
$\tilde{q}$	5	Penalization coefficient for stiffness in crimping and wrinkling evaluation in eq. (55)
i_{dc}	20	Number of design cycles (outer loop)
i_{max}	10	Maximum number of the optimizer iterations (inner loop)
k	[0.5, 1.1]	Steepness coefficient in S shape function in eq. (30) and (43). It defines how discretely thickness of the face-sheet is defined. Value changes during design cycles from min to max [min, max]
Δ_{max}	0.2	Maximum change of design variable between design cycles
aggregate_const	False	Aggregation is switched off because of poor results in test examples
ρ_{KS}	20	Coefficient in KS function in eq. (82)
A_{ign}	0	Defines the area of the elements with the highest FI to be ignored in the next design cycle. Implemented only for aggregate_const=False
b_0, b_ε	0, 0.1	Blending parameters from eq. (65), (67), b_0=0 means no blending
cut_low_FI_threshold	$-\infty$	Derivatives of constraints below this threshold will be skipped. i.e. set to 0 in Jacobian matrix, saving time to their evaluation
Face-sheet materials		E_{11}, E_{22}, G_{12}, G_{23}, G_{13}, ν_{12}, θ, t, ρ, S_{11t}, S_{11c}, S_{22t}, S_{22c}, S_{12}
Core materials		E_{11}, E_{22}, E_{33}, G_{12}, G_{23}, G_{13}, ν_{12}, θ, t, ρ, S_{23}, S_{13}
Design layups		Each layup contains predefined: potential number of bottom face-sheet layers, number of top face-sheet layers or symmetry to bottom, face-sheet material candidates, core material candidates
Patches		Each patch is defined by element numbers. Elements in the patch share layup

4.4 Summary of the implemented method

Key possibilities and limitations which are given by the method itself and its implementation are:

1) Shell elements (CQUAD4, CQUAD8, CTRIA3, CTRIA6) can be in design domain. There are no limitations on elements out of the optimization domain.

2) Multiple design layups can be used, including laminates (without sandwich core). Limitation is that the optimization is not able to remove the core automatically.

3) Orthotropic materials are defined by engineering constants.

4) Patches can be defined (group of elements shearing layup). Blending is implemented through penalization so that the user can control how strongly the continuation of layers should be enforced.

5) Multiple load cases can be used in the Nastran file or in additional files (e.g., with additional elements out of the optimization domain).

6) Optimization aims to discrete results – choosing among predefined core thicknesses and densities, layer orientations, etc. "Continuous" options need to be approximated by many design materials, which prolongs optimization.

7) Convergence would be more difficult when materials differ dramatically in properties.

8) The method is gradient based, so it finds the local extreme, there is no guarantee to find the global extreme, even though interpolation helps to increase the chance of finding a good result.

5 Examples and results

Examples of various complexities were used to define default optimization parameters, to test convergence and quality of results. The test examples are:

1. One element in edge-wise compression and one with shear and bending which test the ability to converge to known optimal design.

2. Separated elements with simple loads test convergence to known optimum and originally used to find default optimization parameters since there are multiple elements with sequentially increasing loads of different types.

3. Panels with out-of-plane compression or side load search for the optimal layup on each element and, in the next variant, when the whole panel is one patch. Panels were also used to check and modify the default parameters, because their element loads may change during optimization due to varying stiffness, which was not the case of previous examples.

4. Long box with ribs loaded with underpressure on a top side and torque to test the use of multiple patches and different design layups when the box contained sandwich panels and UD laminated flanges.

5. Conceptual design of an airliner interior component – a stowage which is loaded by the critical side load case.

6. Conceptual design of an airliner galley with multiple load cases.

All examples run on desktop computer with 80 GB DDR3 RAM, Intel Xeon E5-2620 at 2.00 GHz processor with 12 logical threads, 64bit Windows operation system, Python 3.7 and MSC.Nastran 2020. The size of the examples was not limited by memory, but rather by reasonable optimization time. Since the optimization code is not parallelized, more optimizations were often running simultaneously to use computer capacity, so that the calculation time specified in the description should be considered as approximate.

Material properties in examples

Laminated composites are used for the face-sheets with values according to Idaflieg [65] which correspond to the properties after hand layup for volume content 0.35 as listed in Table 5.1. Area density of the reinforcement were selected as is commonly used in sport aircraft (200 g/m^2 carbon fabric, 160 g/m^2 carbon UD tape, and 300 g/m^2 glass fabric). Composite density is calculated by the rule of mixture as

$$\rho = \rho_f V_f + \rho_m V_m \quad , \tag{83}$$

where ρ_f is fiber density (1.77 g/cm^3 for carbon, 2.55 g/cm^3 for glass) and epoxy matrix density ρ_f = 1.4 g/cm^3, V_f = 0.35, and V_m = 0.65 are fiber and matrix volume contents.

Corresponding thickness of the composite layer is

$$t = \frac{m_f}{V_f \rho_f} \quad ,$$

(84)

where m_f is the area density of the fiber reinforcement.

Foam core properties are for Airex C70.75 from the datasheet [66] (Table 5.2), starting with commonly used density 60 kg/m^3 and with two foams with higher density. Honeycomb core properties are for hexagonal shape 5052 aluminum alloy from datasheet [67] (Table 5.3). For the core, average values were taken for density. Minimum values were taken for mechanical properties to be conservative in design. When the minimum value was not known, 80% of the typical value was used. Honeycomb properties E_{11}, E_{22}, G_{12} are not covered in the datasheet due to low importance; for numerical reasons (included in the calculation of element stiffness by FSDT) small nonzero values were used.

Private material properties were used to solve the examples in cooperation with the industrial partner (airliner stowage and galley). These material data are not directly listed in the thesis. Interested readers may follow the material properties given in these tables to obtain a rough overview.

*Table 5.1: Face-sheet layer properties [65], *guessed values.*

		Carbon fabric	Carbon UD	Glass fabric
V_f		0.35	0.35	0.35
ρ_{dry}	g/m^2	200	160	300
ρ	g/cm^3	1.4	1.4	1.67
t	mm	0.327	0.256	0.336
E_{11}	MPa	39470	77000	16600
E_{22}	MPa	39470	3400	16600
ν_{12}		0.037	0.23	0.03
G_{12}	MPa	1620	2870	3800
G_{23}*	MPa	1620	1620	3800
G_{13}*	MPa	1620	1620	3800
S_{11t}	MPa	146	420	95
S_{11c}	MPa	146	420	95
S_{22t}	MPa	146	50	95
S_{22c}	MPa	146	200	95
S_{12}	MPa	30	50	30

Table 5.2: Foam core properties [66].

Airex		C70.55	C70.75	C70.130	Comment
ρ	kg/m^3	60	80	130	average
t	mm	5, 10, 15	5, 10, 15	5, 10, 15	
E_{11}	MPa	35	50	95	min
E_{22}	MPa	35	50	95	min
E_{33c}	MPa	55	80	145	min
v_{12}		0.1	0.1	0.1	guess
G_{12}	MPa	18	24	45	min
G_{23}	MPa	18	24	45	min
G_{13}	MPa	18	24	45	min
S_{13}	MPa	0.7	1	2.1	min
S_{23}	MPa	0.7	1	2.1	min

Table 5.3: Honeycomb core properties [67].

HexWeb CRIII-3/16-5052 - 3.1			Comment
ρ	kg/m^3	50	average
E_{11}	MPa	0.1	neglected
E_{22}	MPa	0.1	neglected
E_{33c}	MPa	413	0.8 of typical
v_{12}		0	neglected
G_{12}	MPa	0.1	neglected
G_{23}	MPa	122	0.8 of typical
G_{13}	MPa	310	min
S_{13}	MPa	1.07	min
S_{23}	MPa	0.62	min

5.1 One element examples

Compression and bending examples test the basic ability of the algorithm to achieve optimal material selection when only one element is concerned. These examples are simple enough to check if the solution is truly optimal and aims to reveal potential shortcomings of the implemented algorithm. Examples were optimized for several cases of loads and material candidates.
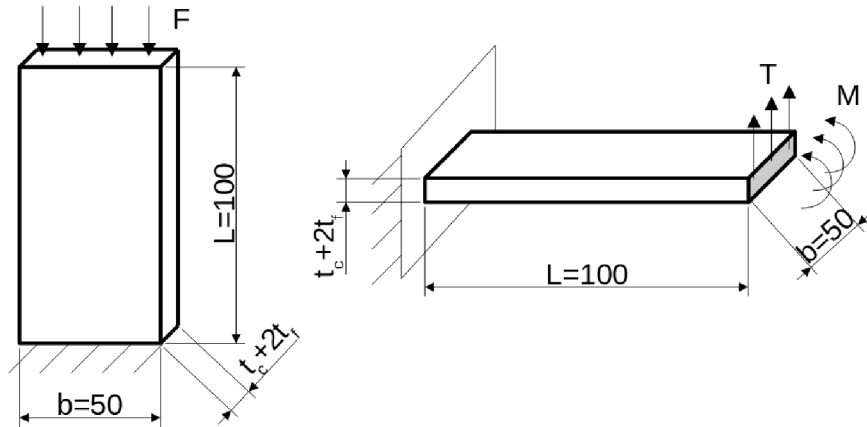

Figure 27: Schema of test cases for edge-wise compression and bending with transverse shear.

5.1.1 Edge-wise compression

Compression example (Figure 27 left) is limited by compressive allowable stress in face-sheets (depending only on face-sheet layup), crimping (depending on the core material and thickness), and wrinkling (depending on both the core and face-sheets).

Design materials:

- Two fabric candidates for the face-sheet layers (0° and 45° carbon fabric) for up to 5 layers (each with thickness 0.327 mm). Face-sheets are symmetric (same top and bottom face).

- Six core candidates (foams 60, 80, and 130 kg/m^3 all with 5 and 10 mm thickness).

The task consists of 17 design variables, which are linked through 6 material (linear) constraints. Failures define 15 nonlinear constraints. The optimizations took less than two minutes (mostly Nastran execution).

Table 5.4: Results for the element loaded by a set of compressive forces F.

| Loads						
F [N]	**2000**	**4000**	**8000**	**12000**	**16000**	**20000**
Values at the end of optimization						
Discreteness	1.000	1.000	1.000	1.000	1.000	1.000
m [g]	6.56	7.81	10.86	17.84	21.69	25.54
FI max	0.68	0.94	1.00	1.00	1.00	1.00
Rounded layup						
Face-sheet	$0/$	$0/$	$0_2/$	$0_3/$	$0_4/$	$0_5/$
t_{core} [mm]	5	5	5	10	10	10
ρ_{core} [kg/m^3]	80	130	130	130	130	130
Properties after rounding						
m [g]	6.58	7.83	12.41	20.23	24.81	29.39
FI faces	0.41	0.82	0.83	0.83	0.83	0.83
FI cr	0.33	0.36	0.71	0.53	0.71	0.89
FI wr	0.29	0.38	0.38	0.38	0.38	0.38
True optimum						
	$\rho_{core} = 60\text{kg/m}^3$	$\rho_{core} = 60\text{kg/m}^3$	$t_{core} = 10\text{mm}, \rho_{core} = 80\text{kg/m}^3$			
m_{opt} [g]	6.08	6.08	12.16			

Optimization was done for a series of loads from 2 kN to 20 kN as shown in the columns of Table 5.4. The table further shows values at the end of the optimization, i.e., before rounding: all tasks converged successfully to discreteness 1.000 and feasible solution (FI ≤ 1). Layup was rounded to the face-sheet layers with orientation 0°, which is the direction of the load. The number of face-sheet layers is optimal, however, three tasks found a solution where the core is over dimensioned, as marked in red, compared to the true optimum in the bottom of the table, so the mass is larger.

Table 5.5 contains graphs for mass, discreteness (element average, face-sheet average, core), and failure indices as they evolved during optimization. Each point in the graph denotes a design point at the end of the optimizer run for the given design cycle.

- For the lowest force (2000 N), the measures evolve mostly before design cycle 4 and finally changes a bit. The load does not cause failure, but it seems that a heavier than necessary core was determined in the beginning where the crimping FI is around 1.

- For 4000 N and 8000 N, the discreteness increased sequentially and the crimping dropped down after initial violation. For 4000 N, the face FI has a peak close to the end, but finally remains under 1. For 8000 N, the face FI remains close to 1 constantly.

- For higher loads, the discreteness quickly gets close to 1. The crimping FI has a high start due to the initial mixture with lighter core materials and penalization. The face FI decreases at the beginning and remains close to 1. The wrinkling FI is also initially violated and later remains well below 1.

- Most of the graphs for the face FI drops down during the final rounding. Corresponding increase is during the final rounding as is visible on mass graphs. This is caused by the S shape function in the face-sheet properties.

Table 5.5: Mass, discreteness, and failure indices during design cycles.
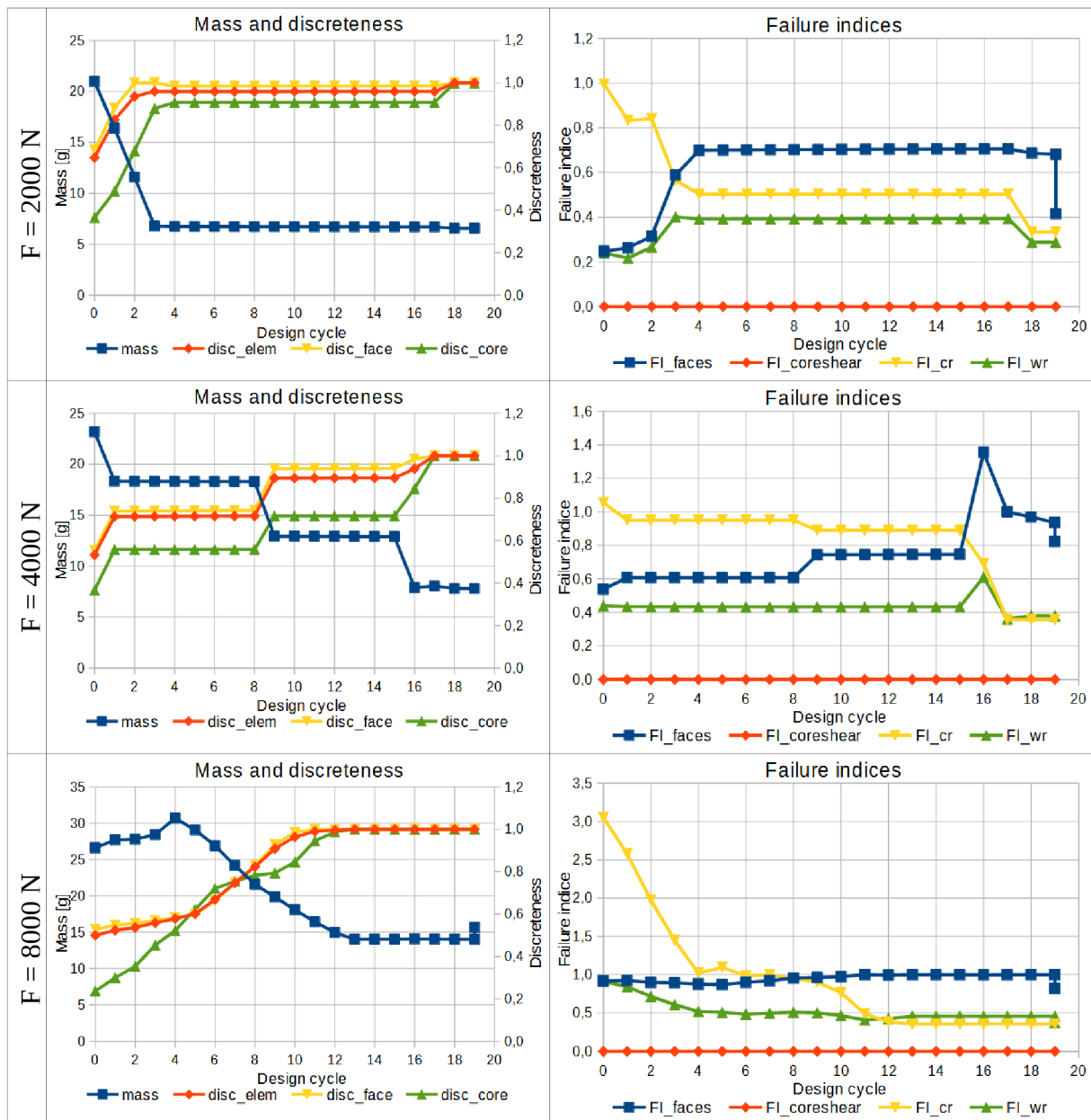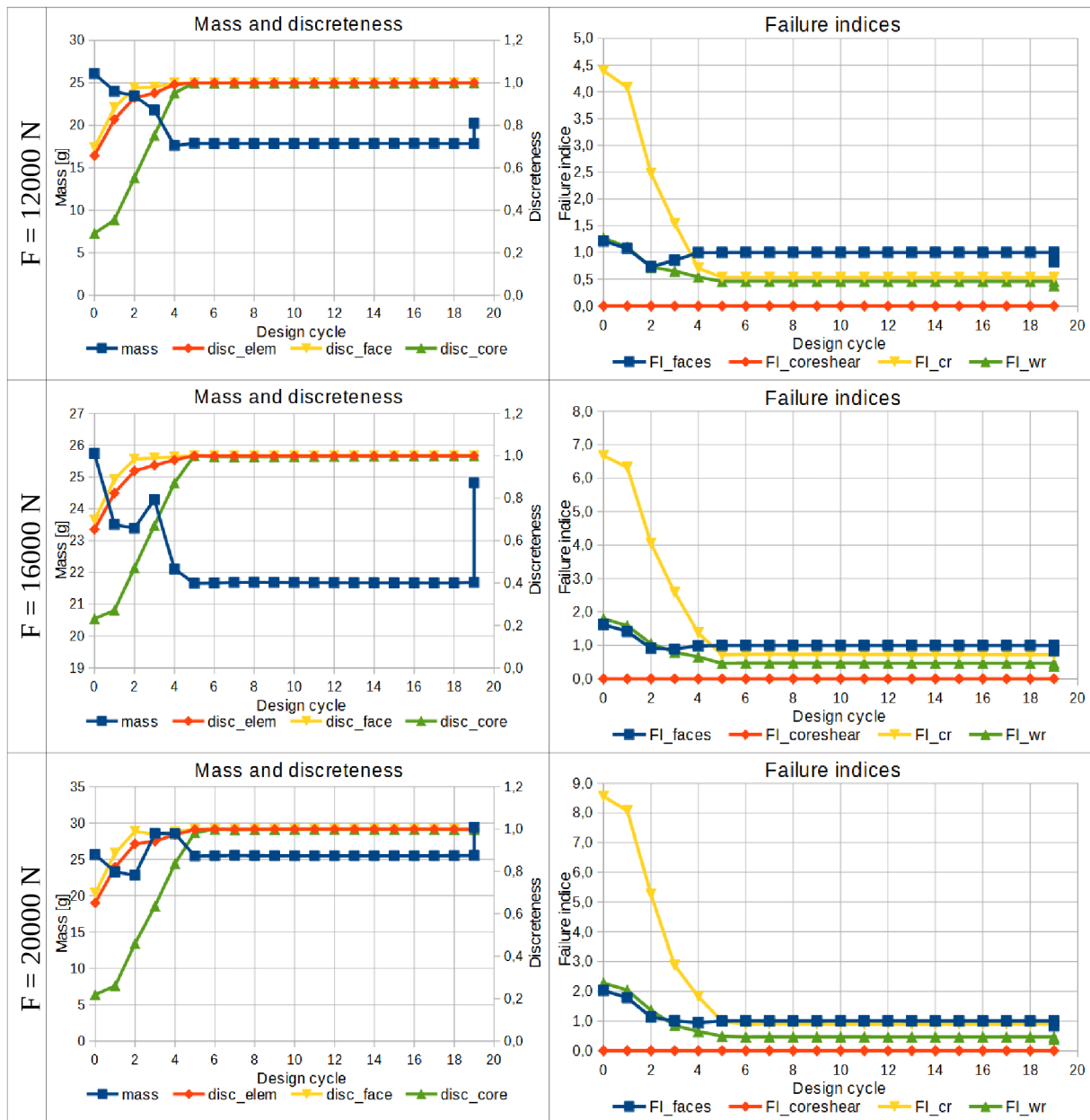
5.1.2 Beam bending and transverse shear

The same dimensions and design materials were used for the beam example which consists again of one element, now fixed on one edge and loaded on the opposite end by the transverse shear force T and the bending moment M (Figure 27 right). The algorithm works with internal loads at the element center so that the loads at this point drives the design and so T_{center} and M_{center} are used for reference in Tables 5.6 and 5.7. Compared to the compression example, core shear failure may occur in this case, but not crimping. Bending moment should lead to higher thickness core and more face-sheet layers. Wrinkling and core shear will drive core density, but core thickness helps also to decrease core shear failure.

*Table 5.6: Results for the element loaded by transverse force and bending moment.*

| Loads							
T_{center} [N]	**200**	**200**	**200**	**400**	**400**	**800**	**1200**
M_{center} [Nm]	**10**	**50**	**90**	**22**	**24**	**50**	**70**
Values at the end of optimization							
Discreteness	1.000	1.000	1.000	0.999	1.000	1.000	0.999
m [g]	6.56	16.00	23.45	11.52	11.06	15.99	19.77
FI max	0.88	1.00	1.00	1.00	1.00	1.00	1.00
Rounded layup							
Face-sheet	0/	0_3/	0_4/	0_2/	0°/	0_3/	0_3/
t_{core} **[mm]**	5	10	10	5	10	10	10
ρ_{core} **[kg/m³]**	80	130	130	130	130	130	130
Properties after rounding							
m [g]	6.58	20.23	24.81	12.41	11.08	20.23	20.23
FI faces	0.83	0.69	0.92	0.90	0.99	0.69	0.96
FI coreshear	0.70	0.16	0.15	0.60	0.36	0.63	0.95
FI wr	0.54	0.29	0.38	0.37	0.44	0.29	0.41
True optimum							
		t_{core}=10mm ρ_{core}=60 kg/m³	t_{core}=10mm ρ_{core}=60 kg/m³	face: 0/ t_{core}=10mm ρ_{core}=80 kg/m³	face: 0/ t_{core}=10mm ρ_{core}=80 kg/m³		
m_{opt} **[g]**		16.73	21.31	8.58	8.58		

The overview of the results is in Table 5.6. Evolution of the measures are in Table 5.7. The set of loads at the element center is selected to investigate cases with low transverse shear and increasing bending moment as well as larger transverse shear and increasing bending moment.

The optimization was successful in reaching a feasible and discrete solution, but not optimal in all cases. Three cases reached the optimum, four did not, but only one of them ended with more than necessary number of face-sheet layers, so the optimization mostly used a denser core than necessary.

- Load case T_{center}= 200 N and M_{center}= 10 Nm led to the core with density 80 kg/m^3, the thickness and number of face-sheet layers were minimal. All graphs stabilized after design cycle 4.

- Load case T_{center}= 200 N and M_{center}= 50 Nm led to 3 layers of face-sheet and thicker core, but stacked at high density 130 kg/m^3. Graphs stabilized after design cycle 5, but there are large steps in mass and face FI in the final rounding. Note that the mass before rounding 16 g is close to the optimum 16.73 g with softer core. That shows that the algorithm was able to find a local minimum close to the global one, but rounding to a discrete number of face-sheets degraded the solution.

- Load case T_{center}= 200 N and M_{center}= 90 Nm was very similar – heavier than necessary core and visible increase of the mass in the final rounding.

- Load cases with T_{center}= 400 N and M_{center}= 22 Nm or M_{center}= 24 Nm are interesting because of the lighter solution achieved with higher loads. The solution with lower load combined a thinner core with stronger face-sheets. Graphs evolved slowly and the core discreteness is low for a very long time, especially in the less loaded case, which points that the core was not clearly selected for most of the run time. Finally, a feasible solution was found, but not with minimal mass.

- Last two load cases with T_{center}= 800 N and M_{center}= 50 Nm, and T_{center}= 1200 N and M_{center}= 70 Nm had not much options fort core selection due to high shear load and (maybe thanks to it) their graphs stabilized soon and led to the optimal solution.

Table 5.7: Mass, discreteness, and failure indices during design cycles.

$T_{center}=1200$ N. $M_{center}= 70$ Nm

$T_{center}= 800$ N. $M_{center}= 50$ Nm
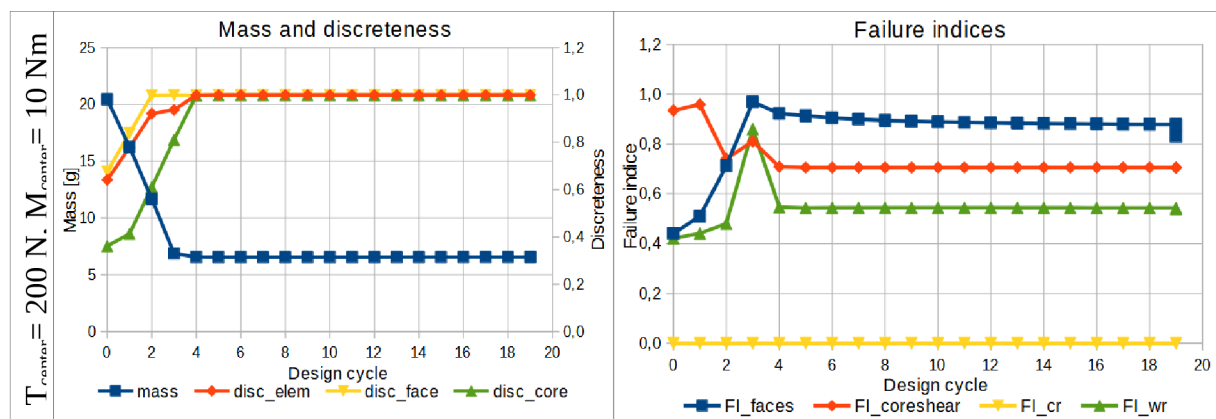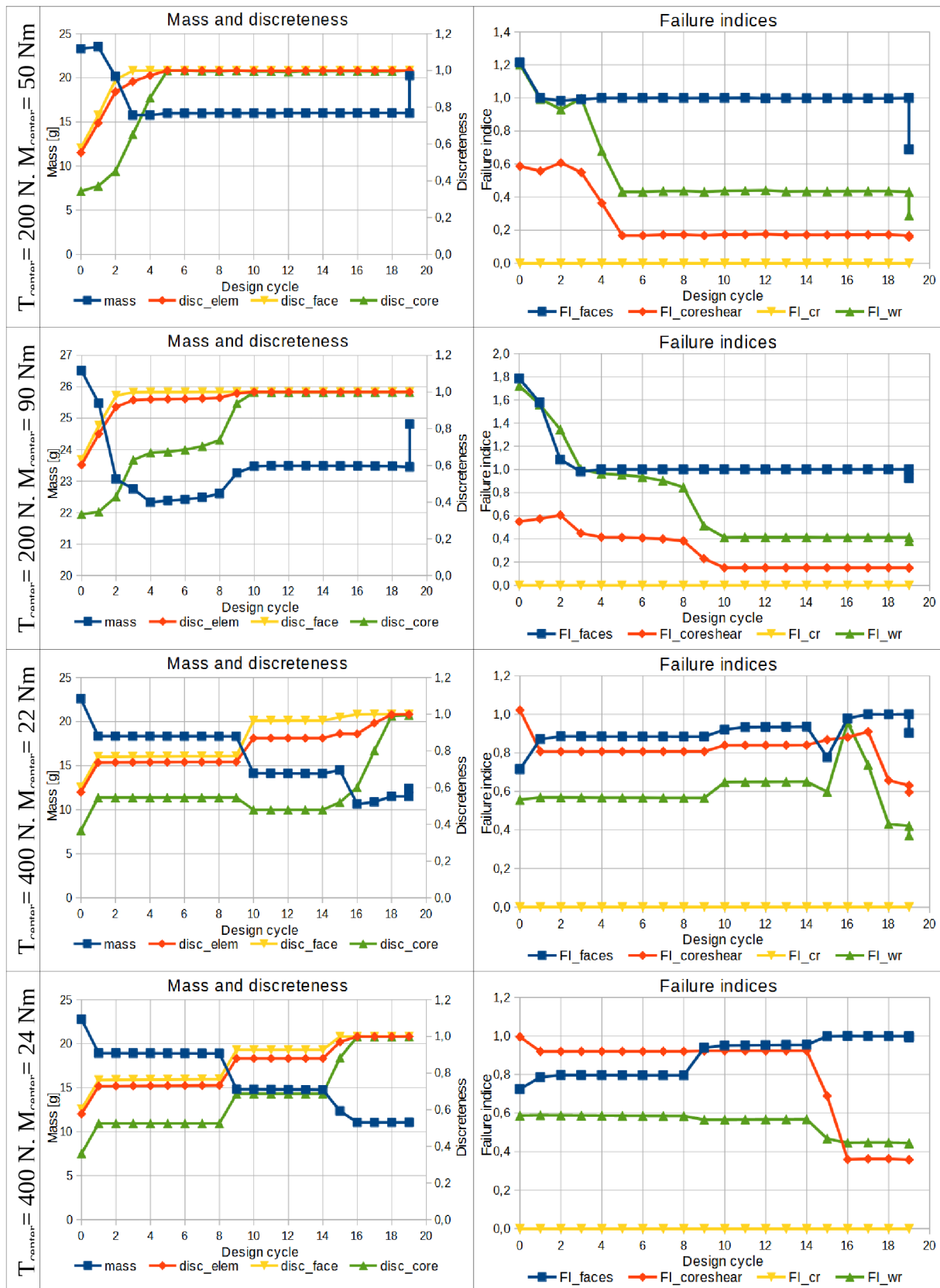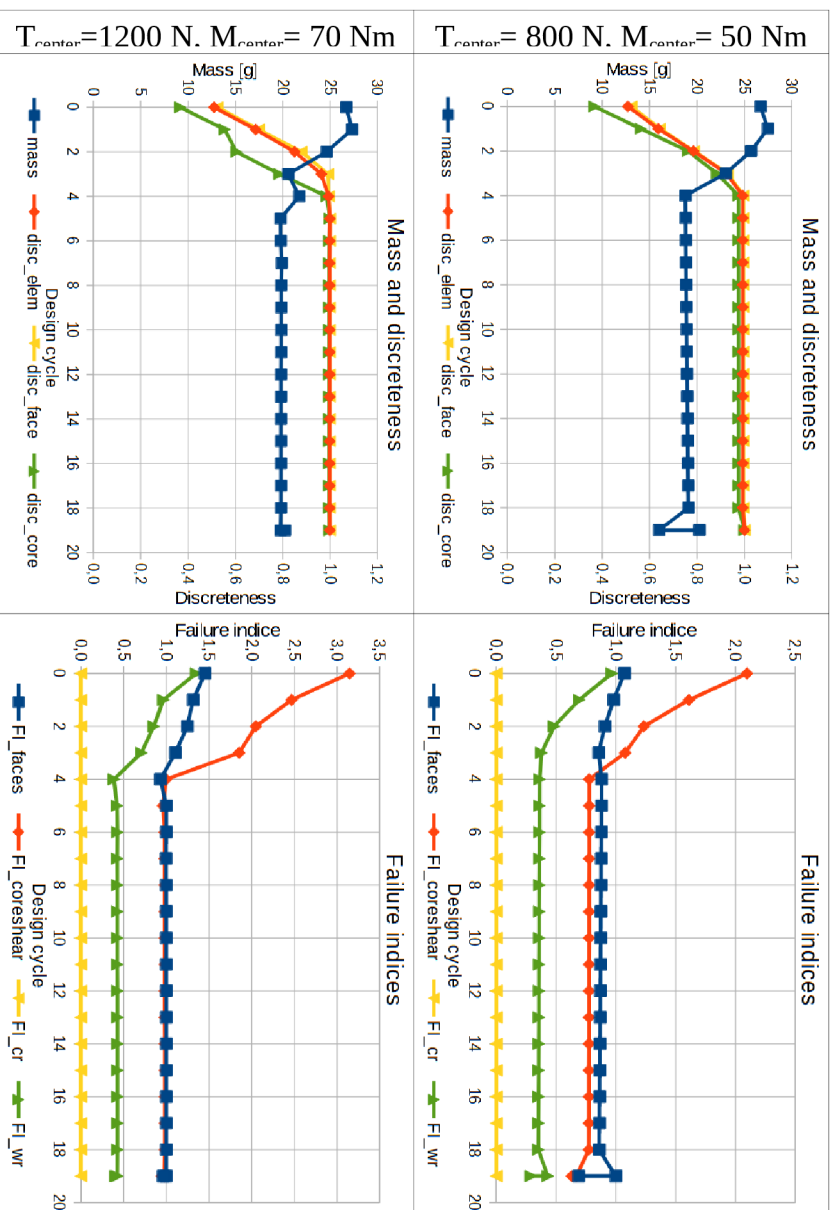
5.2 Separated elements

The next example contains 14 elements which are separated, so that the element forces and moments, shown in Figure 28, will not change during optimization. Elements are fixed on one side. Eight elements are loaded with increasing compression force F, while other six elements are loaded with increasing transverse force T which cause bending moment at the element center M_{center}.

Design materials:

- Four UD carbon/epoxy composites for the face-sheet layers (0°, 90°, +45°, and -45°) for up to 5 layers (each with thickness 0.256 mm). Face-sheets are symmetric (same top and bottom face).

- Four core candidates (foams 80 and 130 kg/m^3 both with 5 and 10 mm thickness).

The task consists of 350 design variables which are linked through 84 material (linear) constraints. Failures define 210 nonlinear constraints. Optimization took 6 minutes with more than half spent on Jacobian evaluation.
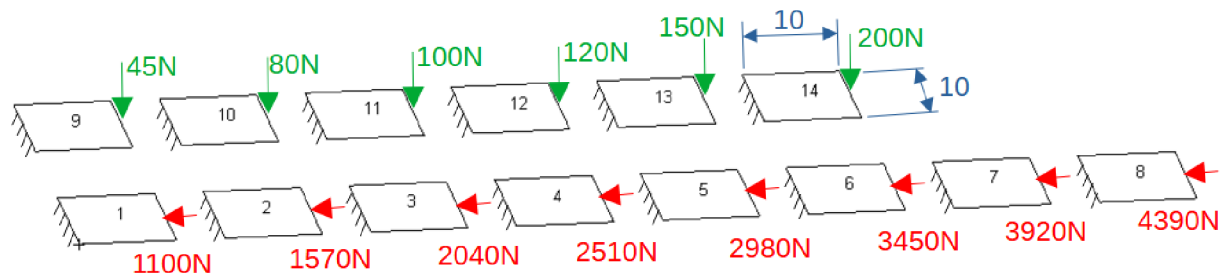

Figure 28: Separated elements with loads and boundary conditions.

The optimization converged well as can be seen in Figure 29 as the evolution for the selected measures show. All of them stabilized after design cycle 8. Average discreteness reached the value 1.000 on all elements for the core as well as face-sheets. Mass has a small step due to the rounding of face-sheet thickness. Maximal failure indices plotted in the graph dropped from higher initial values to finish close to 1 for all failure types.
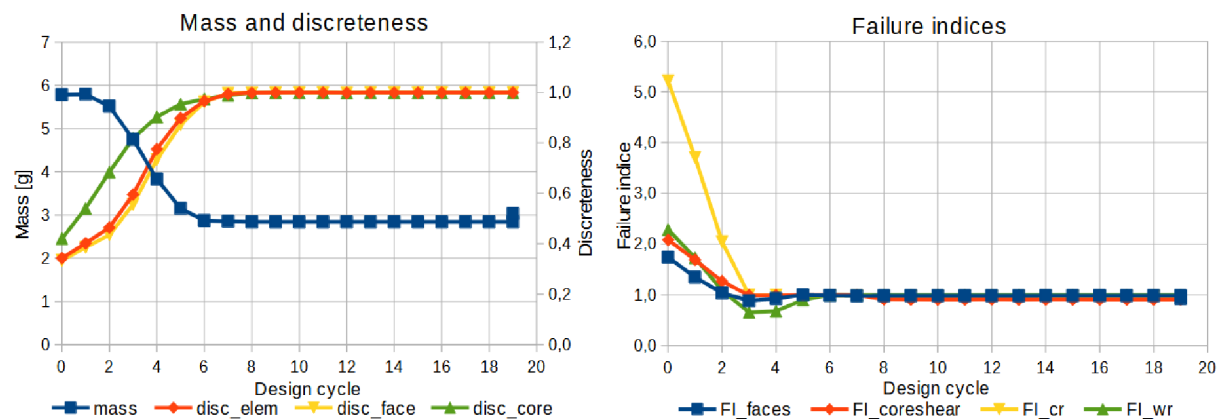

Figure 29: Mass, discreteness, and failure indices during design cycles.

Table 5.8 shows the loads for each element (in-plane force F for elements 1-8, or transverse force and bending moment at the element M_{center} for elements 9-14). Optimization found correctly the optimal number of face-sheet layers on all elements, but elements 1-3 have thicker core than necessary and element 1 has also higher core density than needed. That might be due to the initial failure constraint violation when the optimization got on the track of the stronger core and later when it was not violated any more and rather discrete, the variables stack to the heavier core.

This example was extensively used for selecting robust default parameters for the optimization. Primary concern was to achieve discrete results without failing elements, which were achieved in this case, but with the price of some elements to be heavier than necessary.

Table 5.8: Resulting layups and failure indices.

Element	1	2	3	4	5	6	7	8
F [N]	1100	1570	2040	2510	2980	3450	3920	4390
Rounded layup								
Face-sheet	0/	0/	0/	0_2/	0_2/	0_2/	0_2/	0_3/
t_{core} [mm]	10	10	10	10	10	10	10	10
ρ_{core} [kg/m^3]	80	80	80	80	80	80	80	80
FI_{faces}	0.50	0.71	0.93	0.58	0.68	0.79	0.90	0.68
FI_{cr}	0.24	0.35	0.45	0.56	0.66	0.77	0.87	0.98
FI_{wr}	0.53	0.75	0.98	0.61	0.72	0.84	0.95	0.71
True optimum								
t_{core} [mm]	5	5	5					
ρ_{core} [kg/m^3]	60	80	80					

Element	9	10	11	12	13	14
T [N]	45	80	100	120	150	200
M_{center} [Nmm]	225	400	500	600	750	1000
Rounded layup						
Face-sheet	0/	0/	0/	0/	0/	0/
t_{core} [mm]	5	5	5	10	10	10
ρ_{core} [kg/m^3]	60	80	80	80	80	80
FI faces	0.04	0.07	0.09	0.06	0.07	0.09
$FI_{core\ shear}$	0.81	0.69	0.86	0.54	0.68	0.91
FI_{wr}	0.06	0.07	0.09	0.06	0.07	0.10

Constraint aggregation

Constraint aggregation was done for a set of aggregation parameters ρ_{KS} from 2 to 100, which is used in eq. (82). Table 5.9 shows results. When $\rho_{KS} = 20$ and more, the optimization did not converge as can be seen from low discreteness. Consequently, the mass m after rounding is height and the maximum failure index is above 1. Lower ρ_{KS} resulted in a feasible solution with discreteness close to 1. Aggregation with $\rho_{KS} = 5$ and 10 gave the lowest mass, but it is still more compared to non-aggregated solution due to the heavier than necessary core.

It was expected that constraint aggregation will decrease the calculation time, but the example took approximately the same time (around 6 minutes) with and without aggregation. Mild speed increase due to the lower number of failure constrains was balanced with worse convergence.

Table 5.9: Overview of (rounded) results with various aggregation parameters ρ_{KS}.

ρ_{KS}	2	3	5	10	20	50	100	Not aggregated
Discreteness	0.99	1.00	1.00	1.00	0.57	0.38	0.35	1.00
m [g]	3.42	3.35	**3.12**	**3.12**	4.19	4.64	4.38	**3.03**
max FI	0.98	0.98	0.98	0.98	1.32	1.65	1.97	0.98

5.3 Panel with pressure or side load

This example consists of a 700×1400 mm panel loaded by the normal pressure 50 kPa with fixed edges in the first variant and simply supported edges in the second variant. Third variant has one edge fixed, the middle of the opposite edge is loaded by 6000 N in each of the 9 nodes (the distribution is to decrease stress concentration). It was meshed with 16×32 quad8 elements (second order quadrilateral elements with 8 nodes) as shown in Figure 30. This example follows the results published in the article [68].
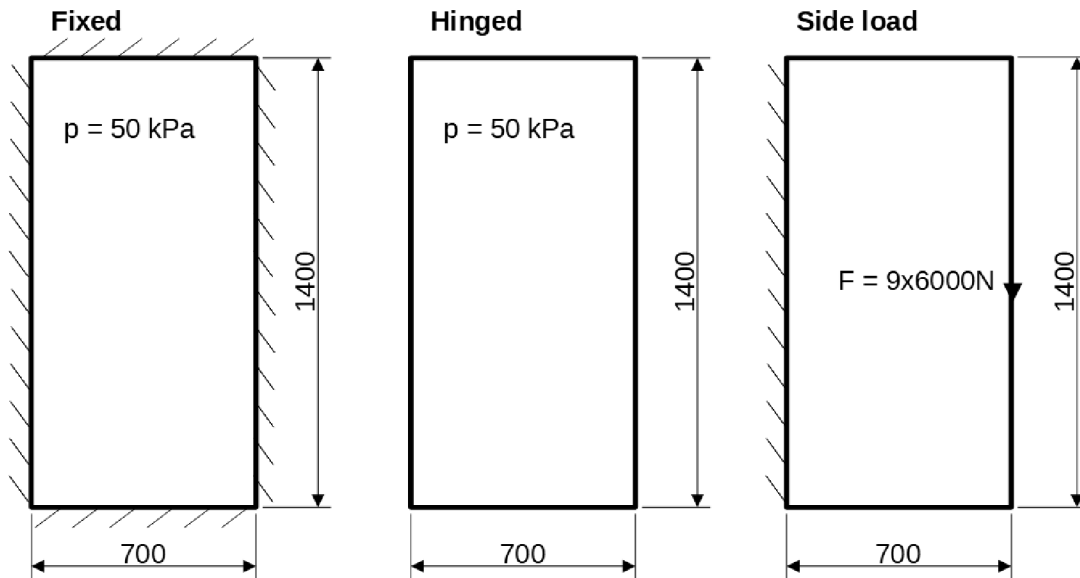

Figure 30: Panel with different boundary conditions [68].

Design materials:

- Four unidirectional layer candidates for the face-sheet layers (0°, 90°, -45°, and 45° UD carbon) for up to 5 layers. Face-sheets are symmetric (same top and bottom face).

- Six core candidates (foams 60, 80, and 130 kg/m^3 all with 5 and 10 mm thickness).

5.3.1 Variable stiffness

Although the settings for various optimization parameters are not presented for their extension, this example was used to find robust default parameters since element loads depend on element stiffness and evolve during optimization, contrary to previous simple examples which focused on the basic function of the optimization which quick runtime easy to test the code.

In these settings, each of the 512 elements had its own design variables, which led to 12800 design variables linked through 3072 material (linear) constraints and 7680 failure (nonlinear) constraints. Optimization took around 3 hours (fixed and hinged plates), resp. 3.5 hours (side loaded panel), with 80% of the time spent on Jacobian evaluation.

Table 5.10: Mass, discreteness, and failure indices during design cycles.
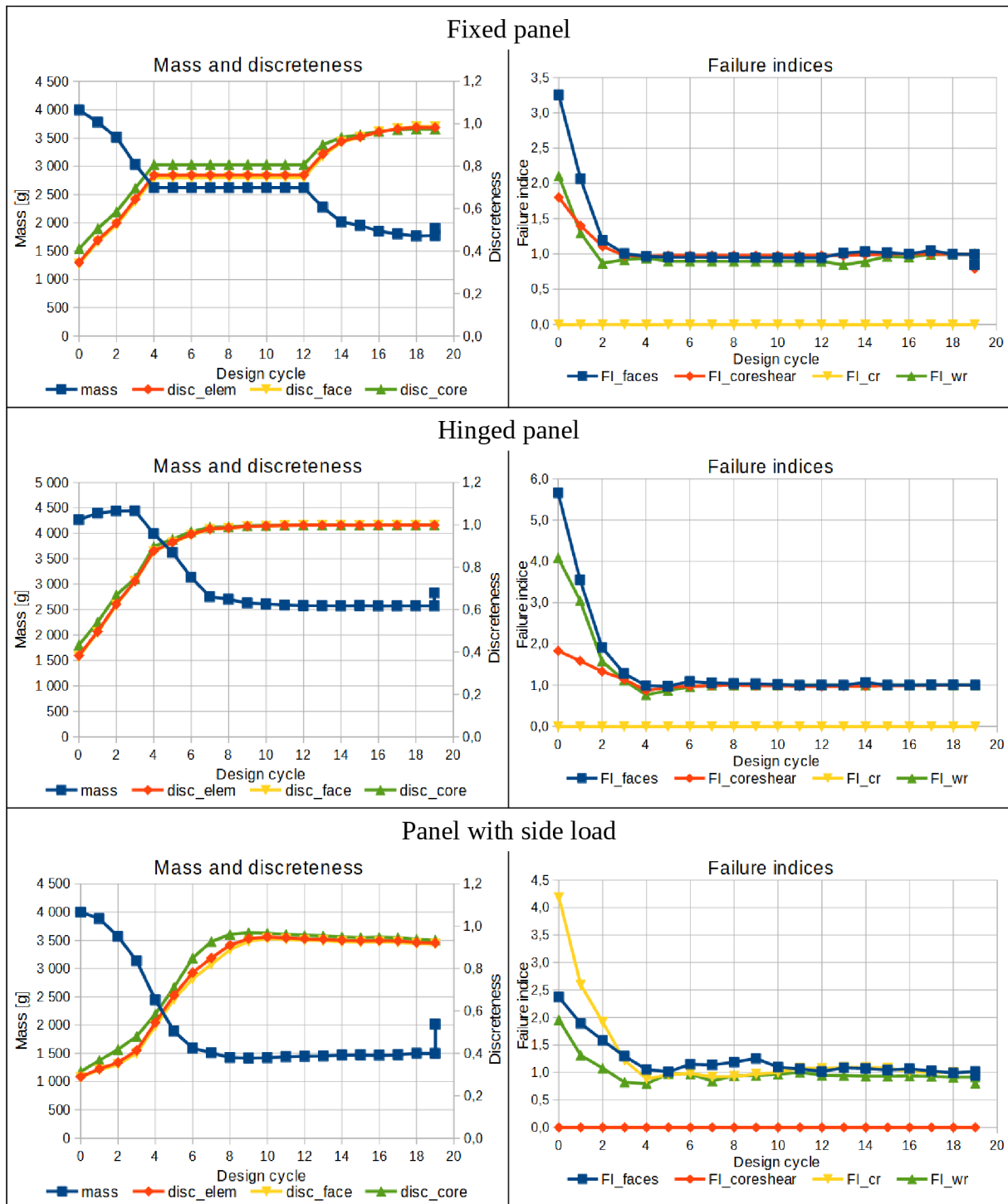
Fixed panel converged to discreteness 0.983 with max. FI 1.01 due to slight violation of the wrinkling criterion after rounding. Graphs in Table 5.10 for the fixed panel show that the discreteness increased at the beginning, stayed constant in the middle, and rose at the end towards 0.983, so the convergence was not as smooth as in other examples, but the failure constraints remained around 1 for most of the design cycles. Figure 31 shows the final discreteness and failure index distribution. Discreteness of the face-sheets is above 0.85, some

elements have core discreteness only above 0.53, which can be explained that the optimization did not fully decide for the core on such elements, but important is that these elements do not have a failure, as can be seen on the right plot. Layup in Figure 32 is with numbering from the outer layer to the core, the opposite face-sheet is symmetric. The figure shows that the fixed panel has empty outer layers 1-3. A pattern in orientation is that the layup of most elements is oriented towards the nearest edge or corner. The core has weaker material in the middle and on the diagonals connecting corners. Stronger core is close to edges. The algorithm carries out an alternative rounding to a heavier core if that core material has a design variable above 1%. In this particular example, the mass increased by 0.5% and max. FI decreased to 0.98.

Hinged panel has straight convergence. Graphs in Table 5.10 stabilized after design cycle 9, but the final max. FI is 1.01 due to slight violation of the wrinkling criterion after rounding. Figure 31 shows high discreteness in face-sheets (above 0.95) and even higher for core discreteness. Max. FI is also on most elements with high values close to 1. Layup in Figure 32 is different from the fixed panel and shows little covering in layers 1 and 2. Segmentation is visible. Middle segment has 0° orientation, the segments close to the corners are oriented diagonally to the bridge area of each segment. Core is almost everywhere with the strongest option.

Panel with side load has no symmetry in loading nor in layup. In the graph in Table 5.10, the discreteness reaches high values at design cycle 9 but slightly decreases after that to finish with average discreteness 0.92 due to waves on FI which ends on 0.96. Figure 31 shows that discreteness is rather uniformly lower, but some elements are weaker in face-sheet discreteness starting at 0.49. Max. FI is high on a few elements, low FI is in the center and top right corner, but there are still two face-sheet layers in Figure 32, which might be associated with a significant step up during rounding in Table 5.10. Otherwise, layers 1-3 are populated only on a few elements with stress concentration. Layers are oriented mostly in +45 or -45 from the fixed edge towards the load area. Core is reinforced in the segment with compressive load.
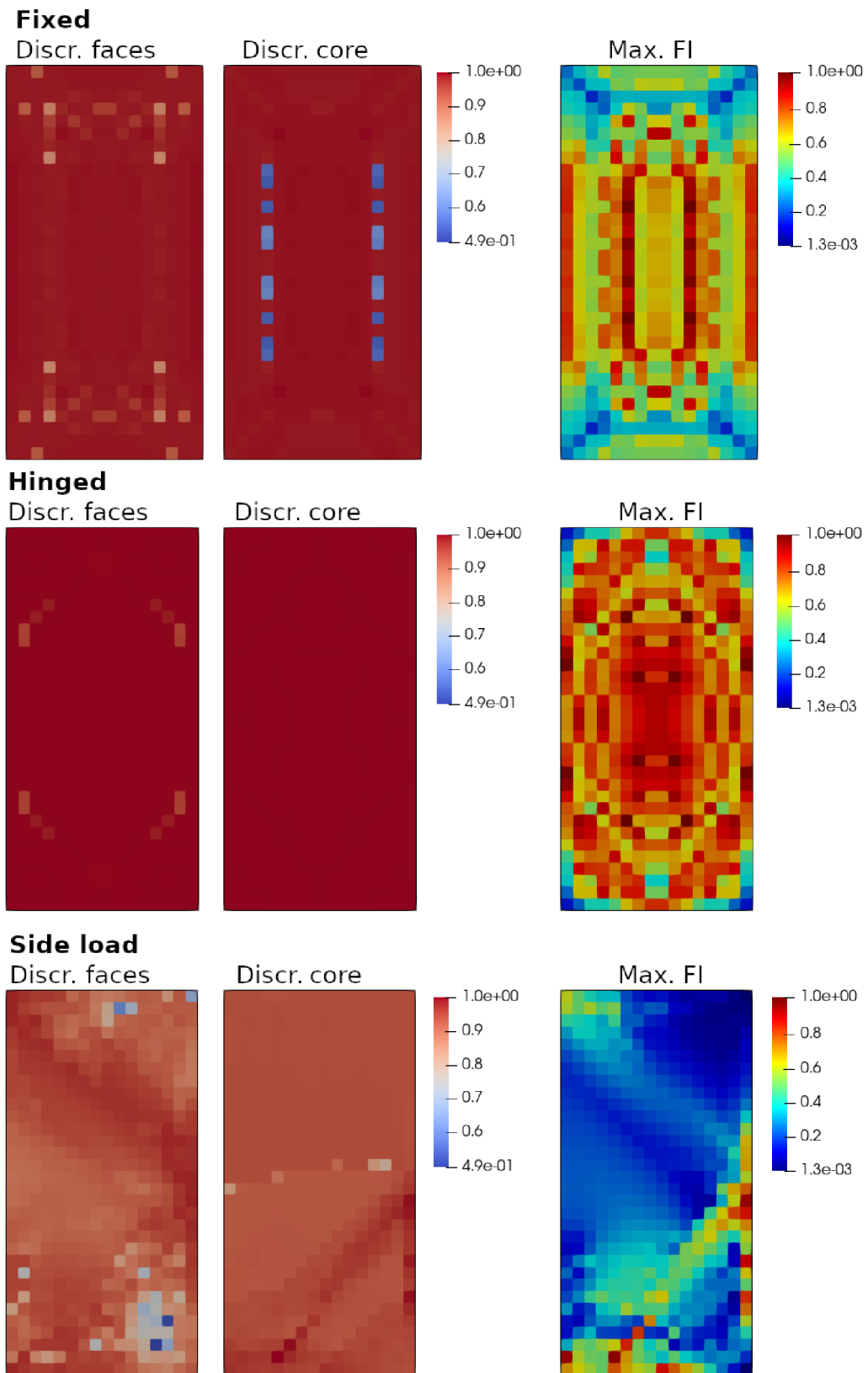
Figure 31: Core and face-sheet discreteness, maximum failure index.
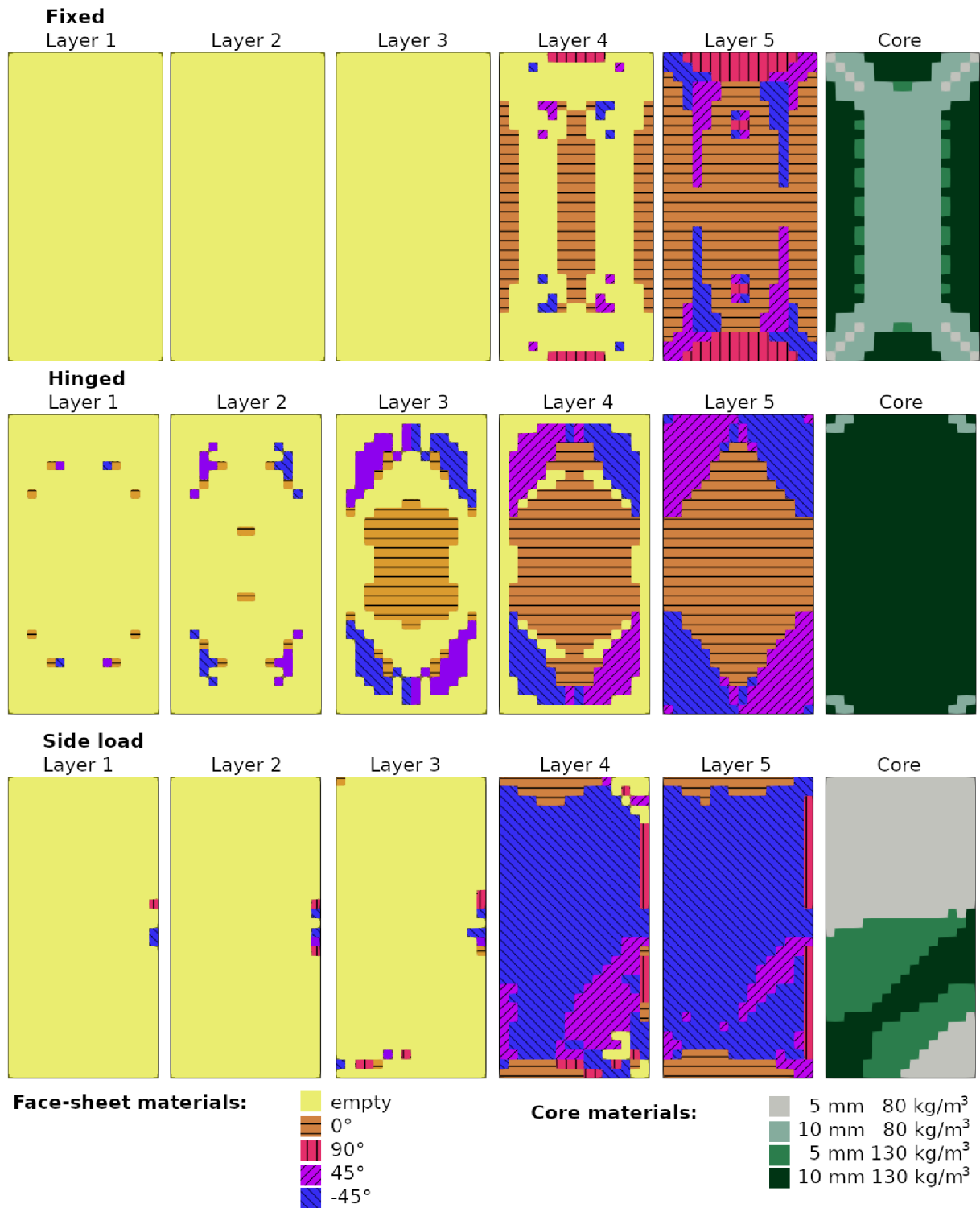
Figure 32: Layup for different boundary conditions, opposite face-sheet is symmetric.
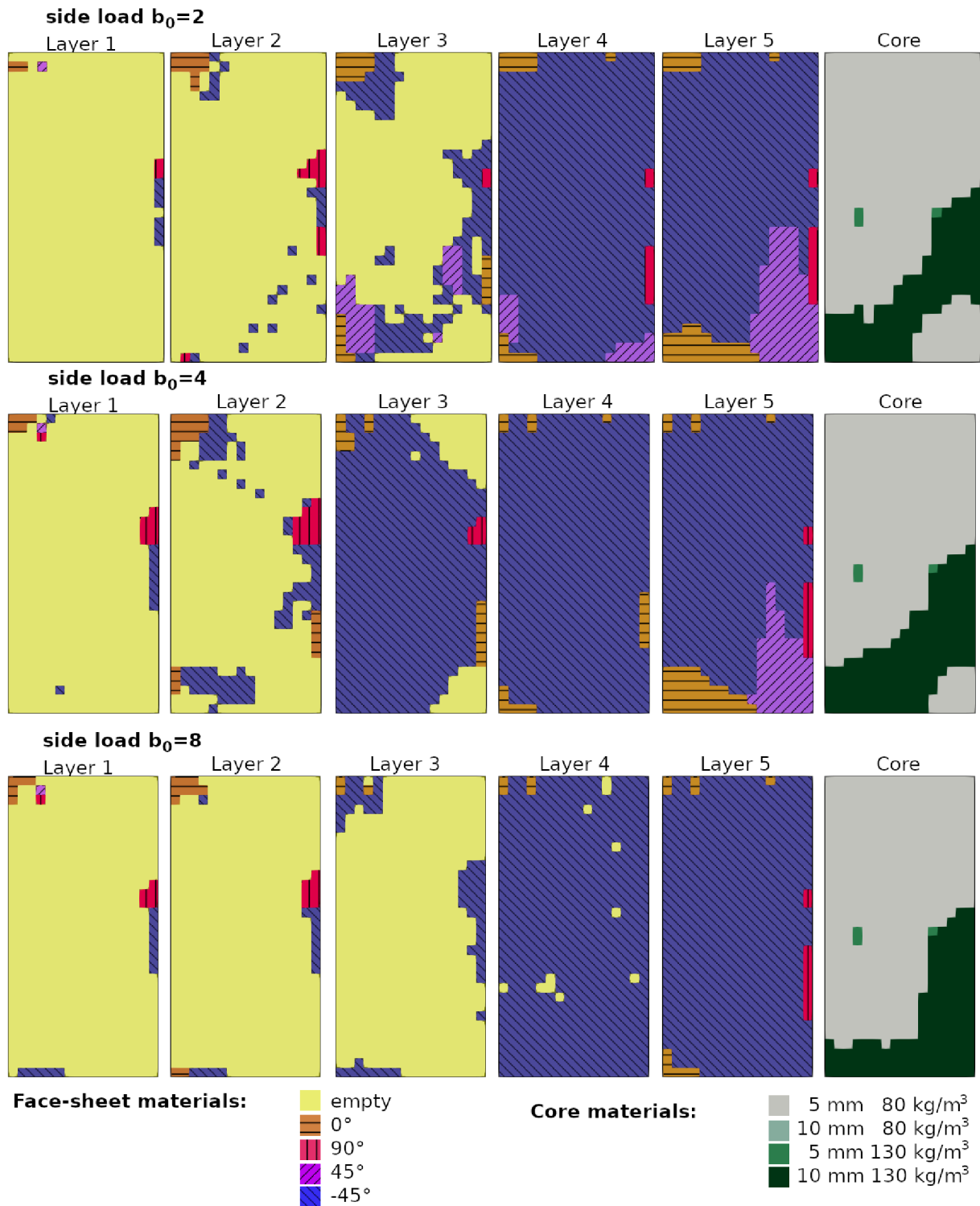
Figure 33: Layup for the panel with side load with different blending parameter b_0.

Blending

Blending was used for all panels, but hinged and fixed panels did not give much distinct results from the solution without blending, thus only the panel with side load is presented. It was calculated for $b_\varepsilon=0.1$ and three values of b_0 (2, 4, and 8). Because of difficult

convergence, the number of optimizer iterations i_{max}=20 was doubled compared to the default value. Figure 33 shows the final layup of the panel with side load for different parameters b_0. It can be seen that the areas with the same material are more compact as b_0 increases, so that b_0=8 has almost continuously filled layers 4 and 5 with -45°. In all cases, the core has practically only two foams present. For b_0=8, heavier core stacked to the corner, which can be interpreted as a trial to decrease the boundary between different core materials. When blending was used, the mass increased variously according to the parameters b_ε and b_0. For b_ε=0.1, b_0=8, it increased by 7%.

Effect of stress concentration

Panel with side load is, according to Figure 30, loaded by a force distributed to 9 nodes to diminish the stress concentration. In the following comparison, the force is concentrated to one node as used to be in engineering practice according to Saint-Venant's principle when stress concentration is ignored during engineering interpretation.

Table 5.11 compares the results with different parameters A_{ign} denoting a portion of the elements with ignored failure constraints. When the force is concentrated and none element is ignored (A_{ign} = 0), the optimization did not converge as can be deducted from low discreteness 0.51 and mass almost two times larger than in the case of distributed load. This behavior can be interpreted by the optimizer which has a priority on a solution feasibility, so that the objective function (penalized mass) is not much taken into account. As a result, only one element under the concentrated load is failing. As A_{ing} increased to 0.01 (ignoring 5 elements from total 515 elements), the discreteness and mass improved, but A_{ing} = 0.015 (ignoring 7 elements) or more was needed to reach discreteness and mass similar to the original case with distributed load where layup was very similar to the original case in Figure 32.

It appears that ignoring some elements is necessary when a model contains concentrations which cannot be designed with available materials to fulfill failure constraints. The price for element ignoring is that the final design contains several failing elements which position was not determined by the user, but important is that the optimizer is able to converge.

Table 5.11: Comparison of force application and parameters to ignore area A_{ign}.

	Distributed load	Concentrated force				
A_{ign}	**0**	**0**	**0.01**	**0.015**	**0.02**	**0.025**
Number of ignored elements	0	0	5	7	10	12
Number of failing elements	0	1	4	7	10	9
Discreteness	0.92	0.51	0.78	0.96	0.95	0.96
m [g]	**2019**	3908	2786	1997	1989	1984

Constraint aggregation

The effect of constraint aggregation was tested on cases with each boundary condition for aggregation parameters ρ_{KS} from 2 to 100. Discreteness, mass, and maximum failure index are compared with the solution without aggregation in Table 5.12.

For the *fixed panel*, the best results are with ρ_{KS} = 10 (lowest mass and not violated constraints) and the results do not differ too much from the solution without aggregation (mass increase by 12%). For lower ρ_{KS}, the discreteness is above 0.8 which is still not much, but the mass is quite high for ρ_{KS} = 2. Contrary, for ρ_{KS} = 20 and more, discreteness is unsatisfactory and the constraints are strongly violated.

For the *hinged panel*, the lowest mass is for ρ_{KS} = 5, but it is already by 55% heavier than the solution without aggregation. Discreteness is above 0.9 for ρ_{KS} up to 5, then it drops to low values together with high constraint violation. Contrary to expectations, the optimization time increased due to aggregation from approximately 3 hours to 4 hours.

For the *panel with side load*, the low mass is also for ρ_{KS} = 5 with mass increased by 55%. Constraints are violated for higher ρ_{KS}. Discreteness is low for all aggregated results. Since the discreteness is the lower for not aggregated solution compared to the fixed and hinged panels, it might be concluded that this example converges harder, but the constraint aggregation decreases the quality more than in the previous cases.

Table 5.12: Overview of (rounded) results with various aggregation parameters ρ_{KS}.

Fixed							
ρ_{KS}	**2**	**3**	**5**	**10**	**20**	**50**	**100**	**Not aggregated**
Discreteness	0.86	0.81	0.82	0.59	0.35	0.37	0.38	0.98
m [g]	3871	3274	2976	**2127**	1809	1808	1805	**1901**
max FI	0.65	0.65	0.69	0.79	4.11	3.27	3.22	1.01

Hinged							
ρ_{KS}	**2**	**3**	**5**	**10**	**20**	**50**	**100**	**Not aggregated**
Discreteness	0.97	0.97	0.93	0.57	0.35	0.35	0.36	1.00
m [g]	4077	4056	**3991**	4028	1800	1799	1807	**2574**
max FI	0.91	0.83	0.94	1.24	7.92	6.71	5.53	1.01

Side load							
ρ_{KS}	**2**	**3**	**5**	**10**	**20**	**50**	**100**	**Not aggregated**
Discreteness	0.36	0.45	0.50	0.44	0.41	0.43	0.44	0.92
m [g]	4042	3780	**2914**	1803	1801	1799	1797	**2019**
max FI	0.86	0.83	0.96	1.85	2.22	3.07	2.79	0.96

Refined mesh

New models were made with the element size two times lower, leading to 2048 elements instead of 512, thus the number of design variables increased to 51200, material constraints to 12288, and failure constraints to 30720. This resulted in the optimization time more than 16 hours (5-7 times more than the original mesh). Layups are not presented, since they were similar with the fine mesh as with the original mesh in Figure 32. Overall results in Table 5.13 show that the solution quality rather decreased. Although the optimal mass can theoretically alter due to the higher number of element centers (where failures are evaluated), the maximum FI increased in all cases and violated constraints. For the fixed panel, max. FI increased by 9%, for the hinged panel by 1%, and for the panel with side load FI=1.03 occurred. The decrease in solution quality for the panel with side load is visible also in discreteness which dropped to 0.70, thus A_{ign} parameter was tried, set to ignore 1% of elements, but the solution did not improve significantly.

Possible explanation of the increase in max. FI is that a high number of variables is more difficult to solve for the optimizer and/or that the optimization parameters were primarily defined to achieve good results on the original mesh and so are not so robust for larger tasks.

Table 5.13: Comparison of original mesh 16×32 and refined to 32×64.

	Fixed		**Hinged**		**Side load**			
Mesh	**16×32**	**32×64**	**16×32**	**32×64**	**16×32**	**32×64**	**16×32**	**32×64**
A_{ign}	**0**						**0.01**	
Discreteness	0.98	1.00	1.00	0.97	0.92	0.70	0.96	0.78
max. FI	1.01	1.10	1.01	1.02	0.96	1.03	1.65	1.75
Number of failing elements	4	12	8	8	0	1	5	16
m [g]	1901	1868	2828	3141	2019	2289	2052	2116

5.3.2 Patch design

Panels were optimized with the use of one patch on all elements, so that the independent design variables were only on one element and the other element layups are driven by the same variables, which leads to a uniform layup on the whole panel. The number of design variables was only 25, 6 material constraints, but 7680 failure constraints remain. Optimization took 2-2.5 hours, which is only by ~35% less than the case where every element has its own layup.

Results from these settings are in Table 5.14. All variants of boundary conditions finished with discrete results and with a feasible solution (FI < 1). All cases ended with the strongest core. For the fixed panel, face-sheet is over dimensioned, because 2 layers with 0° orientation would transfer the loads without failure violation, but 3 layers were in the end of the

optimization. Hinged panel seems to be correct with 2 layers. Panel with side load has 5 layers in the face-sheet where removing one would violate constraints. The orientation corresponds to the results with blending in Figure 33 where layers 1, 2, and 3 were mostly empty.

Table 5.14: Results for one patch over the panel.

	Fixed	Hinged	Side load
Discreteness	1.00	1.00	1.00
max. FI	0.83	0.71	0.94
Face-sheet	45/-45$_2$/	0$_2$/	-45$_5$/
Core	10 mm 130 kg/m^3		

5.4　Box with top underpressure and torque

5.4.1 Sandwich panels

Long box example with ribs is in Figure 34. It is cantilevered on the left end and loaded by tensile underpressure 15 kPa on the top side and torque on the circumference of the ribs through RBE3 elements, 2 Nm on each. Size of the load was selected to fit the load capacity of the sandwich with the layup used in this thesis. It resembles aircraft wing loading, but it is not any specific case. The mesh consists of 990 quad8 elements. Each panel was defined as one patch, so that the model contains 25 patches. That together with design materials lead to 375 design variables, 150 material constraints, and 14850 failure constraints.

Design materials:

- Two fabric candidates for the face-sheet layers (0° and 45° carbon fabric) for up to 5 layers (each with thickness 0.327 mm). Face-sheets are symmetric (same top and bottom face).

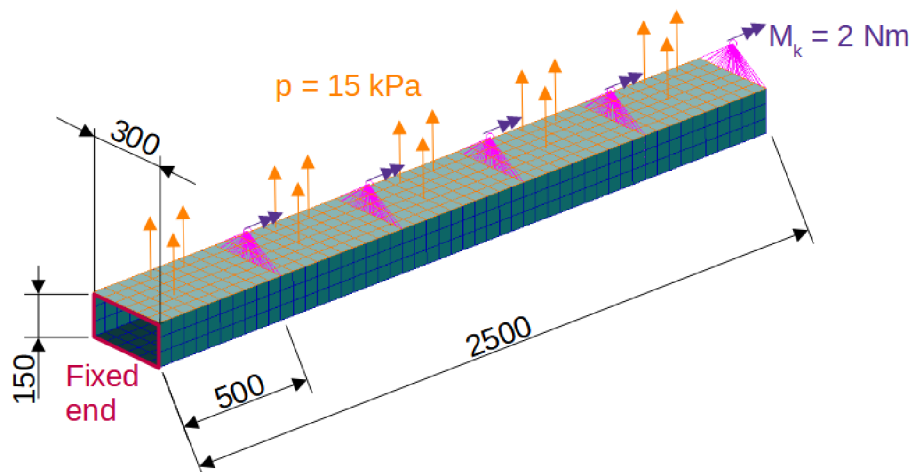- Four core candidates (foams 80 and 130 kg/m^3 both with 5 and 10 mm thickness).

Figure 34: Schema of the box example.

Optimization parameters were altered to find better a solution as concluded in Table 5.15. All settings led to a feasible solution, but the differences in the final mass are large. Default setting is the first column with the maximum number of optimizer iterations i_{max}=10 and maximum change of the design variables within a design cycle Δ_{max}=0.2. Altering of these parameters helped to achieve a better result by smaller step in variables (Δ_{max}) and more iterations on each design cycle (i_{max}) as can be concluded from discreteness 1.00 for cases with i_{max}=20 and the lowest mass when combined with Δ_{max}=0.15. Therefore, graphs and layups will be shown for these settings. Optimization time increased by ~50% from approximately 2 hours (default settings) to more than 3 hours (the best solution).

Table 5.15: Result comparison for different i_{max} and Δ_{max}.

i_{max}	10	15	20	10	15	20
Δ_{max}		0.2			0.15	
Discreteness	0.96	0.96	1.00	0.93	0.99	1.00
max. FI	0.79	0.79	0.79	0.79	0.79	0.90
m [kg]	9.863	10.018	6.928	9.912	8.536	6.613

Maximal failure index in Figure 35 drop soon below 1 and remains relatively stable. Discreteness grows up to design cycle 6, remains stable, and finally grows to 1. Mass has the opposite behavior with a large drop rather close to the end. The ramp in the middle of discreteness is due to the convergence criteria prescribed to the optimizer (the goal discreteness of the design cycle in Figure 25 is reached immediately) and so the next design cycle may start without significant change of the model.
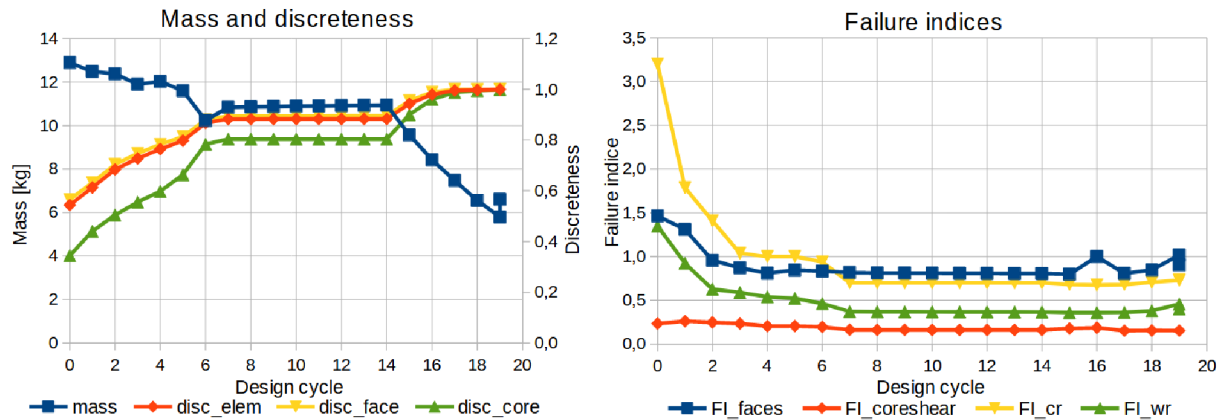

Figure 35: Mass, discreteness, and failure indices during design cycles for $i_{max}=20$, $\Delta_{max}=0.15$

Table 5.16 shows the final layups of the patches. As expected, a stronger core and more face-sheet layers are close to the root where the maximum of bending moment and torque is. Top panels have a stronger core which can be easily explained by the underpressure load and by the fact that the top panels are loaded in compression from the bending moment. Top and bottom panels contain only 0° oriented face-sheets as expected. Front and back panels close to the root (segments 1 and 2) have also face-sheets in 0° orientation probably due to participation in bending moment transfer. Other segments of the back and rear panels have orientations 45° which points to torque loads. All ribs have only a light core and one face-sheet layer, some with 0° and some 45° orientation, which both safely satisfy the failure constraints so the optimizer need not prefer any of them.

Figure 36 shows the maximum failure indices on the panels. It is obvious that the ribs are not much loaded as well as the tip section. Front and back panels in section 3 are less effectively used, which seems that lighter layup is probably possible there.

Table 5.16: Layup of segments 1-5 from the fixed root to the free tip for $i_{max}=20$, $\Delta_{max}=0.15$

| Segment	1 (root)	2	3	4	5 (tip)
Top	0_5/ 10 mm 130 kg/m^3	0_3/ 10 mm 130 kg/m^3	0_2/ 10 mm 130 kg/m^3	0/ 5 mm 130 kg/m^3	0/ 5 mm 130 kg/m^3
Bottom	0_5/ 10 mm 80 kg/m^3	0_3/ 5 mm 80 kg/m^3	0_2/ 5 mm 80 kg/m^3	0/ 5 mm 80 kg/m^3	0/ 5 mm 80 kg/m^3
Front	0_3/ 10 mm 130 kg/m^3	0_2/ 10 mm 130 kg/m^3	45_2/ 5 mm 130 kg/m^3	45/ 5 mm 130 kg/m^3	45/ 5 mm 80 kg/m^3
Back	0_3/ 10 mm 130 kg/m^3	0_2/ 10 mm 130 kg/m^3	45_2/ 5 mm 130 kg/m^3	45/ 5 mm 130 kg/m^3	45/ 5 mm 80 kg/m^3
Ribs	0/ 5 mm 80 kg/m^3	0/ 5 mm 80 kg/m^3	45/ 5 mm 80 kg/m^3	45/ 5 mm 80 kg/m^3	0/ 5 mm 80 kg/m^3
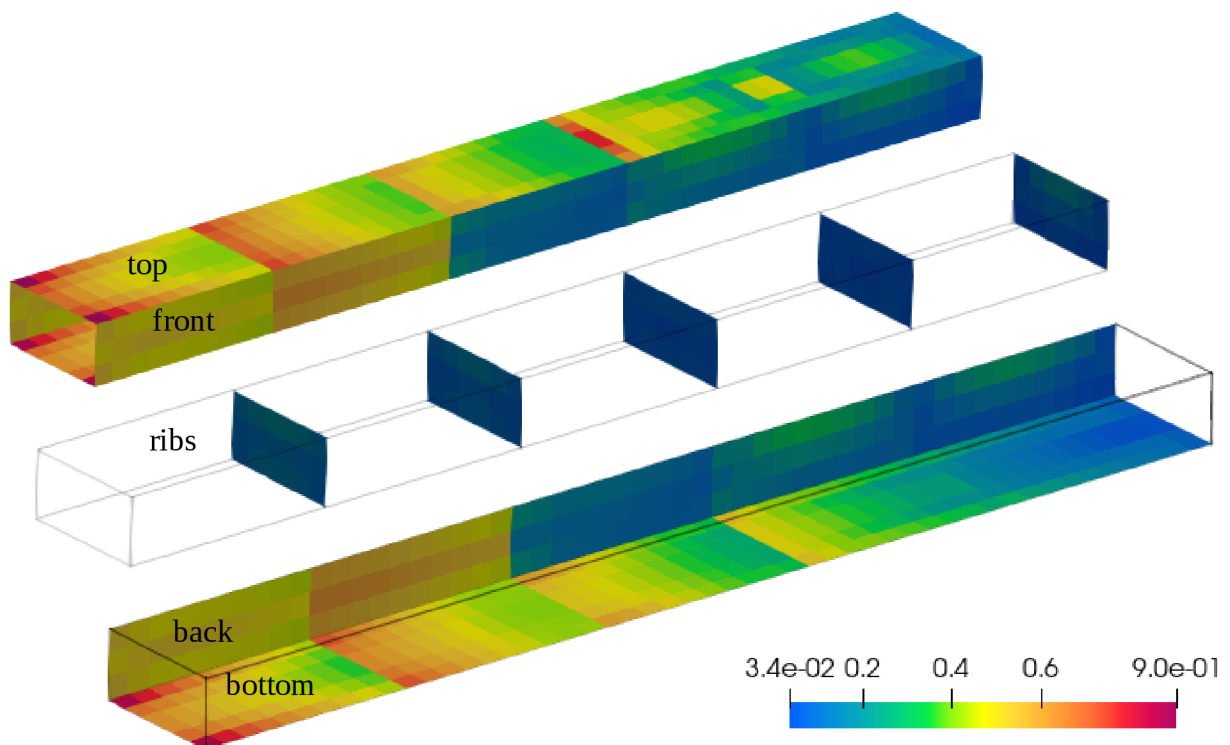
Figure 36: Maximum failure index for $i_{max}=20$, $\Delta_{max}=0.15$.

5.4.2 Sandwich panels with flanges

This variant of the box example contains flanges as shown in Figure 37. Flanges have different layups from the rest. Only a number of UD carbon layers is optimized on the flanges since the design layup contains 40 candidate layers without fabrics and without sandwich core. Flange elements are in patches on every segment, but the left and right flange symmetry is enforced by the design, because both top flanges are in one patch, and both bottom flanges are also in one patch. Other elements have sandwich design layups with the same materials as were used in the sandwich only box. Patches of the sandwich panels are smaller on the top and bottom due to flanges, otherwise they are the same as previously.

The model contains 990 shell elements which are divided to 25 sandwich patches and 10 flange patches. That gives 795 design variables, 550 material constraints, and 19850 failure constraints. Since the flanges increase the capacity to carry out the bending moment, the underpressure on the top elements was increased to 50 kPa, the torque on the ribs was kept on 2 Nm per rib.
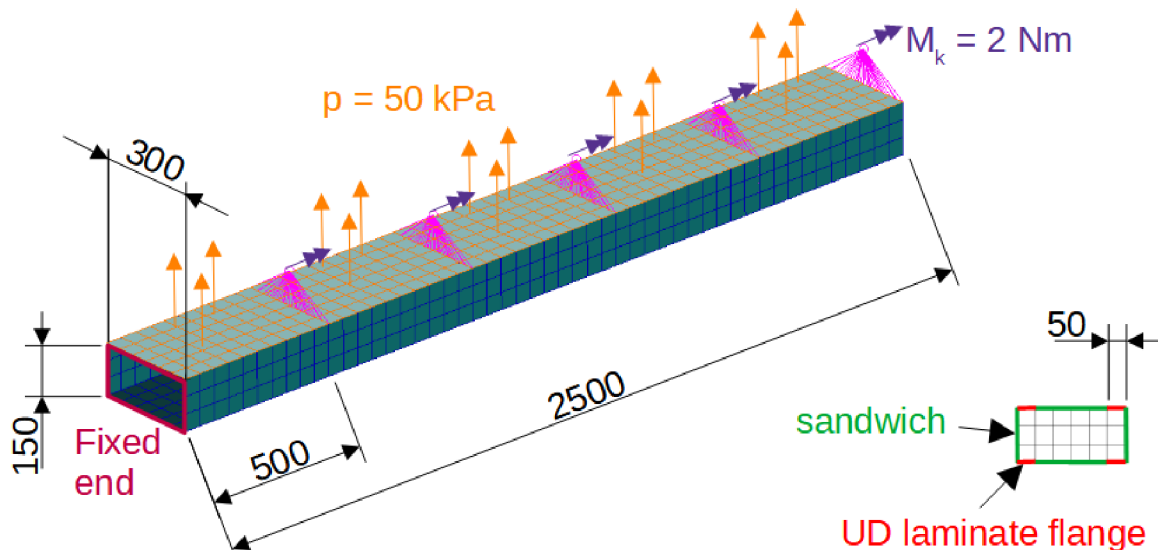

Figure 37: Schema of the box with flanges.

Optimization was run for the same settings as in sandwich-only box, i.e., i_{max}=10, 15, 20 and Δ_{max}=0.2, 0.15 as shown in Table 5.17. All cases satisfy the failure constraints and have discreteness 0.98 or higher. The case with i_{max}= 20 and default Δ_{max}=0.2 is the only one with discreteness 1.00 and clearly lower mass than other cases which reached similar values in discreteness, maximum failure index as well as final mass. Even in the best case, the maximum failure index 0.87 is still well below 1, which might signify that the solution can be still improved.

Table 5.17: Result comparison for different i_{max} and Δ_{max}.

i_{max}	10	15	20	10	15	20
Δ_{max}		0.2			0.15	
Discreteness	0.98	0.99	1.00	0.98	0.98	0.98
max. FI	0.85	0.85	0.87	0.86	0.85	0.86
m [kg]	13.235	13.065	10.774	13.213	12.970	13.691

Figure 38 shows that discreteness stabilized after design cycle 6 and failure indices remained below 1 even when the mass changed significantly during design cycles.
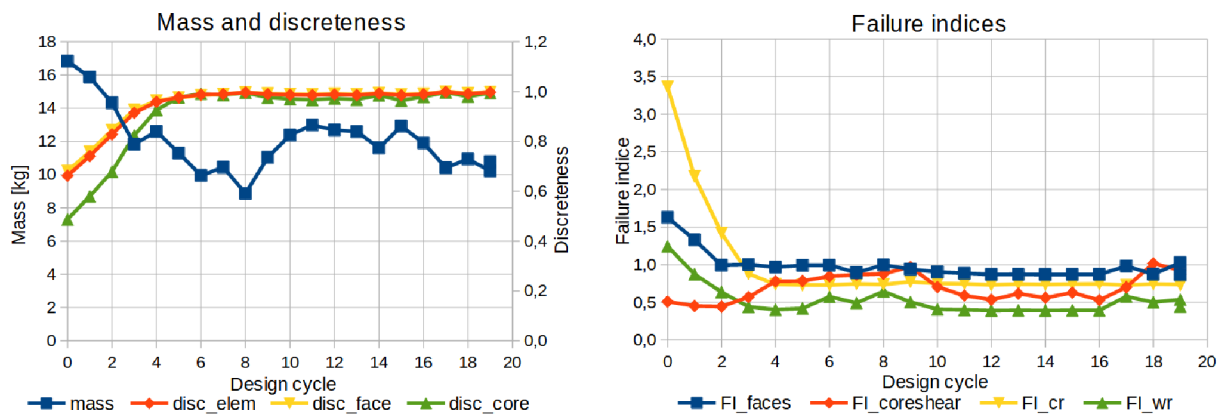

Figure 38: Mass, discreteness, and failure indices during design cycles for $i_{max}=20$, $\Delta_{max}=0.2$.

Layups of the best solution are in Table 5.18. Top panels have a strong core on segments 1-4 due to compression from bending moment and local bending from the underpressure, whereas the bottom panels have a light core which corresponds to the expected tensile loading. Orientations on the top and bottom panels are 0° with more maximum allowable number of face-sheet layers on segments 1-3. Front and back panels have 45° layers and a strong core on segments 1 and 2 as corresponds to shear from torque. Ribs have mostly a light core and one 45° face-sheet layer, but the tip rib ended with three layers probably as a support for the top panel end.

Figure 39 shows the maximal failure indices for the best solution. The highest values are on the bottom and especially top sandwich panels on segments 1 and 2 close to the root and on the other top panels above ribs. Rather low FI on the front and back panels suggest that they could be lighter as well as ribs 1 and 5. Flanges do not reach extra high FI, which denotes that they did not reach the optimum because 7-40 UD layers are enough to remove some of them without overwhelming increase of failure index.

Table 5.18: Layup of segments 1-5 from the fixed root to the free tip for $i_{max}=20$, $\Delta_{max}=0.2$.

| Segment	1 (root)	2	3	4	5 (tip)
Top	0_5/ 10 mm 130 kg/m^3	0_5/ 10 mm 130 kg/m^3	0_5/ 10 mm 130 kg/m^3	0_3/ 10 mm 130 kg/m^3	0_3/ 10 mm 80 kg/m^3
Bottom	0_5/ 5 mm 80 kg/m^3	0_5/ 5 mm 80 kg/m^3	0_5/ 5 mm 80 kg/m^3	0_2/ 5 mm 80 kg/m^3	0/ 5 mm 80 kg/m^3
Front	45_5/ 10 mm 130 kg/m^3	45_3/ 10 mm 130 kg/m^3	45_3/ 5 mm 130 kg/m^3	45_2/ 5 mm 130 kg/m^3	45/ 5 mm 130 kg/m^3
Back	45_5/ 10 mm 130 kg/m^3	45_3/ 10 mm 130 kg/m^3	45_2/ 5 mm 130 kg/m^3	45_2/ 5 mm 130 kg/m^3	45/ 5 mm 130 kg/m^3
Ribs	45/ 5 mm 130 kg/m^3	45/ 5 mm 80 kg/m^3	45/ 5 mm 80 kg/m^3	45/ 5 mm 80 kg/m^3	$45/0_2$/ 5 mm 80 kg/m^3
Top flanges	$0_{40\,UD}$	$0_{26\,UD}$	$0_{22\,UD}$	$0_{7\,UD}$	$0_{9\,UD}$
Bottom flanges	$0_{40\,UD}$	$0_{25\,UD}$	$0_{12\,UD}$	$0_{8\,UD}$	$0_{5\,UD}$
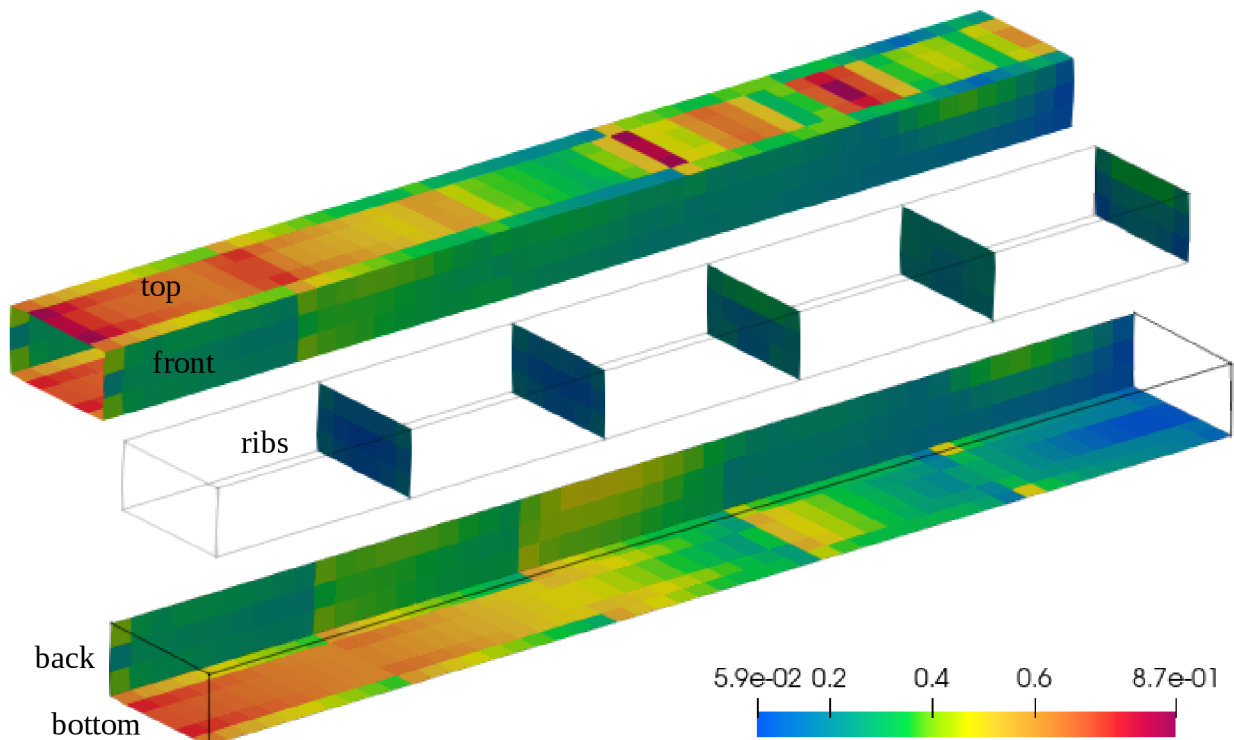
Figure 39: Maximum failure index for $i_{max}=20$, $\Delta_{max}=0.2$.

5.5 Aircraft interior components

5.5.1 Stowage

Real stowage of an airliner was selected as a practical component. The mesh is in Figure 40. The stowage is loaded in a side direction with acceleration acting on the point masses connected to the structure through RBE3 elements. Boundary conditions consist of fixation at attachment points where the stowage is connected to the floor through RBE2 elements. The model contains springs, rods, and other connectivity elements as are usual for such a component. Optimization does not limit their use and, in this example, the model for optimization was taken from practice without modifications. It contains 4993 quad4 elements on 11 flat panels selected as patches, which together with design materials led to 99 design variables, 33 material constraints, and 44937 failure constraints.
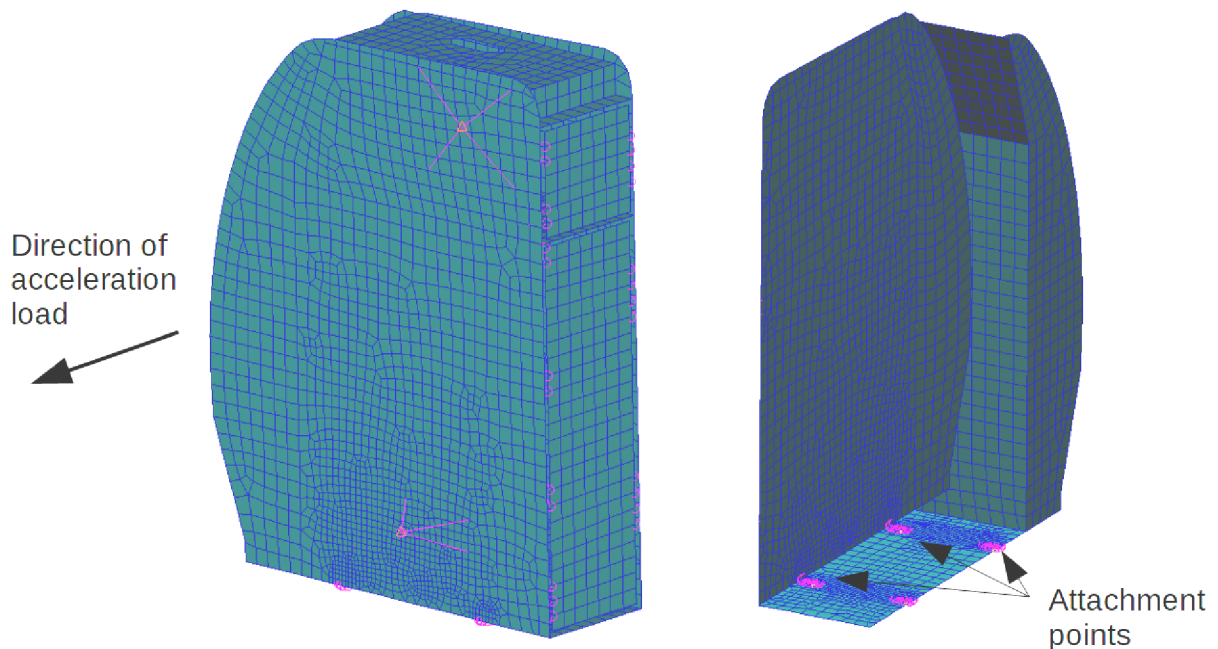

Figure 40: FE model of the stowage.

Design materials:

- Only one material can be in the face-sheet (0° glass fabric) in 2 or 4 layers (each with thickness 0.336 mm), thus it is modeled as two possible layers of double thickness (0.672 mm and 0.672 mm).

- Six core candidates: honeycomb with thicknesses 6.35, 12.7, 18.8 mm and with orientations 0° or 90°.

Attachments are not the subject of optimization, but the model typically does not simulate their area in detail, so that RBE2 elements cause local stress concentration. Because of the stress peaks, the stowage was optimized for several A_{ign} parameters as shown in Table 5.19. When ignoring was not used ($A_{ign}=0$), the discreteness of the model was below 1 and the mass

was high because thick face-sheets remained at the end of the optimization. The area of failing elements around the attachment is low as can be seen in the bottom view in Figure 41. Therefore, the optimization led to the same results for 0.1%, 0.5%, as well as 1% ignored area.

Table 5.19: Result comparison for different A_{ign}.

A_{ign}	0	0.001	0.005	0.01
Discreteness	0.94	1.00	1.00	1.00
m [kg]	33.664	17.025	17.025	17.025

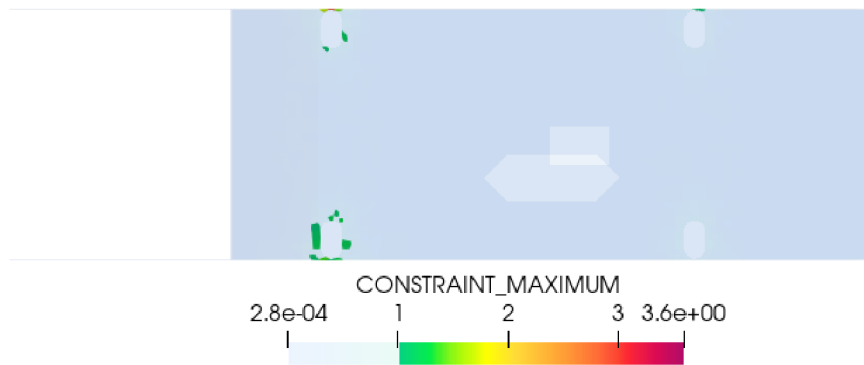*Figure 41: Bottom view on elements with FI>1 for $A_{ign}=0.005$.*

Figure 42 shows the graphs for the case with $A_{ign}=0.005$. All measures stabilized after design cycle 6. Discreteness reached 1, failure indices for core shear, crimping and wrinkling remained below 1 during all design cycles. Face-sheet failure decreased from the initial high value to 3.6 which is the value around the attachments as shown in Figure 41.
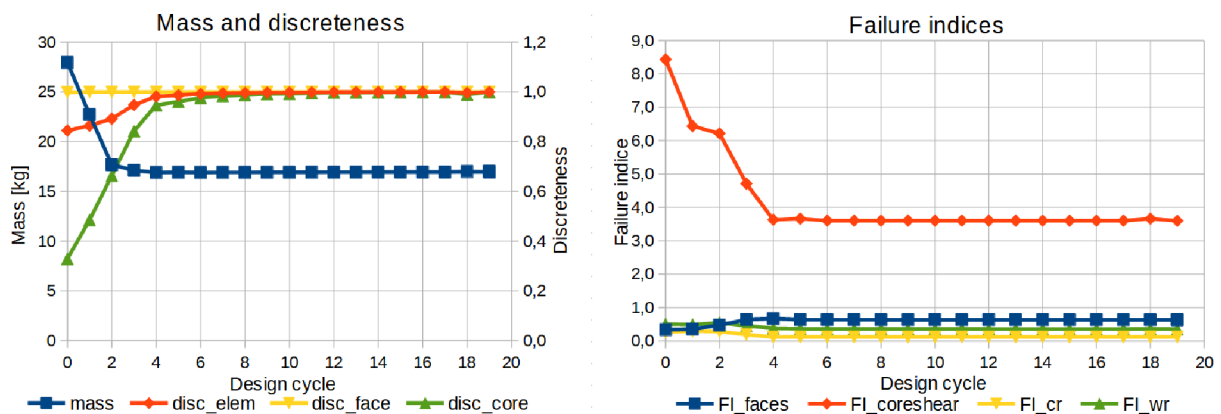
Figure 42: Mass, discreteness, and failure indices during design cycles for $A_{ign}=0.005$.

Optimization resulted in all panels with only two plies in the face-sheets for nonzero A_{ign}. Optimization removed additional two plies. Figure 43 shows the core thicknesses of the panels and their orientations marked by black lines. It is difficult to guess the best orientation

of the middle panels, but the side walls have a vertical orientation which was expected from the overall side load. Most of the core thicknesses are at the lowest value, which points to the fact that the stowage should be rather designed by technological considerations and loads are not critical in linear static analysis.

Figure 43: Orientations and thicknesses on the stowage for $A_{ign}=0.005$.

5.5.2 Galley

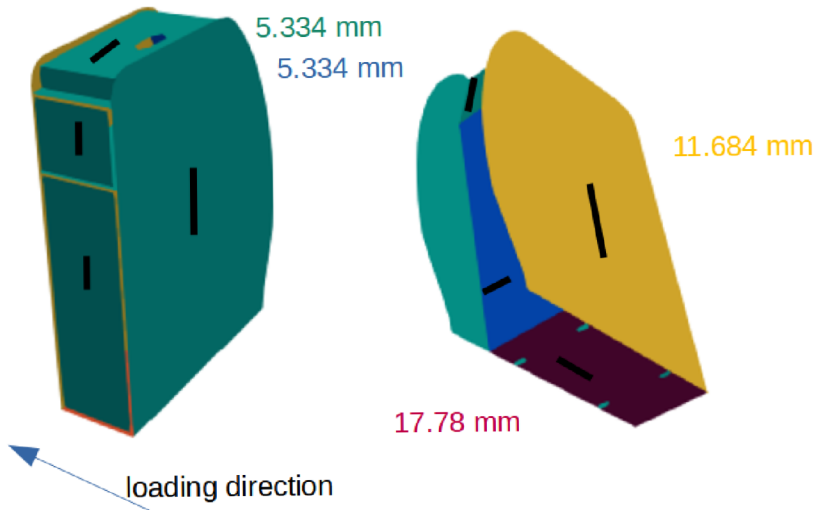The final example represents application of the program to the conceptual design of an airliner galley. The galley covers the rear bulkhead of the passenger compartment. It serves to accommodate trolleys in the bottom section, equipment such as a coffee machine, and boxes for refreshments. Shell FE model is typically used to analyze the strength and deformation of the galley. Loads from the inner staff are applied as a pressure on the shelf faces or through acceleration acting on concentrated masses connected to the shell structure through RBE2 and RBE3 elements. The galley is connected to the primary structure through the floor, side and top attachment points that can be modeled by RBE2 elements and springs, reflecting the stiffness of each connection.

The optimization model (Figure 44) was done in the same manner but with rough mesh so that the total number of shell elements was 4252, which was necessary to reach the optimization results in reasonable time. Number of patches (panels) was 54 which led to 486 design variables, 162 number of material constraints, but the number of failure constrains was 38268. Six separate load cases were applied, defined by load factors in each of the basic directions (forward, aft, left, right, up, down). Each load case was in a separate Nastran input file due to the different arrangement of RBE elements. Optimization with this number of elements and load cases took over 14 hours.
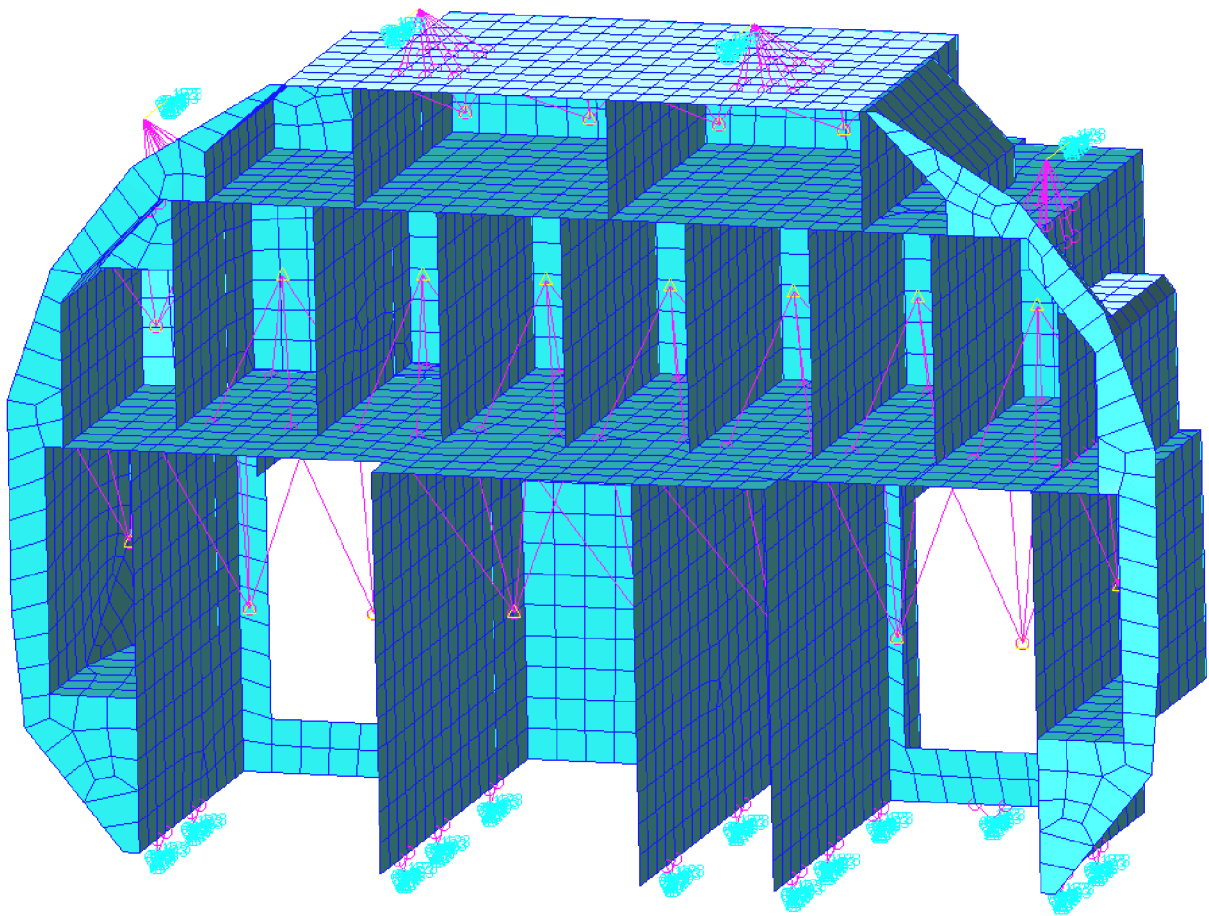

Figure 44: Optimization model with RBE arrangement for load case in up direction.

Design materials were the same as in the stowage example. Aim of the optimization was to select the global layup for the panels. Local reinforcement (metal doublers and inserts) cannot be defined by the optimization algorithm, so it has to be defined manually after the optimization. Omitting local reinforcement leads to local failures of the panels, so that using A_{ign} to ignore a certain portion of the elements is necessary to achieve meaningful results.

Table 5.20 shows the final discreteness and mass for a set of A_{ign}. Discreteness was 1.00 in all cases with nonzero A_{ign}. It is obvious that none ignoring led to a very heavy solution. When 5% area was ignored, mass of the panels was only slightly higher than in cases with more ignored elements. In cases with $A_{ign}=0.05$ and more, all panels contain only two plies in face-sheets and the mass difference is given only by the heights of the panel cores.

Table 5.20: Result comparison for different A_{ign}.

A_{ign}	0	0.02	0.05	0.1	0.15	0.2
Discreteness	0.95	1.00	1.00	1.00	1.00	1.00
m [kg]	147.004	124.357	82.521	82.215	79.446	77.216

Figure 45 shows that the discreteness and mass stabilized after design cycle 8, which denotes good convergence as was, e.g., in one-element examples for the optimal solution. Maximal failure indices remained at values under 1 for core shear, crimping, and wrinkling, but the model failures are in face-sheet layers, which are mostly on ignored elements, but are not filtered out from the graph.
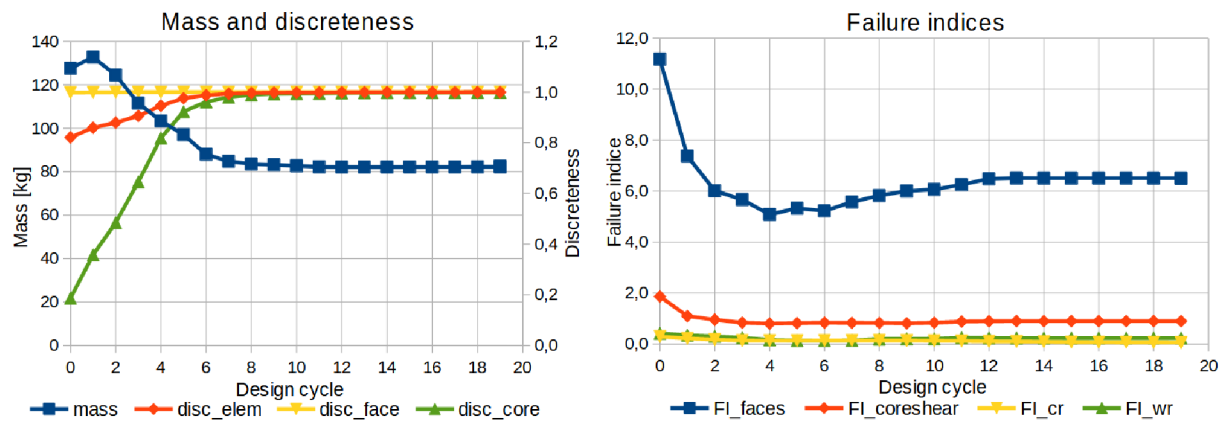
Figure 45: Mass, discreteness, and failure indices during design cycles for $A_{ign}=0.05$.

Figure 46 shows the color plot corresponding to the core material, i.e., thickness and orientation. Since the orientation depends on FE element orientation, black lines were added manually according to the element orientations on each panel. In this example, the optimizer had to evaluate element loads on each element of the panel for 6 different load cases, so it is difficult to evaluate specifically the correctness of the resulting core orientations and thicknesses.
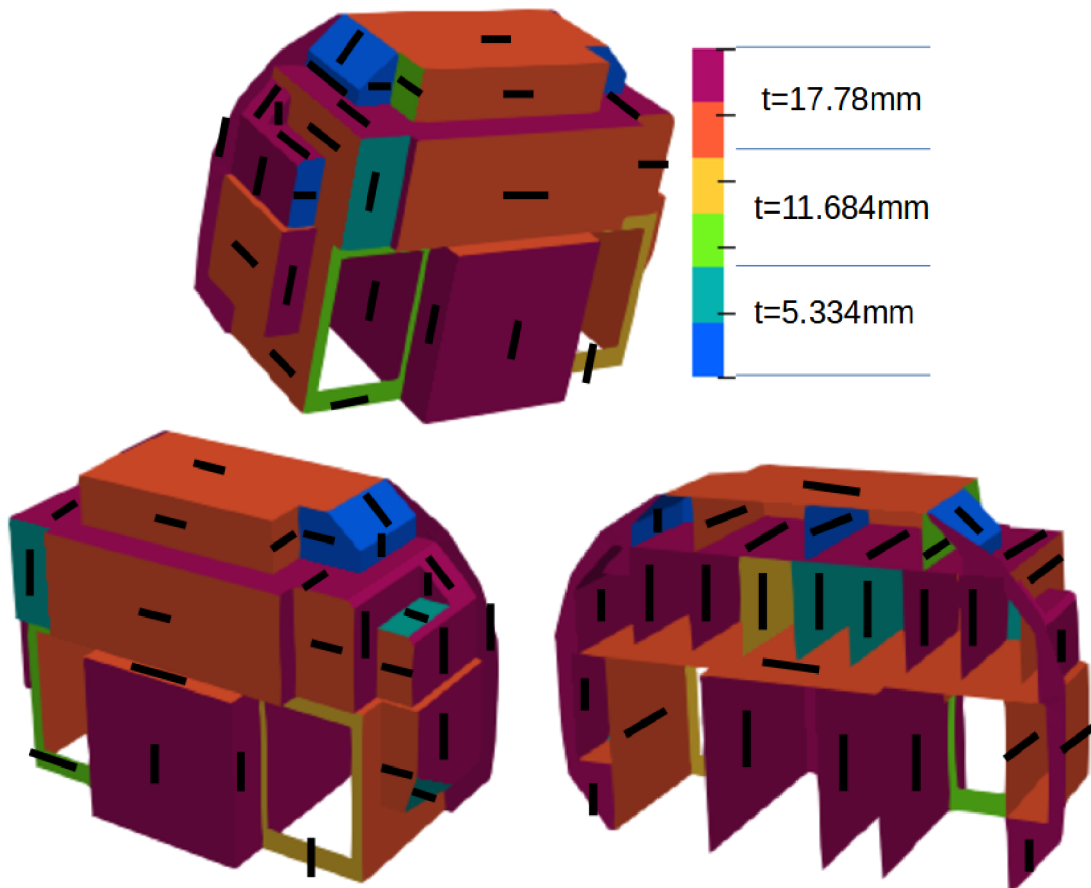
Figure 46: Galley results with panels orientations and thicknesses for $A_{ign}=0.05$.

Figure 47 shows the failing elements, which are mostly in the ignored area. It is a useful output for the designer so that these areas can be reinforced with doublers and inserts. Imperfections of the model can also cause failures, which might be considered because some elements might be failing just because of a poor quality of the mesh due to rough element size.
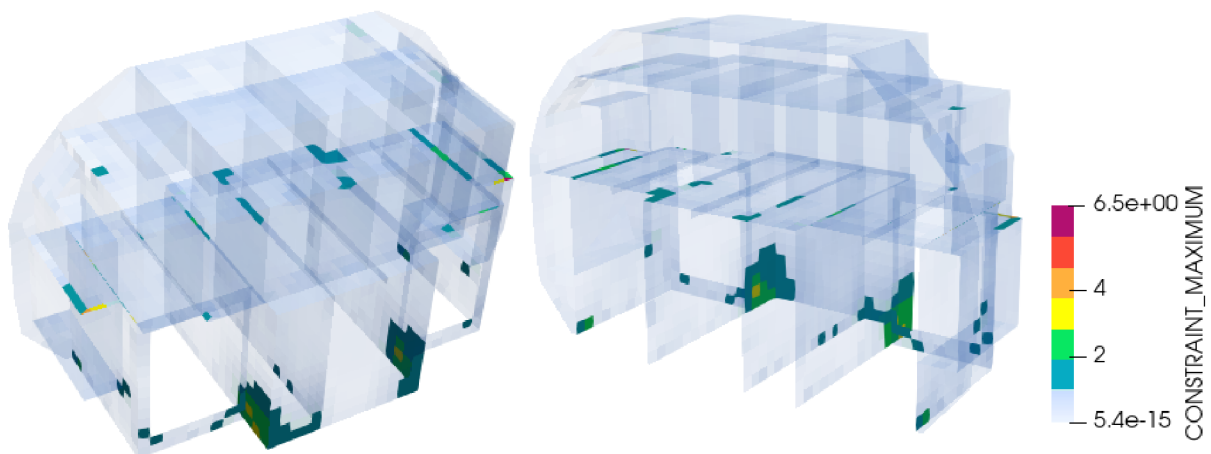
Figure 47: Elements with max FI > 1, for $A_{ign}=0.05$.

5.6 Summary of examples

Findings from the test examples can be summarized to these points:

1) Final discreteness and maximum failure index can be used for the first assessment of the results. In most cases, the final design was without failure constraint violation. Some examples finished with a slight violation. Final discreteness was usually close to 1, which denotes that the continuous variables converged successfully to a discrete solution which is required in the composite design.

2) The optimizer was not able to reach a discrete solution when the failure constraints could not be fulfilled by the strongest candidate materials (or) due to local stress concentration. The difficulty can be avoided by the use of A_{ign} parameter prescribing area of the elements which failure constraints are ignored.

3) Constraint aggregation did not work satisfactorily. Best solutions were achieved with ρ_{KS} lower than reported in the literature, but it still did not reach the quality of a solution without aggregation. Aggregation was expected to decrease the optimization time, but examples with aggregation required similar or even longer time due to worse convergence. These differences, compared to the literature, could be explained by a different approach to derivatives and evolution of the design cycles.

4) Although default optimization parameters were defined to achieve a robust solution in most cases, lower mass was achieved with altered parameters in some examples (the box example performed better with higher number of iterations i_{max}).

5) Simple examples revealed that the program is capable of reaching the true optimum in some cases, but not in all of them, which is not surprising when gradient optimization is used. Box with flanges, as a representative of a larger task, contained patches with a relatively low failure index, which also points to nonoptimal solution.

6) Optimization time ranged from minutes for one element to 14 hours for the galley with multiple load cases. Most of the time is spent on Jacobian evaluation, related to the number of failure constraints, thus time increases with number of candidate materials on the layup, the number of elements, and the number of load cases. Number of design variables also increases time, but not as significantly as was demonstrated by the panel where one large patch did not shorten the time as dramatically compared to the case without patches.

6   Conclusion

Theses described a new approach to sandwich optimization for the task of mass minimization with sandwich failure constraints. The method is based on Discrete Material Optimization (DMO), which applies the principles of multimaterial topology optimization to composite optimization. The method uses continuous design variables which converge to discrete values by the end of the optimization due to penalization.

Outcomes and contributions of the thesis:

1) The novelty of this approach is that it evaluates the gradients on elements separately and the interaction of the neighboring elements is carried out by the controlled evolution of the model. Gradient evaluation is separated from the FE model, which is theoretically less efficient, but enables to use an ordinary Nastran model which can contain common types of elements such as springs, RBE elements, etc.

2) Sandwich failure criteria within the concept of DMO require to deal with a combination of the candidate materials. Among sandwich failures, crimping and wrinkling were not found to be published previously in the scope of DMO.

3) The method was implemented as a Python program. It is able to deal with basic features such as: general Nastran input with shell elements in the optimization domain, multiple user-defined layups, multiple load cases, and patches.

4) Test examples were used to find robust default optimization parameters. It was shown that optimization is able to achieve a discrete solution without failure constraint violation or only slight violation.

5) Test example with concentrated load at one node revealed difficulties of the optimizer to converge due to locally high failures. This issue was successfully solved by defining a parameter which prescribes a small portion of the element failures to be ignored.

6) Examples demonstrated potential of the program for conceptual design of the sandwich structure layup. As a result, the workflow of a designer can change as shown in Figure 26, where the comparison with and without optimization is shown. Running the optimization program takes longer machine time, but modification of the optimization parameters is quick compared to manual layup modification and checking the results each time to satisfy requirements when the optimization program is not used.

The method can be further improved to fit a wider scope of engineering tasks. New manufacturing constraints can be added as they will be required by specific components. Implementation of the adjoint method for derivative calculation could help with additional requirements on displacement and buckling. Other potential for scientific work is in combination with different methods, such as GA, to decrease the risk of reaching a local minimum.

7   Literature

[1]   BIRMAN, Victor and KARDOMATEAS, George A. Review of current trends in research and applications of sandwich structures. *Composites Part B: Engineering*. June 2018. Vol. 142, p. 221–240. DOI 10.1016/j.compositesb.2018.01.027.

[2]   *Composite Materials Handbook - Volume 6 Structural Sandwich Composites* [online]. Warrendale, PA : SAE International, 2013. [Accessed 30 July 2020]. ISBN 978-0-7680-8062-9. Available from: https://saemobilus.sae.org/content/R-427/

[3]   ZENKERT, Dan. *An Introduction to Sandwich Structures: Student edition*. 2nd edition. Stockholm : KTH, 2005.

[4]   LÖFFELMANN, František and MALIŠ, Michal. *LU13-2015-TL4.DE Návrh vrstvení trupu TL-4000*. 30 March 2015. Letecký ústav, VUT v Brně.

[5]   PELED, D. and FROSTIG, Y. High-order bending of sandwich beams with transversely flexible core and nonparallel skins. *Journal of Engineering Mechanics*. 1994. Vol. 120, no. 6, p. 1255–1269. DOI 10.1061/(ASCE)0733-9399(1994)120:6(1255). Scopus

[6]   LÖFFELMANN, František and MALIŠ, Michal. *LU15-2015-TL4.ST Pevnostní kontrola trupu TL-4000*. 28 April 2015. Letecký ústav, VUT v Brně.

[7]   FROSTIG, Y. and PELED, D. High-order bending of piecewise uniform sandwich beams with a tapered transition zone and a transversely flexible core. *Composite Structures*. 1 January 1995. Vol. 31, no. 2, p. 151–162. DOI 10.1016/0263-8223(95)00012-7.

[8]   GHIASI, Hossein, PASINI, Damiano and LESSARD, Larry. Optimum stacking sequence design of composite materials Part I: Constant stiffness design. *Composite Structures*. 1 September 2009. Vol. 90, no. 1, p. 1–11. DOI 10.1016/j.compstruct.2009.01.006.

[9]   THOMSEN, O.T. and VINSON, J.R. Modeling of tapered sandwich panels using a high-order sandwich theory formulation. *AIAA Journal*. 2002. Vol. 40, no. 9, p. 1867–1875. DOI 10.2514/2.1866. Scopus

[10]   GHIASI, Hossein, FAYAZBAKHSH, Kazem, PASINI, Damiano and LESSARD, Larry. Optimum stacking sequence design of composite materials Part II: Variable stiffness design. *Composite Structures*. 1 December 2010. Vol. 93, no. 1, p. 1–13. DOI 10.1016/j.compstruct.2010.06.001.

[11]   E. F. BRUHN. *Analysis and design of flight vehicle structures*. Carmel : Jacobs Publishing, 1973. MK 10180

[12]   SONMEZ, Fazil O. Optimum Design of Composite Structures: A Literature Survey (1969–2009). *Journal of Reinforced Plastics and Composites*. 1 January 2017. Vol. 36, no. 1, p. 3–39. DOI 10.1177/0731684416668262.

[13]   KOLLAR, Laszlo P. and SPRINGER, George S. *Mechanics of Composite Structures*. West Nyack, NY, USA : Cambridge University Press, 2003.

[14]   NIKBAKT, S., KAMARIAN, S. and SHAKERI, M. A review on optimization of composite structures Part I: Laminated composites. *Composite Structures*. 1 July 2018. Vol. 195, p. 158–185. DOI 10.1016/j.compstruct.2018.03.063.

[15]   *ASM Handbook, Volume 21: Composites*. ASM International, 2001. ISBN 0-87170-703-9.

[16]   BENDSØE, M. P. Optimal shape design as a material distribution problem. *Structural optimization*. 1 December 1989. Vol. 1, no. 4, p. 193–202. DOI 10.1007/BF01650949.

[17]   *HexWeb Honeycomb Sandwich Design Technology*. 2000. Hexcel Composites.

[18]   STEGMANN, J. and LUND, E. Discrete material optimization of general composite shell structures. *International Journal for Numerical Methods in Engineering*. 2005. Vol. 62, no. 14, p. 2009–2027. DOI 10.1002/nme.1259.

[19]   CATAPANO, Anita and MONTEMURRO, Marco. A multi-scale approach for the optimum design of sandwich plates with honeycomb core. Part I: homogenisation of core properties. *Composite Structures*. 1 December 2014. Vol. 118, p. 664–676. DOI 10.1016/j.compstruct.2014.07.057.

[20]   LUND, Erik and STEGMANN, Jan. On structural optimization of composite shell structures using a discrete constitutive parametrization. *Wind Energy*. 2005. Vol. 8, no. 1, p. 109–124. DOI 10.1002/we.132.

[21]   CATAPANO, Anita and MONTEMURRO, Marco. A multi-scale approach for the optimum design of sandwich plates with honeycomb core. Part II: the optimisation strategy. *Composite Structures*. 1 December 2014. Vol. 118, p. 677–690. DOI 10.1016/j.compstruct.2014.07.058.

[22]   LUND, Erik. Buckling topology optimization of laminated multi-material composite shell structures. *Composite Structures*. 1 November 2009. Vol. 91, no. 2, p. 158–167. DOI 10.1016/j.compstruct.2009.04.046.

[23]   GIGLIO, M., GILIOLI, A. and MANES, A. Numerical investigation of a three point bending test on sandwich panels with aluminum skins and Nomex™ honeycomb core. *Computational Materials Science*. 1 April 2012. Vol. 56, p. 69–78. DOI 10.1016/j.commatsci.2012.01.007.

[24]   SØRENSEN, Søren N. and LUND, Erik. Topology and thickness optimization of laminated composites including manufacturing constraints. *Structural and Multidisciplinary Optimization*. 1 August 2013. Vol. 48, no. 2, p. 249–265. DOI 10.1007/s00158-013-0904-y.

[25]   HEIMBS, Sebastian. Virtual testing of sandwich core structures using dynamic finite element simulations. *Computational Materials Science*. 1 April 2009. Vol. 45, no. 2, p. 205–216. DOI 10.1016/j.commatsci.2008.09.017.

[26]   SJØLUND, J. H., PEETERS, D. and LUND, E. Discrete Material and Thickness Optimization of sandwich structures. *Composite Structures*. 1 June 2019. Vol. 217, p. 75–88. DOI 10.1016/j.compstruct.2019.03.003.

[27]   FINK, Axel and EINZMANN, Constantin. Discrete tailored asymmetric sandwich structures. *Composite Structures*. 15 April 2020. Vol. 238, p. 111990. DOI 10.1016/j.compstruct.2020.111990.

[28]   VELEA, Marian N., WENNHAGE, Per and ZENKERT, Dan. Multi-objective optimisation of vehicle bodies made of FRP sandwich structures. *Composite Structures*. 1 May 2014. Vol. 111, p. 75–84. DOI 10.1016/j.compstruct.2013.12.030.

[29]   HOFF, N. J. and MAUTNER, S. E. The Buckling of Sandwich-Type Panels. *Journal of the Aeronautical Sciences*. 1 July 1945. Vol. 12, no. 3, p. 285–297. DOI 10.2514/8.11246.

[30]   SULLINS, R.T., SMITH, G.W. and SPIER, E.E. *Manual for structural stability analysis of sandwich plates and shells* [online]. 1969. NASA. Available from: https://ntrs.nasa.gov/citations/19700004831Washington, D.C.

[31]   MALIŠ, Michal, ŠPAČEK, Petr, JEZA, Lukáš and SCHOŘ, Pavel. *Compost: Composite Posptrocessor v1.45 User guide*. 2012. Institute of Aerospace Engineering, Faculty of Mechanical Engineering, Brno University of Technology.

[32]   *TCT - Transnational Composite Training STRESS: Sandwich Sizing Process*. 2006. Airbus S.A.S.

[33]   SERESTA, Omprakash, GÜRDAL, Zafer, ADAMS, David B. and WATSON, Layne T. Optimal design of composite wing structures with blended laminates. *Composites Part B: Engineering*. 1 June 2007. Vol. 38, no. 4, p. 469–480. DOI 10.1016/j.compositesb.2006.08.005.

[34]   PÍŠTĚK, Antonín and PEŠÁK, Miroslav. Optimization of Stiffened Panel with the Help of Mathematical Programming, Experimental Verification. In : *26th International Congress of the Aeronautical Sciences ICAS* [online]. Anchorage, Alaska, USA, 2008. p. 13. ISBN 0-9533991-9-2. Available from: https://www.icas.org/ICAS_ARCHIVE/ICAS2008/PAPERS/517.PDF

[35]   PÍŠTĚK, Antonín. *Optimalizace leteckých konstrukcí s využitím metody konečných prvků*. Dizertační práce. Brno : Vojenská akademie Antonína Zápotockého, 1980.

[36]   BERLAND, Håvard. Automatic differentiation. [online]. 14 September 2006. Available from: https://www.pvv.ntnu.no/~berland/resources/autodiff-triallecture.pdf

[37]   VIRTANEN, Pauli, GOMMERS, Ralf, OLIPHANT, Travis E., HABERLAND, Matt, REDDY, Tyler, COURNAPEAU, David, BUROVSKI, Evgeni, PETERSON, Pearu, WECKESSER, Warren, BRIGHT, Jonathan, VAN DER WALT, Stéfan J., BRETT, Matthew, WILSON, Joshua, MILLMAN, K. Jarrod, MAYOROV, Nikolay, NELSON, Andrew R. J., JONES, Eric, KERN, Robert, LARSON, Eric, CAREY, C. J., POLAT, İlhan, FENG, Yu, MOORE, Eric W., VANDERPLAS, Jake, LAXALDE, Denis, PERKTOLD, Josef, CIMRMAN, Robert, HENRIKSEN, Ian, QUINTERO, E. A., HARRIS, Charles R., ARCHIBALD, Anne M., RIBEIRO, Antônio H., PEDREGOSA, Fabian and VAN MULBREGT, Paul. SciPy 1.0: fundamental algorithms for scientific computing in Python. *Nature Methods*. March 2020. Vol. 17, no. 3, p. 261–272. DOI 10.1038/s41592-019-0686-2.

[38]   KRAFT, Dieter. *A Software Package for Sequential Quadratic Programming* [online]. 1988. Deutsche Forschungs- und Versuchsanstalt für Luft- und Raumfahrt. [Accessed 16 July 2020]. Available from: http://degenerateconic.com/wp-content/uploads/2018/03/DFVLR_FB_88_28.pdf

[39]   WÄCHTER, Andreas and BIEGLER, Lorenz T. On the implementation of an interior-point filter line-search algorithm for large-scale nonlinear programming. *Mathematical Programming*. 1 March 2006. Vol. 106, no. 1, p. 25–57. DOI 10.1007/s10107-004-0559-y.

[40]   SVANBERG, Krister. The method of moving asymptotes—a new method for structural optimization. *International Journal for Numerical Methods in Engineering*. 1987. Vol. 24, no. 2, p. 359–373. DOI 10.1002/nme.1620240207.

[41]   STOLPE, M. and SVANBERG, K. An alternative interpolation scheme for minimum compliance topology optimization. *Structural and Multidisciplinary Optimization*. 1 September 2001. Vol. 22, no. 2, p. 116–124. DOI 10.1007/s001580100129.

[42]   CHENG, G. D. and GUO, X. ε-relaxed approach in structural topology optimization. *Structural optimization*. 1 June 1997. Vol. 13, no. 4, p. 258–266. DOI 10.1007/BF01197454.

[43]   DUYSINX, P. and SIGMUND, O. New developments in handling stress constraints in optimal material distribution. *7th AIAA/USAF/NASA/ISSMO Symposium on Multidisciplinary Analysis and Optimization* [online]. 2 September 1998. [Accessed 16 July 2020]. DOI 10.2514/6.1998-4906. Available from: https://arc.aiaa.org/doi/10.2514/6.1998-4906

[44]   BRUGGI, Matteo. On an alternative approach to stress constraints relaxation in topology optimization. *Structural and Multidisciplinary Optimization*. 1 August 2008. Vol. 36, no. 2, p. 125–141. DOI 10.1007/s00158-007-0203-6.

[45]   KREISSELMEIER, G. and STEINHAUSER, R. SYSTEMATIC CONTROL DESIGN BY OPTIMIZING A VECTOR PERFORMANCE INDEX. CUENOD, M. A. (ed.), *Computer Aided Design of Control Systems*. 1 January 1980. P. 113–117. DOI 10.1016/B978-0-08-024488-4.50022-X.

[46]   LE, Chau, NORATO, Julian, BRUNS, Tyler, HA, Christopher and TORTORELLI, Daniel. Stress-based topology optimization for continua. *Structural and Multidisciplinary Optimization*. 1 April 2010. Vol. 41, no. 4, p. 605–620. DOI 10.1007/s00158-009-0440-y.

[47]   KENNEDY, Graeme J. and HICKEN, Jason E. Improved constraint-aggregation methods. *Computer Methods in Applied Mechanics and Engineering*. 1 June 2015. Vol. 289, p. 332–354. DOI 10.1016/j.cma.2015.02.017.

[48]   PARÍS, J., NAVARRINA, F., COLOMINAS, I. and CASTELEIRO, M. Block aggregation of stress constraints in topology optimization of structures. *Advances in Engineering Software*. 1 March 2010. Vol. 41, no. 3, p. 433–441. DOI 10.1016/j.advengsoft.2009.03.006.

[49]   HOLMBERG, Erik, TORSTENFELT, Bo and KLARBRING, Anders. Stress constrained topology optimization. *Structural and Multidisciplinary Optimization*. 1 July 2013. Vol. 48, no. 1, p. 33–47. DOI 10.1007/s00158-012-0880-7.

[50]   KENNEDY, Graeme J. A full-space barrier method for stress-constrained discrete material design optimization. *Structural and Multidisciplinary Optimization*. 1 September 2016. Vol. 54, no. 3, p. 619–639. DOI 10.1007/s00158-016-1428-z.

[51]   SOHOULI, A., YILDIZ, M. and SULEMAN, A. Design optimization of thin-walled composite structures based on material and fiber orientation. *Composite Structures*. 15 September 2017. Vol. 176, p. 1081–1095. DOI 10.1016/j.compstruct.2017.06.030.

[52]   SØRENSEN, Søren N., SØRENSEN, René and LUND, Erik. DMTO – a method for Discrete Material and Thickness Optimization of laminated composite structures. *Structural and Multidisciplinary Optimization*. 1 July 2014. Vol. 50, no. 1, p. 25–47. DOI 10.1007/s00158-014-1047-5.

[53]   SØRENSEN, René and LUND, Erik. Thickness filters for gradient based multi-material and thickness optimization of laminated composite structures. *Structural and Multidisciplinary Optimization*. 1 August 2015. Vol. 52, no. 2, p. 227–250. DOI 10.1007/s00158-015-1230-3.

[54]   *Design Sensitivity and Optimization User's Guide - MSC Nastran 2020*. 2020. Hexagon, MSC Software.

[55]   VANDERPLAATS, G. N. NASA-CR-177985: *ADS - A Fortran Program for Automated Design Synthesis Version 3.00:* [online]. NASA Contractor Report. Fort Belvoir, VA : Defense Technical Information Center, 1988. [Accessed 27 August 2020]. Available from: http://www.dtic.mil/docs/citations/ADA213595

[56]   ZHOU, Ming, FLEURY, Raphael and KEMP, Martin. Optimization of Composite - Recent Advances and Application. In : *13th AIAA/ISSMO Multidisciplinary Analysis Optimization Conference* [online]. Fort Worth, Texas : American Institute of Aeronautics and Astronautics, 13 September 2010. [Accessed 26 August 2021]. ISBN 978-1-60086-954-9. Available from: https://arc.aiaa.org/doi/10.2514/6.2010-9272

[57]   KUENZI, Edward W. *Minimum Weight Structural Sandwich* [online]. 1965. U.S. Department of Agriculture, Forest Service, Product Laborarory. Available from: https://www.fpl.fs.fed.us/documnts/fplrn/fplrn086_rev_a.pdf

[58]   THEULEN, J. C. M. and PEIJS, A. A. J. M. Optimization of the bending stiffness and strength of composite sandwich panels. *Composite Structures*. 1 January 1991. Vol. 17, no. 1, p. 87–92. DOI 10.1016/0263-8223(91)90062-4.

[59]   SJØLUND, J. H. and LUND, E. Structural gradient based sizing optimization of wind turbine blades with fixed outer geometry. *Composite Structures*. 1 November 2018. Vol. 203, p. 725–739. DOI 10.1016/j.compstruct.2018.07.031.

[60]   SOREMEKUN, Grant, GÜRDAL, Zafer, KASSAPOGLOU, Christos and TONI, Darryl. Stacking sequence blending of multiple composite laminates using genetic algorithms. *Composite Structures*. 1 April 2002. Vol. 56, no. 1, p. 53–62. DOI 10.1016/S0263-8223(01)00185-4.

[61]   LUND, Erik. Discrete Material and Thickness Optimization of laminated composite structures including failure criteria. *Structural and Multidisciplinary Optimization*. 1 June 2018. Vol. 57, no. 6, p. 2357–2375. DOI 10.1007/s00158-017-1866-2.

[62]   KASSAPOGLOU, Christos. *Aerospace Series (PEP): Design and Analysis of Composite Structures: With Applications to Aerospace Structures*. 2nd edition. Wiley, 2013. ISBN 978-1-118-53694-0.

[63]   LEY, Robert P., LIN, Weichuan and MBANEFO, Uy. *Facesheet Wrinkling in Sandwich Structures NASA/CR-1999-208994* [online]. 1999. NASA. [Accessed 26 July 2020]. Available from: https://ntrs.nasa.gov/archive/nasa/casi.ntrs.nasa.gov/19990017863.pdfVirginia

[64]   CONN, Andrew R., GOULD, Nicholas I. M. and TOINT, Philippe L. *Trust Region Methods* [online]. Society for Industrial and Applied Mathematics, 2000. [Accessed 23 August 2020]. MOS-SIAM Series on Optimization. ISBN 978-0-89871-460-9. Available from: https://epubs.siam.org/doi/book/10.1137/1.9780898719857

[65]   *Dimensionierungsrichtwerte für den Segel und Motorsegelflugzeugbau*. 1988. Interessengemeinschaft Deutscher Akademischer Fliegergrupen (IDAFLIEG).

[66]   Data Sheet 01.2020: Airex C70. [online]. 2020. [Accessed 16 July 2020]. Available from: https://www.3accorematerials.com/uploads/documents/TDS-AIREX-C70-E-01.2020.pdf

[67]   *HexWeb CR III: Corrosion resistant Specification Grade Aluminum Honeycomb* [online]. 2017. Hexcel. Available from: https://hexcel.com/user_area/content_media/raw/HexWeb_CRIII_DataSheet.pdf

[68]   LÖFFELMANN, František. Discrete material optimization with sandwich failure constraints. *Structural and Multidisciplinary Optimization* [online]. 14 July 2021. [Accessed 30 August 2021]. DOI 10.1007/s00158-021-03006-x. Available from: https://link.springer.com/10.1007/s00158-021-03006-x

[69]   REDDY, J. N. *Mechanics of Laminated Composite Plates and Shells: Theory and Analysis, Second Edition*. 2 edition. Boca Raton : CRC Press, 2003. ISBN 978-0-8493-1592-3.

[70]   JURAČKA, Jaroslav. *Kompozitní konstrukce v letectví, LU01-2007-OST.ST, rev.3*. 2011. Letecký ústav, VUT v Brně. Brno

[71]   KIM, Alicia. *SE207 Structural Optimization: course notes*. 2016.

8 List of symbols and abbreviations

A, A_{ign}	element area, relative ignored area
A_{44}, A_{45}, A_{55}	transverse shear stiffness matrix members
A	membrane stiffness matrix
AD	Automatic Differentiation
ADS	Automated Design Synthesis
b_0, b_ε	blending parameters
B	bending-membrane coupling stiffness matrix
d	distance of face-sheet centers, discreteness
DMO	Discrete Material Optimization
DDMO	Decoupled Discrete Material Optimization
D, **D**	bending stiffness (matrix)
E, E_f	elastic modulus, effective face-sheet modulus
f(**x**)	goal function
F	force vector
FE, FEA, FEM	finite element, finite element analysis, finite element method
FI, $FI_{\sigma, \tau, cr, wr}$	failure index for face-sheets, core shear, crimping, wrinkling
FSDT	First Order Shear Deformation Theory
g(**x**)	constraint function
GA	genetic algorithm
GFRP	Glass Fiber Reinforced Polymer
G_c	core shear modulus
i, i_{dc}, i_{max}	i-th candidate material, number of design cycles, number of optimizer iterations
IPOPT	Interior Point Optimizer
j	j-th layer, design cycle
J	Jacobian matrix
k, k'	k-th element, coefficient in the logistic function
k_{wr}	wrinkling coefficient
K	shear correction factor
K	stiffness matrix
KS	Kreisselmeier-Steinhauser function
L	Lagrange function
m	real mass
M	penalized mass in the goal function, bending moment
MMA	Method of Moving Asymptotes
MSCADS	MSC Automated Design Synthesis
MUST	MUltidisciplinary Synthesis Tool
n_E, n_M, n_{MF}, n_{MC}, n_L, n_P	number of elements, materials, face-sheet materials, core materials, layers, pairs for blending
n.p.	neutral plane
N, N_{cr}	linear load, critical load
p	penalization coefficient
PUR	polyurethane
PVC	polyvinyl chloride
q, $\tilde{q}$	distributed load, penalization coefficient
Q	shear force

$\mathbf{Q}$, $\bar{\mathbf{Q}}$	layer stiffness matrix, layer stiffness matrix in element coordinate system
RAMP	Rational Approximation of Material Properties
RBE2, RBE3	Rigid Body Element
S	shear stiffness, allowable stresses in the face-sheet and core
SIMP	Solid Isotropic Materials with Penalization
SLP	Sequential Linear Programming
SLSQP	Sequential Least SQuares Programming
$\mathbf{u}$	displacement vector
UD	uni-directional composite
t_1, t_2, t_c, t_f	thickness of first and second face-sheet, core, face-sheet
t_M,	thickness in goal function
T	transverse force load
v	element volume
V, V_f, V_m	total volume, composite fiber volume content, composite matrix volume content
w	deflection, weight coefficient
W_c, W_f	core mass, face-sheet mass
x_{ijk}, x_{Tk}	material variable, thickness variable
z	position of the layer from the neutral plane
Δ, Δ_{12} pair	finite difference of the variable, difference between variables in blending
Δ_{max}	allowable change of design variable per design cycle
ε	strain
γ	shear strain
θ, θ_p	material orientation, principle direction angle
λ	Lagrange multiplier
ν	Poisson's number
ρ, ρ_{KS}, ρ_L, ρ_M	material density, KS function coefficient, layer density, density in goal function
$\bar{\rho}$	shifted layer density
σ, σ_{PN}	stress, P-norm function
τ	shear stress

9 Appendix

9.1 Layer stress calculation

In this work, the First Order Shear Deformation Theory (FSDT) is used to calculate layer stresses during optimization according to the element inner loads which are printed by the FE solver. Stresses can be also taken as the output from the FE, solver but analytical formulas are needed for evaluation of the derivatives of design constraints dependent on stresses. The FSDT differs from the Classical Laminated Plate Theory (CLPT) in removing Kirchhoff hypothesis so that transverse normals after deformation do not remain perpendicular to the plate mid-surface. Practical consequence is that transverse shear stresses need to be evaluated.

Assumptions and restrictions of the theory [69]:

1) The layers are perfectly bonded together.

2) The material of each layer is orthotropic linearly elastic.

3) Each layer is of uniform thickness.

4) The strains and displacements are small.

5) The transverse shear stresses on the top and bottom surfaces of the laminate are zero.

Relations in this chapter are from Reddy [69] and Juračka [70]. Generalized plane stress is assumed. Out-of-plane components $\sigma_{33} = 0$, $\varepsilon_{33} \neq 0$ are not further elaborated. Considering the orthotropic material of the layer, its constitutive stress-strain relations are given by the lamina stiffness matrix $\mathbf{Q}$ in

$$\begin{Bmatrix} \sigma_1 \\ \sigma_2 \\ \tau_{12} \end{Bmatrix} = \begin{bmatrix} Q_{11} & Q_{12} & 0 \\ Q_{12} & Q_{22} & 0 \\ 0 & 0 & Q_{66} \end{bmatrix} \begin{Bmatrix} \varepsilon_1 \\ \varepsilon_2 \\ \gamma_{12} \end{Bmatrix} = \begin{bmatrix} \dfrac{E_{11}}{1-\nu_{12}\nu_{21}} & \dfrac{\nu_{12}E_{22}}{1-\nu_{12}\nu_{21}} & 0 \\ \dfrac{\nu_{12}E_{22}}{1-\nu_{12}\nu_{21}} & \dfrac{E_{22}}{1-\nu_{12}\nu_{21}} & 0 \\ 0 & 0 & G_{12} \end{bmatrix} \begin{Bmatrix} \varepsilon_1 \\ \varepsilon_2 \\ \gamma_{12} \end{Bmatrix} \quad , \tag{85}$$

where $\nu_{21} = \nu_{12} \dfrac{E_{22}}{E_{11}}$. For sandwich structures transverse shear properties need to be considered. It is assumed that shear stiffness is given by the core material, so the shear stress and strain relation is

$$\begin{Bmatrix} \tau_{26} \\ \tau_{16} \end{Bmatrix} = \begin{bmatrix} Q_{44} & 0 \\ 0 & Q_{55} \end{bmatrix} \begin{Bmatrix} \gamma_{26} \\ \gamma_{16} \end{Bmatrix} = \begin{bmatrix} G_{23} & 0 \\ 0 & G_{13} \end{bmatrix} \begin{Bmatrix} \gamma_{26} \\ \gamma_{16} \end{Bmatrix} \quad . \tag{86}$$

Transformation to the plate coordinate system leads to the eq. (85) and (86) in the forms

$$\begin{Bmatrix} \sigma_{xx} \\ \sigma_{yy} \\ \tau_{xy} \end{Bmatrix} = \begin{bmatrix} \bar{Q}_{11} & \bar{Q}_{12} & \bar{Q}_{16} \\ \bar{Q}_{12} & \bar{Q}_{22} & \bar{Q}_{26} \\ \bar{Q}_{16} & \bar{Q}_{26} & \bar{Q}_{66} \end{bmatrix} \begin{Bmatrix} \varepsilon_{xx} \\ \varepsilon_{yy} \\ \gamma_{xy} \end{Bmatrix} \quad ,$$

$$\begin{Bmatrix} \tau_{yz} \\ \tau_{xz} \end{Bmatrix} = \begin{bmatrix} \bar{Q}_{44} & \bar{Q}_{45} \\ \bar{Q}_{45} & \bar{Q}_{55} \end{bmatrix} \begin{Bmatrix} \gamma_{yz} \\ \gamma_{xz} \end{Bmatrix}$$

(87)

where transformed members of the matrix $\bar{Q}$ are

$$\begin{aligned}
\bar{Q}_{11} &= Q_{11}\cos^4\theta + 2(Q_{12}+2Q_{66})\sin^2\theta\cos^2\theta + Q_{22}\sin^4\theta \\
\bar{Q}_{12} &= (Q_{11}+Q_{22}-4Q_{66})\sin^2\theta\cos^2\theta + Q_{12}(\sin^4\theta+\cos^4\theta) \\
\bar{Q}_{22} &= Q_{11}\sin^4\theta + 2(Q_{12}+2Q_{66})\sin^2\theta\cos^2\theta + Q_{22}\cos^4\theta \\
\bar{Q}_{16} &= (Q_{11}-Q_{12}-2Q_{66})\sin\theta\cos^3\theta + (Q_{12}-Q_{22}+2Q_{66})\sin^3\theta+\cos\theta \\
\bar{Q}_{26} &= (Q_{11}-Q_{12}-2Q_{66})\sin^3\theta\cos\theta + (Q_{12}-Q_{22}+2Q_{66})\sin\theta+\cos^3\theta \\
\bar{Q}_{66} &= (Q_{11}+Q_{22}-2Q_{12}-2Q_{66})\sin^2\theta\cos^2\theta + Q_{66}(\sin^4\theta+\cos^4\theta) \\
\bar{Q}_{44} &= Q_{44}\cos^2\theta + Q_{55}\sin^2\theta \\
\bar{Q}_{45} &= (Q_{55}-Q_{44})\sin\theta\cos\theta \\
\bar{Q}_{55} &= Q_{55}\cos^2\theta + Q_{44}\sin^2\theta
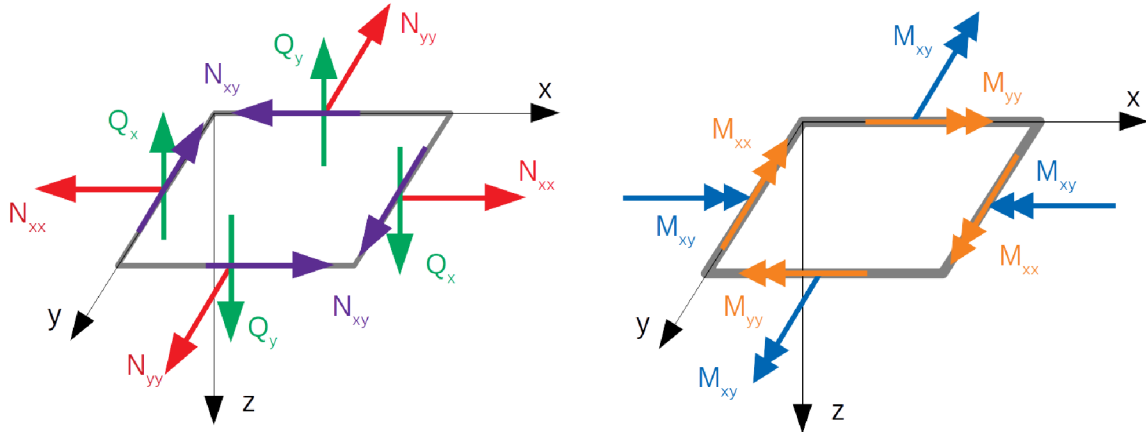\end{aligned}$$

(88)

Figure 48: Element force and moment resultants according to Reddy [69].

Constitutive equation for the whole laminate has the form

$$\begin{Bmatrix} N \\ M \end{Bmatrix} = \begin{bmatrix} A & B \\ B & D \end{bmatrix} \begin{Bmatrix} \varepsilon^0 \\ \kappa \end{Bmatrix} \quad ,$$

(89)

where N and M are the in-plane and moment linear loading vectors as depicted in Figure 48, ε^0 and κ are the membrane and bending strain vectors

$$N = \begin{Bmatrix} N_{xx} \\ N_{yy} \\ N_{xy} \end{Bmatrix} \quad , \quad M = \begin{Bmatrix} M_{xx} \\ M_{yy} \\ M_{xy} \end{Bmatrix} \quad , \quad \varepsilon^0 = \begin{Bmatrix} \varepsilon_{xx}^0 \\ \varepsilon_{yy}^0 \\ \varepsilon_{xy}^0 \end{Bmatrix} \quad , \quad \kappa = \begin{Bmatrix} \kappa_{xx} \\ \kappa_{yy} \\ \kappa_{xy} \end{Bmatrix} \quad .$$

(90)

Extensional stiffness matrix **A**, bending stiffness matrix **D**, and bending-extensional coupling stiffness matrix **B** are 3×3 symmetric matrices which members are

$$A_{ij} = \sum_{k=1}^{N} \bar{Q}_{ij,k}(z_{k+1} - z_k) \quad, \quad B_{ij} = \frac{1}{2}\sum_{k=1}^{N} \bar{Q}_{ij,k}(z_{k+1}^2 - z_k^2) \quad, \quad D_{ij} = \frac{1}{3}\sum_{k=1}^{N} \bar{Q}_{ij,k}(z_{k+1}^3 - z_k^3) \quad,$$

(91)

where N is number of the layers on the element and z (shown in Figure 49) is the layer position according to the neutral plane calculated for non-symmetric layup as

$$z_{np} = \frac{\sum_{k=1}^{N} z_k^I t_k (\bar{Q}_{11k} + \bar{Q}_{22k})}{\sum_{k=1}^{N} t_k (\bar{Q}_{11k} + \bar{Q}_{22k})} \quad.$$
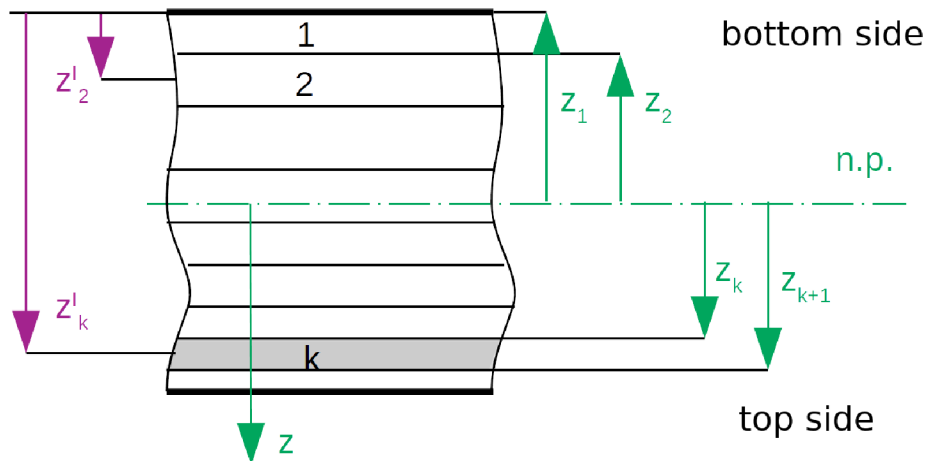
(92)

Figure 49: Layer numbering and position according to Reddy [69].
Bottom and top side are according to Nastran notation.

Additional constitutive equations for the transverse shear are

$$\begin{Bmatrix} Q_y \\ Q_x \end{Bmatrix} = K \begin{bmatrix} A_{44} & A_{45} \\ A_{45} & A_{55} \end{bmatrix} \begin{Bmatrix} \gamma_{yz}^0 \\ \gamma_{xz}^0 \end{Bmatrix} \quad,$$

(93)

where extensional stiffnesses are for laminated composites

$$A_{44} = \sum_{k=1}^{N} \bar{Q}_{44,k}(z_{k+1} - z_k) \quad, \quad A_{45} = \sum_{k=1}^{N} \bar{Q}_{45,k}(z_{k+1} - z_k) \quad, \quad A_{55} = \sum_{k=1}^{N} \bar{Q}_{55,k}(z_{k+1} - z_k) \quad.$$

(94)

K is the shear correction coefficient which takes into account change of the real shear stress across the plate in contrast to constant distribution in this theory. For homogeneous plates it is K = 5/6, for sandwiches K ≈ 1 according to and for sandwiches shear stiffness is assumed to be given only by the core as

$$A_{44} = \bar{Q}_{44,k} \frac{d^2}{t_c} \quad , \quad A_{45} = \bar{Q}_{45,k} \frac{d^2}{t_c} \quad , \quad A_{55} = \bar{Q}_{55,k} \frac{d^2}{t_c} \tag{95}$$

where k denotes core layer, d is distance of face-sheet centers, t_c is core thickness.

For the evaluation of lamina stresses, the global compliance matrix must be constructed as inverted global stiffness matrix from the eq. (89), resp. (93). so that membrane and bending strain vectors are calculated as

$$\begin{Bmatrix} \varepsilon^0 \\ \kappa \end{Bmatrix} = \begin{bmatrix} a & b \\ b & d \end{bmatrix} \begin{Bmatrix} N \\ M \end{Bmatrix} \quad . \tag{96}$$

It is worth noticing that in case of symmetric layup, inversion is simpler since matrix $\mathbf{B} = \mathbf{0}$ so that $\mathbf{b} = \mathbf{0}$, $\mathbf{a} = \mathbf{A}^{-1}$, and $\mathbf{d} = \mathbf{D}^{-1}$.

Strains on the k-th layer are than computed

$$\begin{Bmatrix} \varepsilon_{xx} \\ \varepsilon_{yy} \\ \gamma_{xy} \end{Bmatrix}_k = \begin{Bmatrix} \varepsilon^0_{xx} \\ \varepsilon^0_{yy} \\ \gamma^0_{xy} \end{Bmatrix} + z_k \begin{Bmatrix} \kappa_{xx} \\ \kappa_{yy} \\ \kappa_{xy} \end{Bmatrix} \tag{97}$$

and corresponding stresses in the global coordinate system are

$$\begin{Bmatrix} \sigma_{xx} \\ \sigma_{yy} \\ \tau_{xy} \end{Bmatrix}_k = \bar{Q} \begin{Bmatrix} \varepsilon_{xx} \\ \varepsilon_{yy} \\ \gamma_{xy} \end{Bmatrix}_k \quad , \tag{98}$$

where $\bar{Q}$ is the transformed lamina stiffness matrix from eq. (87). Stresses in the desired direction given by the angle θ (e.g., in the material coordinate system) are given by

$$\begin{Bmatrix} \sigma_1 \\ \sigma_2 \\ \tau_{12} \end{Bmatrix}_k = \begin{bmatrix} \cos^2\theta & \sin^2\theta & 2\sin\theta\cos\theta \\ \sin^2\theta & \cos^2\theta & -2\sin\theta\cos\theta \\ -\sin\theta\cos\theta & \sin\theta\cos\theta & \cos^2-\sin^2\theta \end{bmatrix} \begin{Bmatrix} \sigma_{xx} \\ \sigma_{yy} \\ \tau_{xy} \end{Bmatrix}_k \quad . \tag{99}$$

Transverse shear stresses are considered constant through the composite by the FSDT so that the eq. (93) with inverse constitutive matrix is

$$\begin{Bmatrix} \gamma_{yz} \\ \gamma_{xz} \end{Bmatrix} = \frac{1}{K\left(A_{44}A_{55} - A_{45}^2\right)} \begin{bmatrix} A_{55} & -A_{45} \\ -A_{45} & A_{44} \end{bmatrix} \begin{Bmatrix} Q_y \\ Q_x \end{Bmatrix} \tag{100}$$

and the layer transverse shear stresses can be evaluated again by the equation (87)

$$\begin{Bmatrix} \tau_{yz} \\ \tau_{xz} \end{Bmatrix}_k = \begin{bmatrix} \bar{Q}_{44} & \bar{Q}_{45} \\ \bar{Q}_{45} & \bar{Q}_{55} \end{bmatrix} \begin{Bmatrix} \gamma_{yz} \\ \gamma_{xz} \end{Bmatrix} \tag{101}$$

and finally by transformation to the material coordinate system by θ we get

$$\begin{Bmatrix} \tau_{26} \\ \tau_{16} \end{Bmatrix}_k = \begin{bmatrix} \cos\theta & -\sin\theta \\ \sin\theta & \cos\theta \end{bmatrix} \begin{Bmatrix} \tau_{yz} \\ \tau_{xz} \end{Bmatrix}_k \quad . \tag{102}$$